

NRL Report 6186

UNCLASSIFIED

Determination of the Spin and Parity of
Nuclear Excited States by the
Experimental Measurement of Triple
Correlations in $(p, \gamma\gamma)$ Reactions

C. R. GOSSETT AND L. S. AUGUST

*Nuclear Reactions Branch
Radiation Division*

February 12, 1965



U.S. NAVAL RESEARCH LABORATORY
Washington, D.C.

CONTENTS

Abstract	ii
Problem Status	ii
Authorization	ii
1. INTRODUCTION	
1.1 General Problem	1
1.2 Radiative Proton Capture Reaction	1
1.3 Properties of the (p, γ) Reaction	2
1.4 Properties of Correlation Measurements	3
	6
2. EXPERIMENTAL METHOD	
2.1 Sum-Coincidence Method	9
2.2 Difficulties of the Method	9
2.3 Double Sum-Coincidence Arrangement	11
	13
3. EXPERIMENTAL APPARATUS	
3.1 Accelerator and Beam Optics System	14
3.2 Experimental Equipment	14
	18
4. EXPERIMENTAL ELECTRONICS	
4.1 General Arrangement and Data Control	24
4.2 Sum-Coincidence Circuit	24
4.3 Gain-Stabilizer System	26
	34
5. PROCEDURE AND DATA ANALYSIS	
5.1 Alignment Procedures	42
5.2 Correlation Measurement Procedures	42
5.3 Data Analysis	46
5.4 Predicted Correlation Functions	52
	62
6. EXPERIMENTAL RESULTS	
6.1 Identification of States	70
6.2 Correlation Results	70
6.3 Discussion	73
	84
ACKNOWLEDGMENTS	
	88
REFERENCES	
	89

ABSTRACT

The measurement of triple correlations in $(p,\gamma\gamma)$ reactions to determine spin and parity of nuclear excited states has not been widely used in the past despite the capability of such measurements to produce generally unambiguous assignments. This lack of usage has arisen primarily because of the low efficiency, the complexity, and the difficulty of such measurements when performed by standard techniques. This report describes an experimental arrangement which allows the measurement of triple correlations with an exceptionally high efficiency and multiplicity (the capability of measuring many different correlations simultaneously). This improvement has been obtained primarily from the successful application of a three-crystal double sum-coincidence spectrometer. An explanation of the method and detailed descriptions of the physical apparatus, electronic circuitry, experimental procedures, and data analysis are given, including explanations of a number of deviations from normal in both the design and procedures. As an illustration of the effectiveness and limitations of the experimental arrangement, the results of an extensive triple correlation experiment on the $^{60}\text{Ni}(p,\gamma\gamma)^{61}\text{Cu}$ reaction are presented with the conclusions regarding the spin and probable parity of six of the lowest-lying energy levels and a discussion of the applicability of certain nuclear models to this nucleus.

PROBLEM STATUS

This is a final report on one phase of the problem. Work on other phases is continuing.

AUTHORIZATION

NRL Problem H01-10
Project RR 002-06-41-5006

Manuscript submitted September 25, 1964.

DETERMINATION OF THE SPIN AND PARITY OF NUCLEAR
EXCITED STATES BY THE EXPERIMENTAL MEASUREMENT
OF TRIPLE CORRELATIONS IN $(p,\gamma\gamma)$ REACTIONS

UNCLASSIFIED

1. INTRODUCTION

1.1 General Problem

The principal aim of nuclear spectroscopy is the determination of the parameters associated with nuclear excited states for comparison with the various theoretical models which are developed to explain nuclear structure. Probably the most important of these parameters are the excitation energy of the state and its spin and parity, the former locating the state and the latter characterizing it. These parameters are basic to virtually any comparison with theory, although other experimentally measurable quantities may also be important. Although the properties of some of the levels at higher excitation energies have intrinsic interest with regard to level densities, it is generally the lowest lying excited states that are crucial for comparison with nuclear models.

A measurement of the energy of an excited state is generally possible by a measurement of the energy of the particles or quanta involved in either the excitation or the de-excitation of the state, as observed in the nuclear reaction or radioactive decay which causes the formation of the state. The precision with which such energy measurements may be made depends largely upon the type particle or quanta observed as well as the particular experimental method used. A related consideration is the energy resolution of the measurement, which plays an important part in the determination and identification of closely spaced levels. In addition, in some cases, auxiliary information is necessary in order to ascertain the location of the state, particularly in cases where the causal sequence of the events must be established.

The measurements of spin and parity, on the other hand, are frequently more complex experimentally, as these parameters do not manifest themselves so readily as energy. Some of the methods of determining spin are based upon the probability of observation of transitions between states of certain spin values. Thus, in some cases, inferences for the spin or at least limitations on the values of the spin of a state may be made on the simple basis of the observation or nonobservation of particular transitions. More complex are measurements in which transition probability varies according to these parameters, or direct measurements of transition probability in terms of level widths or lifetimes. A more direct, and often less ambiguous, method is the measurement of the angular momentum involved in transitions, as manifest in the spatial distributions of the particles or quanta involved.

Measurements of spatial distributions may vary from experimentally quite simple to quite complex, depending upon the type reaction or decay studied and the number of particles or quanta involved. Such measurements frequently depend upon the factors important in determining the energy of the state, as it is usually necessary to identify the radiations with the state in question and, where necessary, to experimentally separate such radiations from other radiations which may also be present. Thus, for this type measurement, energy sensitive detectors are generally required, and coincidence arrangements may be necessary to properly identify the causal relationships involved. As a class, these complex measurements of spatial distributions are known as correlations, and in those cases where a favorable reaction or decay allows their use, they provide the most reliable method of measuring the spins of nuclear excited states.

1.2 Radiative Proton Capture Reaction

One reaction which has proved very useful in providing spin assignments by correlation measurements is that of the capture of a proton and the subsequent decay of the compound state by the emission of one or more gamma rays, i.e., the (p, γ) or $(p, \gamma\gamma)$ reactions. When the transition from the capturing level to a state of known spin is observed, correlations of this transition may establish the spin of the capturing level. Or, when cascades of two or more transitions populate an intermediate excited state of the compound nucleus, the directional correlations of the transitions involved may be used to establish the spin of this intermediate level in addition to the spin of the capturing level. The use of transitions involving the emission of electromagnetic quanta (gamma rays) provides a well understood reaction mechanism. Thus, no uncertainty about the extent to which a given mechanism is operating or uncertainty over the interpretation of the mechanism itself exists for the case of gamma emission as it sometimes does in particle emitting (especially direct interaction) reactions.

The (p, γ) reaction has, accordingly, been fairly widely used in certain portions of the periodic table, from the time that energy sensitive gamma detectors (scintillators) became generally available in the early fifties. Most of these observations have been in the region between $Z = 10$ and $Z = 20$, from Ne to Ca. Proton capture reactions have also been observed in the light elements, $Z < 10$, but here the lower Coulomb barrier more often permits particle emission, with which the slower gamma-ray emission poorly competes. Thus, in this region, even when radiative proton capture is observed, the interpretation of the results is frequently complicated by the presence of broad interfering levels which are due to the high transition probabilities for particle emission. The increasingly higher Coulomb barriers above $Z = 10$ are effective in reducing such particle transition probabilities, at least with low bombarding energies for the incident protons, and the (p, γ) reactions become the predominant gamma-emitting reactions.* The widths observed for the capturing levels also generally become narrower and interference of neighboring levels becomes less of a problem.

Prior to 1955, it was believed on theoretical grounds that resonant (p, γ) reactions would not be observed for nuclides with higher Z based on the assumption that for incident proton energies sufficiently high to significantly penetrate the Coulomb barrier, the level density would become so great and the level widths so broad that discrete resonances would not be observed. That this was not so at low proton energies ($E_p < 2$ MeV) for nuclides as high as Ni ($Z = 28$) was discovered in this Laboratory in connection with work on lower Z nuclides, when it was found that gamma-ray resonances were observed which were attributable to the Ni foil backing of the target in question. This interesting observation was followed by a fairly extensive investigation of the (p, γ) reaction on separated isotopes of this element, which were reported in an article by Butler and Gossett (1). The results of that work, which represented the state of the art for such a weak reaction at that time, provide most of the preliminary information upon which the present experiment is based. The present experiment, by use of some more recently developed techniques, permits the extension of those measurements to triple correlations, which allow the determination of the spin and parity parameters for the low-lying state of the ^{61}Cu nuclide, by means of the $^{60}\text{Ni}(p, \gamma\gamma)^{61}\text{Cu}$ reaction, these levels being of particular interest to a recently proposed nuclear model.

*Note that inelastic proton scattering or Coulomb excitation may occur for cases where the proton energy is sufficiently larger than the excitation energy of the first excited state. Also, in special cases where the proton energy exceeds the threshold energy for neutron emission to the first excited state of the residual nuclide, i.e., the $(p, n\gamma)$ reaction, gamma rays may also be emitted.

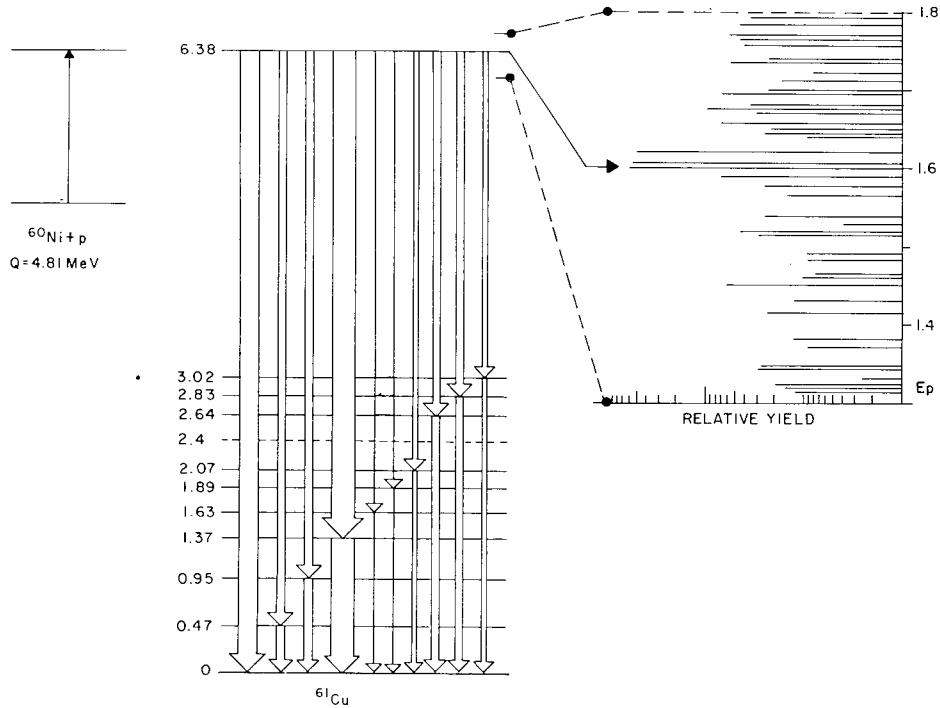


Fig. 1 - A schematic representation of the (p, γ) reaction showing the low-lying energy levels of the residual nucleus ^{61}Cu and the two-part gamma-ray cascades populating them from one particular capturing level (resonance). The widths of the arrows are approximately proportional to the branching of the cascades through these levels. To the upper right, shown to an expanded energy scale, is a schematic yield curve demonstrating in a semi-logarithmic representation the variation in the yield from resonance to resonance. Each resonance observed is a manifestation of an unbound level of the residual nucleus.

1.3 Properties of the (p, γ) Reaction

Some of the main features of the (p, γ) reaction which affect the present experiment are shown schematically in Fig. 1 and will be discussed in this section with reference to the results presented in Ref. 1. As shown on the left in Fig. 1, the energy equivalent of the sum of the rest masses of the proton and the ^{60}Ni (target) nucleus exceeds that of the ^{61}Cu (residual) nucleus in its ground state by the Q-value. As the proton must have sufficient velocity to tunnel through the repulsive Coulomb barrier, the kinetic energy of the proton in the center-of-mass system is added to the Q-value to produce the excitation energy in the compound nucleus, which is an energy on the order of 6 MeV. It is found that if the energy of a monoenergetic beam of incident protons is varied, large fluctuations will occur in the yield of gamma rays from the reaction. These resonances in the yield correspond to the excitation of virtual (unbound to particle emission) excited states in the compound nucleus. A schematic yield curve in a semilogarithmic representation is shown with an expanded energy scale to the right side of the figure. It is noted that the gamma-ray yield varies considerably from resonance to resonance. The experimental manifestation of this property is illustrated in Fig. 2, which shows the experimentally determined gamma-ray yield as a function of proton energy for this reaction. Here a general increase with increasing proton energy in the number of resonances observed and in the strength of these resonances is a manifestation of the increasing penetration of the Coulomb barrier. The lower portion of the figure includes that region of excitation

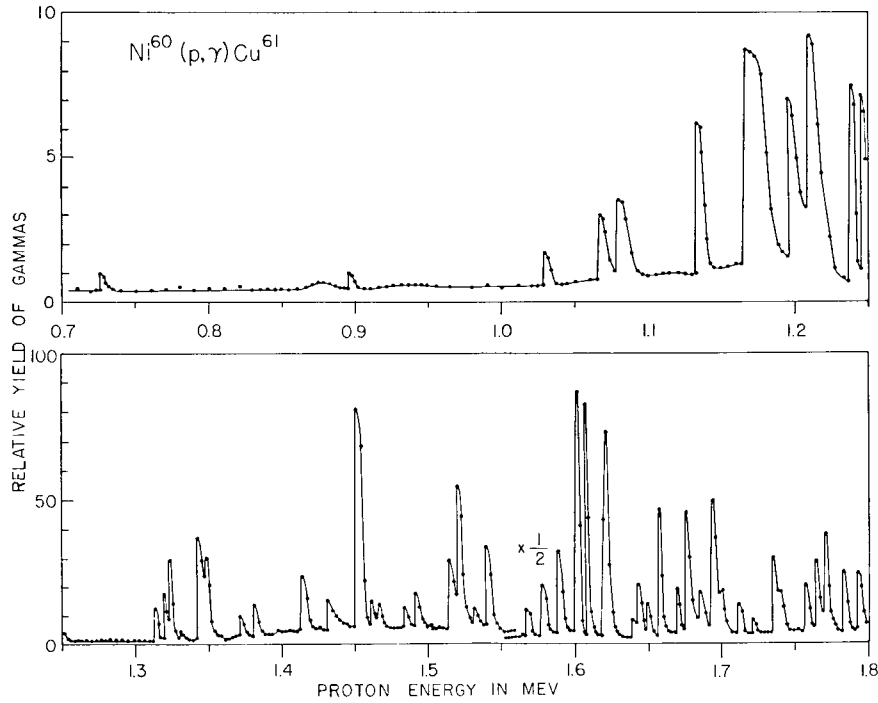


Fig. 2 - An experimental yield curve for the $^{60}\text{Ni}(p, \gamma) ^{61}\text{Cu}$ reaction taken from Ref. 1

energy where resonances sufficiently strong for correlation work are observed. It is noted that the observed resonances appear quite narrow and are generally well separated from each other. Actually, the widths observed in Fig. 2 are due to the instrumental effects of the spread of energy of the incident proton beam and the thickness of the target materials traversed by that beam. Attempts to measure the actual or "natural" width of the resonances by the use of a very high resolution energy analyzer for the incident protons (see Ref. 1) resulted in placing an upper limit of only tens of electron volts for these widths rather than the several hundred to a thousand electron volts evident in Fig. 2. One favorable result of the narrowness of the natural width of the levels compared to their separation in excitation energy is that these levels will not coherently interfere under such conditions.

Another property of the resonances is the branching of the de-exciting gamma-ray transitions through the lower excited states of the residual nucleus, as indicated schematically for one particular resonance by the widths of the arrows representing the gamma-ray transitions on the level diagram of Fig. 1. As shown in this example, only two-part cascades are indicated; in this case, this is a property of the method used to determine the existence of the transitions. Actually, it is probable that some of the excited states, particularly those above the first two or three, additionally cascade through lower levels to give rise to three- or four-part cascades from the capturing resonance to the ground state. The branching from the capturing level through the lower excited states is a function of that particular level, and this branching may vary considerably from resonance to resonance.

The experimental manifestation of the variation in the branching is shown in Fig. 3 which illustrates gamma-ray spectra obtained at a number of the stronger of these resonances. It will be noted that the structure varies considerably from resonance to resonance. The observed spectra are, of course, also dependent upon the response of

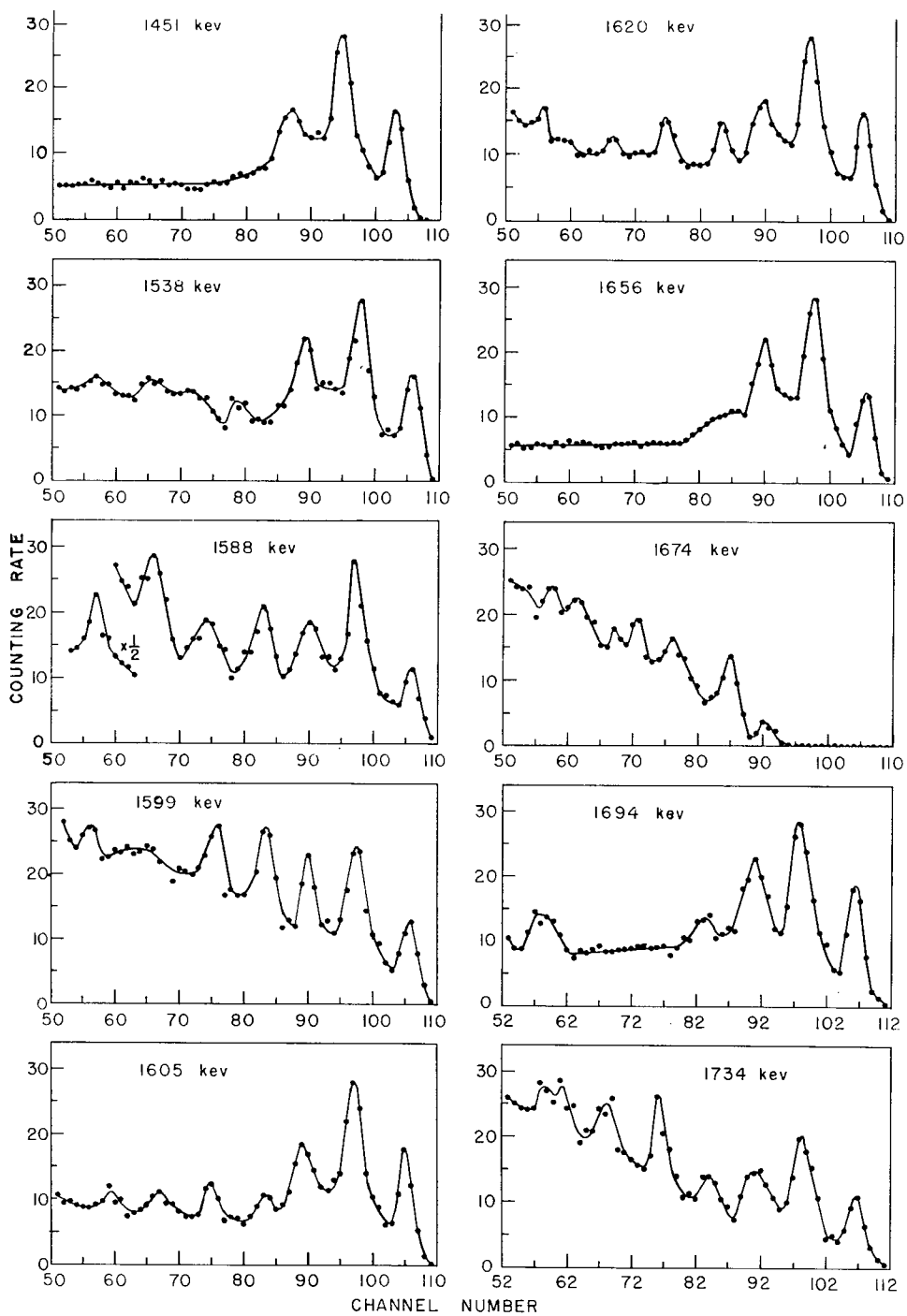


Fig. 3 - The pulse-height spectra for high-energy gamma rays from the $^{60}\text{Ni}(p, \gamma\gamma)^{61}\text{Cu}$ reaction as observed at some of the more intense resonances shown in Fig. 2. (Ref. 1.)

the detector used (in this case scintillating crystals of activated NaI) and the nature of the mechanisms of interaction of the gamma rays with matter. An example of the complexity of the spectra resulting from the interaction of high-energy gamma rays is afforded by the spectrum in the upper-left-hand corner, which is due to a single monoenergetic gamma ray and shows a long flat tail characteristic of the Compton-scattering interaction and the complex three-peak structure characteristic of the pair-production interaction, the peaks arising from the escape of none, one, or both of the annihilation quanta resulting from the decay of the positron created by the pair-production interaction. The complexity of the spectrum resulting from a single gamma ray is, of course, compounded when a number of gamma rays of different energy are present as in most of the cases illustrated in Fig. 3. These factors make the precise determination of the amount of a given gamma ray present in an ungated spectrum rather difficult for all but the highest energy gamma rays present; and even when great care is taken in determining the spectral response of the detector for various energies of gamma rays, the attempt to resolve a complex spectrum into its components is difficult at best.

A further difficulty introduced by the use of the scintillation type detectors is that these detectors are inherently only moderate resolution devices. This can be seen by the observed width of the peaks in the spectra of Fig. 3. This resolution, which for the higher energy gamma rays may be on the order of 3 percent of the energy of the gamma ray, becomes relatively worse for lower energy gamma rays, reaching 10 percent at around 0.4 to 0.5 MeV. Thus, while the use of gamma-ray transitions provides a convenient means of observing transitions through selected states from the point of view of a mechanism which is well understood, the presently available methods of detecting these gamma rays with reasonable efficiency are not as susceptible to high resolution measurements or to ease of interpretation as similar measurements for charged particles may be under certain conditions.

A further important property of the transitions observed at different resonances is that the gamma rays may show spatial distributions of intensity depending on the angular momentum transfer involved in the transitions, as has been previously noted. A very simple example of this property is provided by the measurement of the intensity of a given transition as a function of the angle of the detector to the direction of the beam of protons, called an angular distribution. Thus, for the transition to the ground state, observed as the highest peak in the spectra of Fig. 3, these distributions of intensities were determined in Ref. 1 and are shown in Fig. 4 for some of the stronger resonances in this reaction. In the cases shown, the isotropic distributions with angle generally correspond to capture in a spin 1/2 state, while those showing anisotropies are due to capture in a spin 3/2 state. Distribution measurements for the gamma ray from the capturing level to the ground state such as those reported in Ref. 1 yield only the spin of the capturing level; the more complex measurements necessary to yield the spins of the intermediate excited states, such as were performed in the present experiment, are discussed below.

1.4 Properties of Correlation Measurements

The case of the simple capture of a proton and emission of a single gamma ray is shown schematically in Fig. 5. The first stage of the process, that is, the absorption of the incoming proton to form a state of given spin and parity, is essentially analogous to the de-excitation process. The relevant parameters in the notation of Devons and Goldfarb (2) are: the channel spin, a , which is the sum of the spins of the target nucleus and the proton; the angular momentum carried in by the incoming proton, ℓ_1 or ℓ'_1 , where $\ell'_1 = \ell_1 + 1$ and in the general case admixtures of ℓ_1 and ℓ'_1 may occur; and the spin of the compound state, b . In the de-excitation process the relevant parameters are: the spin of the compound state, b ; the angular momentum carried away by the gamma ray,

Fig. 4 - The angular distributions for the gamma-ray transitions from the capturing level to the ground state from $^{60}\text{Ni}(p, \gamma)^{61}\text{Cu}$ reaction as observed at some of the more intense resonances shown in Fig. 2. (From Ref. 1.)

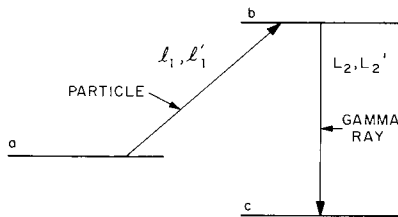
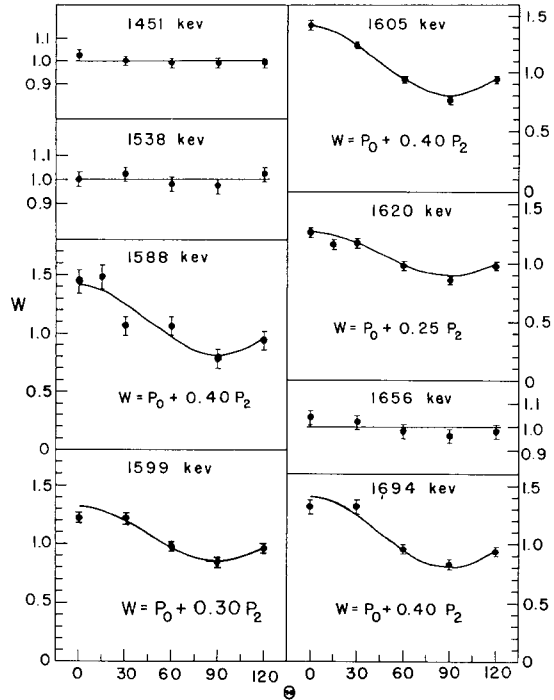


Fig. 5 - Schematic representation of the double correlation for the (p, γ) reaction showing the relevant parameters in the notation of Devons and Goldfarb (2)

L_2 or L_2' , where $L_2' = L_2 + 1$ and in the general case again admixtures of these two multipoles may occur; and the spin of the final state, c .

The case here outlined is the simplest possible and, for instance in the case of radioactive decay, is analogous to the double correlation between two gamma rays. It should be noted that in the reaction case the coincidence between the incoming proton and the gamma ray is essentially automatic and need not be specifically observed, therefore simplifying to some extent the experimental arrangements. This case, known as a double correlation or distribution, is obtained by measuring the intensity of the gamma ray as a function of the angle between the detector and the proton beam direction and was illustrated in the preceding section.

The experimental information which may be obtained in such a case is generally represented by the Legendre expansion in even powers* up to P_4 and limited to this value by the fact that multipolarities greater than quadrupole are not generally observed in reaction work. Thus: $W(\theta) = a_0 + a_2 P_2(\cos \theta) + a_4 P_4(\cos \theta)$. From such a distribution, one may obtain at most only two significant values: that is, the ratios $A_2 = a_2/a_0$ and $A_4 = a_4/a_0$. One notes, however, that even if the spin of a target nucleus and the spin of the final

*Odd powers appear only in cases of constructive interference of neighboring levels.

state are known, the experiment must determine not only the spin of the capturing state, b , but also the values of the two nonquantized variables δ_1 and δ_2 which represent the admixture of the angular momenta carried by the incoming proton and the admixture of the multipoles of the outgoing gamma ray, respectively. It may be seen that the two significant ratios determined from the experimental distribution are far short of sufficient to determine all of the variables of this problem. Even if the possibility of admixture of the incoming angular momenta is removed by the choice of a target nucleus of zero spin, the results of the distribution are generally ambiguous as to the choice of spin of the capturing state and the multipole mixing of the gamma ray. That is, generally more than one combination of the variables is allowable. Frequently, an external criterion, such as the improbability of the observation of large multipole admixtures, is applied to remove the ambiguity. However, this may be a dangerous criterion in some cases.

The essential underdetermination of the variables, which is due to the fact that only one angle can exist between two vectors, may be removed by consideration of the triple correlation, shown schematically in Fig. 6, wherein the gamma-ray transition between the state, c and an additional state, d (generally the ground state of the residual nucleus), is observed. This provides the additional possibility of a multipole admixture, δ_3 , for

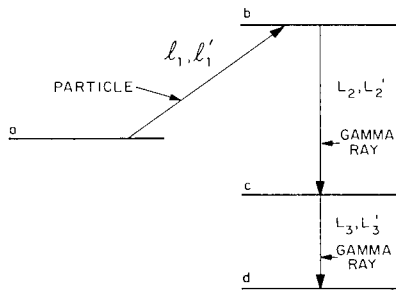


Fig. 6 - Schematic representation of the triple correlation for the $(p, \gamma\gamma)$ reaction showing the relevant parameters in the notation of Devons and Goldfarb (2)

the secondary gamma ray, which may carry an angular momentum, L_3 or L'_3 , where $L'_3 = L_3 + 1$. While additional variables have been added to the problem, the inclusion of another vector introduces the possibility of additional angles in terms of which the angular correlation may be measured. It has, in fact, been shown by Ferguson (3) at Chalk River that instead of the two significant ratios available from the distribution measurement, there are in principle eighteen independent values from the triple correlation, which should be sufficient in all cases to overdetermine the problem. In practice, of course, this many parameters are not generally determined. However, even under certain conditions of measurement which simplify both the experiment and the analysis, it is generally possible except in certain degenerate cases to adequately overdetermine the problem to the extent that unambiguous assignments may be made to both the quantized and unquantized variables. This is particularly true if the spin of the ground state of the target nucleus is zero, as in this report.

In the present experiment, the channel spin is just that of the incident proton because of the zero target spin, the spin of the ground state of the residual nucleus is known from other measurements (4), and the spins of the capturing states have been measured (with some possible ambiguity) by distribution measurements (1). The orbital angular momentum, l_1 , of the incoming proton depends upon the spin and parity of the capturing state. Thus, the principal unknowns to be determined experimentally are the spin of the intermediate state, c , and the multipole admixtures of the two gamma rays, δ_2 and δ_3 . Certain constraints upon the latter are supplied by the fact that in reaction work generally only electric dipole (E1), magnetic dipole (M1), and electric quadrupole (E2) radiations are found. The electric or magnetic character of the gamma ray determines whether a parity change occurs. The correlations, however, are not sensitive to the electric or magnetic character and determine only the multipolarity. Parity may be measured in gamma-ray transitions only by means of polarization experiments. However, it has been customary to make probable parity assignment in those cases where a significant admixture of quadrupole radiation with dipole is observed, on the theory that magnetic quadrupole radiation is sufficiently improbable compared to electric dipole that significant admixtures will not be observed of this type. Thus, while it is clearly questionable to assume an E1 transition

only on the basis of the absence of an observable admixture, it is more reasonable to assume a probable M1-E2 transition when significant admixture is observed, provided that isotropic spin or other mechanism which might retard an E1 transition is not expected to be strongly operating.

In the actual measurement of triple correlations, as in the double correlation, or distribution, the proton beam direction establishes the preferred direction in space and provides an essentially free coincidence. The problem then resolves to the measurement of the intensity of the coincidences between a given pair of cascading gamma rays as a function of the spherical angles: θ , with respect to the beam direction, and ϕ , with respect to one of the detectors. Now in principle, the correlations may be calculated in terms of any arbitrary placement of the gamma-ray detectors throughout the sphere, provided that a sufficient number, adequately distributed, are used. However, in practice the analysis is much simplified if one of the detectors is placed at 0 degrees or 90 degrees to the beam and the other moved on an arc of one of the principal planes. Under these conditions, the correlation function reduces to a simple Legendre expansion in terms of the variable angle, as in the distribution case. Several such experimental configurations are possible and are called geometries. For each geometry, a similar geometry exists which differs only as to whether the first, or primary, gamma ray is captured in the moving detector or in the fixed detector. The usual methods of measuring triple correlations by normal fast-slow coincidence arrangements generally allow for the measurement of a single cascade in only one geometry at a time. The arrangements of the present experiment, however, provide for the simultaneous measurement of many of these as described in the next section, and the geometries used in the present experiment are defined in Sec. 2.3.

2. EXPERIMENTAL METHOD

2.1 Sum-Coincidence Method

Triple-correlation measurements, unlike the experimentally simpler double-correlation, or angular-distribution, measurements, generally permit unambiguous assignments of spin and multipole admixture, if measurements are made in a sufficient number of geometries. Nevertheless, triple-correlation measurements are frequently resorted to only to remove obvious ambiguities from distribution measurements, probably because the necessary coincidence arrangements inherently involve decreased detection efficiency by requiring the detection of an additional gamma ray, and because the normal fast-slow coincidence arrangements permit the measurement of the correlation for only a single cascade and in only one geometry at a time. However, it becomes feasible to use the triple-correlation measurements as the principal means of investigation even with such a weak reaction, as that observed in the present experiment, if a sufficient multiplicity is gained for the measurement, that is, if the correlations are measured simultaneously for each two-part cascade present between the capturing level and the ground state, and if these correlations are measured simultaneously in an adequate number of geometries for each cascade. Such an improvement in the multiplicity has been achieved in this Laboratory by the use of a double sum-coincidence arrangement. This arrangement has permitted, in the present experiment, the simultaneous measurement of up to 24 correlation functions in a time interval sufficient for a single measurement for the least intense of these transitions. The method also provides a considerable simplification of the pulse-height spectrum. Accordingly, the use of the triple-correlation measurements has been adopted for this experiment as the sole method of determining the spin and admixture parameters.

The sum-coincidence method was developed by Hoogenboom (5) at the University of Utrecht. The spectra of Fig. 7 illustrate the basic principles involved. Here in a semi-logarithmic display is shown in the upper curve with open circles the ungated response

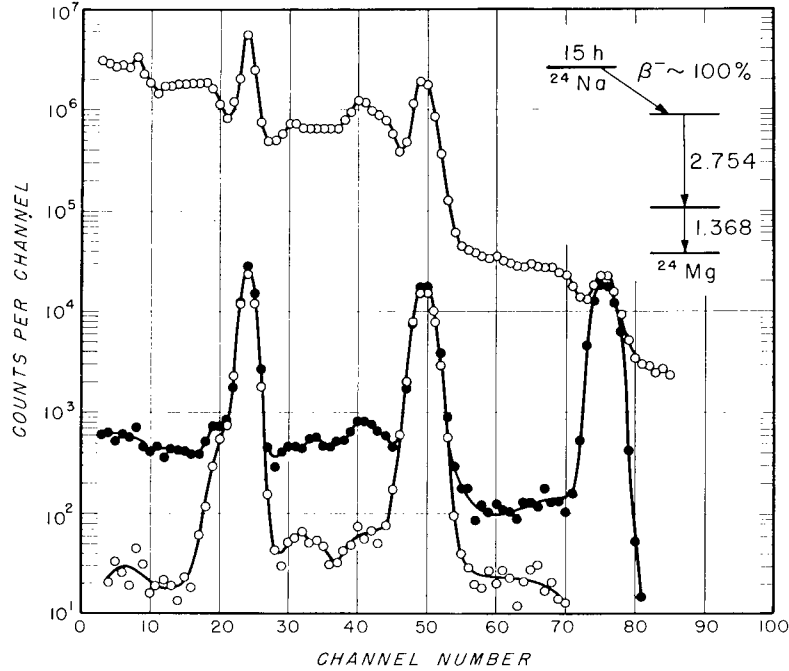


Fig. 7 - An illustration of the sum-coincidence principle using the gamma rays following the decay of ^{24}Na . The upper curve (open circles) is the response of a single NaI detector to the radiation. The middle curve (closed circles) is that portion of the events from the detector selected by a sum condition (amplitude only) between two such detectors. The lower curve (open circles) is that portion of the events selected by the sum condition and an additional fast time-coincidence condition.

of a single detector to the radiation from a ^{24}Na source prepared by irradiation in the NRL reactor. This source provides a simple simulation of the $(p,\gamma\gamma)$ reaction in that it yields two coincident gamma rays of 2.754 and 1.368 MeV in cascade, as indicated in the level diagram of the upper-right-hand corner. In the ungated spectrum, peaks (in about channels 24 and 50) corresponding to the capture of the full energy of each of these gamma rays are noted as well as the Compton distributions, and in the case of the higher energy gamma ray, a single annihilation quanta escape peak (about channel 40) and a suggestion of a double escape peak (see Sec. 1.3). In addition to these, because the detector subtends a fairly large solid angle, a sum distribution due to the simultaneous interaction of both members of a single cascade within the crystal is noted above the total capture peak of the highest energy gamma ray. This distribution is culminated by a sum peak (about channel 75) at an energy corresponding to the capture of the full energy of both members of the cascade.

If an additional detector is placed in a similar arrangement with the same source and its gain adjusted so that it provides an identical response (equal gain condition), and if the outputs of the two detectors are linearly summed and a differential discriminator (hereafter called the sum gate) placed over the sum peak corresponding to the capture of the full energy of both gamma rays, and if this sum condition is applied to select (gate) events from the total output of one of the detectors, then the spectrum of the middle curve, shown with closed circles, will be observed. Here three principal peaks are observed:

the highest corresponding to the sum gate itself, occurring for those events in which both gamma rays deposit their full energy in the crystal being observed; the next peak down corresponding to the case where the higher energy of the two gamma rays has deposited its full energy in the crystal being observed, while the lower energy member of the cascade has simultaneously deposited its full energy in the other crystal; and the lowest peak corresponding to the reverse situation, where the lower energy gamma ray has deposited its full energy in the crystal being observed and the higher energy member its full energy in the other.

Several advantages of this technique are immediately apparent: First, the sum condition restricts attention to those events which have deposited their full energy in the detectors, thus suppressing those events in which the escape of secondary quanta produce smaller pulses which serve merely to obscure the spectrum and thereby producing a single nearly Gaussian peak for each of the gamma rays. Second, the single sum gate allows the detection of either member of a cascade under circumstances where the capture of the full energy of the other member of the cascade in the other detector is assured. Thus, in terms of the correlations discussed in Sec. 1.4, the correlations are observed in two geometries simultaneously. Third, although it is not apparent in the test case shown here which involves only a single two-part cascade, the sum-coincidence method provides a similar response for all two-part cascades having the same total energy for the sum of the two gamma rays. The $(p, \gamma\gamma)$ reaction is, of course, ideally suited to this requirement, since the selection of a given resonance assures that all two-part cascades originating with the capturing level and terminating with the ground state involve the same total sum of the gamma-ray energies which is just the excitation energy of the resonant capturing level. Thus, it is seen that the multiplicity factor gained by a single sum-coincidence arrangement may be very large, since at a given resonance all two-part cascades to the ground state will be observed in two geometries concurrently.

2.2 Difficulties of the Method

This extremely powerful method of sum-coincidence has not been widely used in the measurement of triple correlations because of the existence of certain experimental difficulties which have been largely overcome in the design of the present experiment. One of these difficulties is that, while the sum condition is an inherent coincident condition, because the two pulses must occur within a certain time of each other in order to add, it is a coincident condition of rather poor resolving time ($2\tau \approx 1$ to $1.5 \mu\text{sec}$). This condition may, of course, be improved by requiring an auxiliary fast, or moderately fast, time coincidence between the two detectors, and the results of such a requirement are shown in the lowest curve of Fig. 7 involving open circles. This requirement eliminates the sum peak which corresponds to the capture of both radiations in the same detector, because such events cannot satisfy the coincident condition requiring events in both detectors. In the example shown, which corresponds to relatively high counting rate, it can be seen that the fast coincidence resolving time of about 80 nsec produces a considerable improvement in the spectrum. In examining this spectrum, we find that the peaks rise by about three orders of magnitude above the residual background, due in this case largely to remaining accidentals. This situation provides an excellent sensitivity for the detection of weaker cascades. The circuitry used to achieve the sum-coincidence conditions are described in Sec. 4.2.

A second difficulty, which has been described by Draper and Fleischer (6), concerns the transfer of energy between the two detectors and arises principally in cases of the escape from one detector and the capture in the other of either an annihilation quanta from the pair-production interaction or a back-scattered quanta from the Compton interaction. These transfer events give rise to satellite peaks that occur for cases which meet the sum-coincidence requirement and which would otherwise have been properly treated, had not the transfer occurred, or to events which satisfy the sum requirement only and

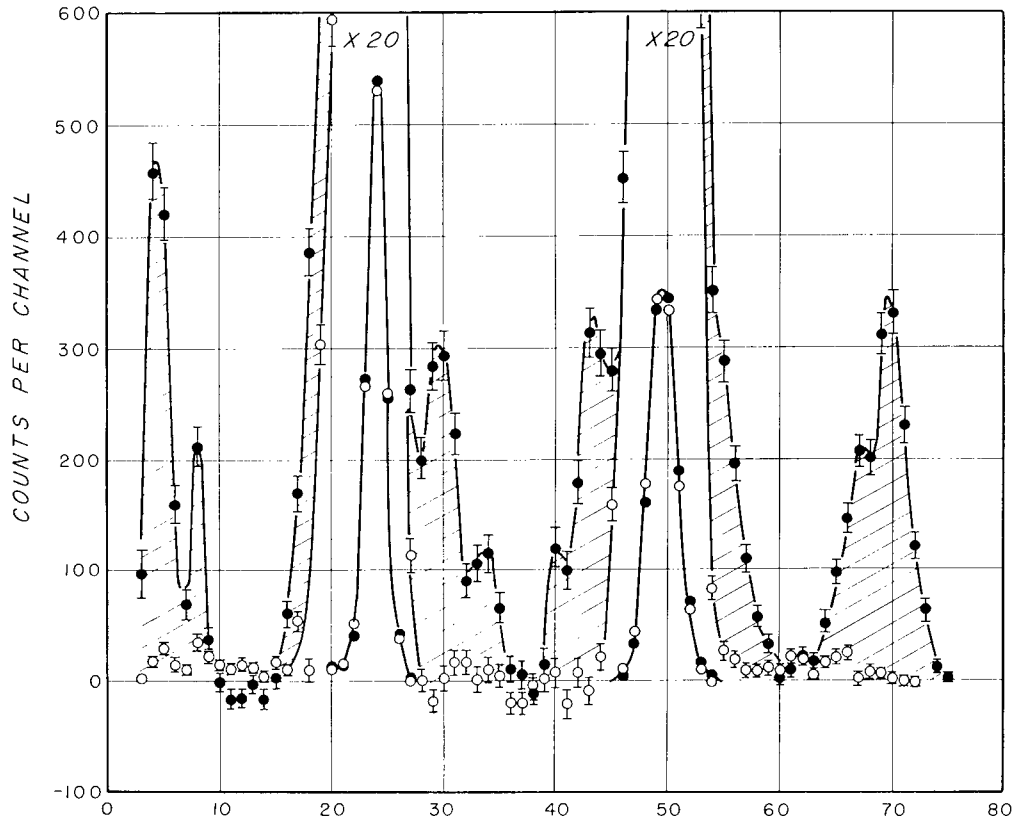
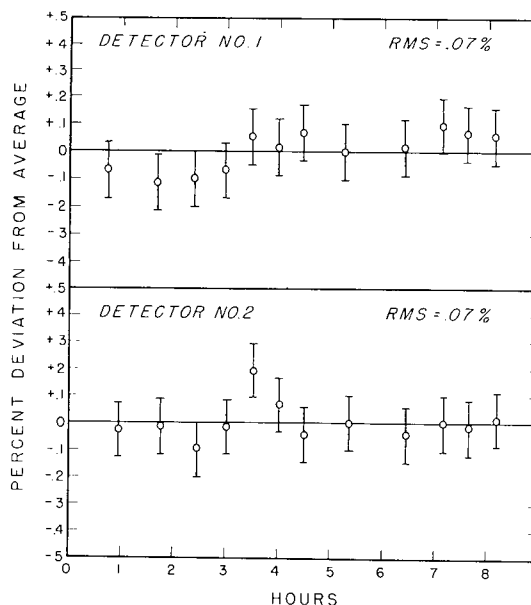


Fig. 8 - Sum-coincidence spectra obtained with (open circles) and without (closed circles) Pb collimators. The difference between the two curves is indicated by the crosshatched areas. The two spectra are normalized to the same peak yields and these peaks are shown with a scale changed by a factor of 20. Experimentally determined accidental coincidence spectra have been subtracted from each spectra to clearly show the "crosstalk" peaks.

for which the transfer itself supplies the fast-coincidence condition. This difficulty has been greatly reduced in the present arrangement by the use of conical Pb collimators which almost completely eliminate such low-energy transfer events except those which pass through the restricted collimator apertures. The effectiveness of these collimators is shown in Fig. 8, where sum-coincidence spectra obtained with and without the collimators (accidental coincidences subtracted) are compared for the ^{24}Na test case. The elimination of the satellite peaks enhances the ability of the sum-coincidence method to detect very weak two-part cascades in the presence of much stronger radiation, as indicated by the bottom curve of Fig. 6, which was obtained with the collimators. The configuration of the collimators is described in Sec. 3.2.

A third, and perhaps the most important, difficulty is related to the gain stability of each of the detector systems. Thus, the application of sum-coincidence measurements to correlations necessarily extended over long time periods requires extreme stability in the response of each of the detectors and of the sum gate in order to prevent distortions of the resultant spectra. In the present experiment, this difficulty has been overcome by the use on each detector of a light-source-based gain stabilization system that produces

Fig. 9 - The stability of the light sources used in the gain stabilizer arrangements. For these measurements the peak due to the light source was positioned between two peaks due to gamma rays from radioactive sources, and the equivalent energy of the light-source peak determined from these peaks. The quantity shown is the deviation of this equivalent energy from the average as determined from measurements made throughout the day. The error bars represent an estimate of the accuracy with which the equivalent energy could be determined considering the statics obtained.



stabilities of the order of 0.1 or 0.2 percent over a working day. The effectiveness of this stabilization system is indicated for two detector systems in Fig. 9. The stabilizer system is described in detail in Sec. 4.3.

2.3 Double Sum-Coincidence Arrangement

The present experiment uses several of the Chalk River geometries which provide that one of the detectors be placed at an angle of 90 degrees to the beam direction and the other detector be moved on an arc of one of the principal planes. Under the condition of the fixed detector at 90 degrees to the beam, each correlation may be expressed as a simple normalized Legendre expansion in even powers restricted to the fourth order: $W(\theta) = 1 + A_2 P_2(\cos \theta) + A_4 P_4(\cos \theta)$. Thus, although each correlation yields two significant ratios, A_2 and A_4 , the latter is considerably less sensitive and in most correlations is near zero. This lack of sensitivity effectively reduces the number of sensitive ratios to two for a single sum-coincidence arrangement.† Therefore, to provide four independent A_2 values, it has proved expedient to provide an additional pair of geometries for each cascade by supplying a second sum-coincidence arrangement. This has been achieved, as illustrated in Fig. 10, by the use of a single additional detector fixed at 90 degrees to the beam and 90 degrees from the other fixed detector. Thus, with the beam in the $+z$ direction and with detectors fixed on the $+x$ and $+y$ axes, the third detector is moved in the $y-z$ plane on an arc between the $+z$ and $-y$ axes in terms of an angle θ to the $+z$ axis. For convenience, the four geometries used have been labeled A, B, C, and D. These are defined in Table 1 in terms of the equivalent Chalk River cases and the spherical angles θ and ϕ . This choice of geometries allows three detectors to operate simultaneously with an angle of no less than 90 degrees between any pair, as required by the collimator arrangements. By placing the moving detector in the horizontal plane the mechanically more complex problem of moving a shielded detector in a vertical plane has been avoided. The physical aspects of the arrangement used in the present experiment are described in Sec. 3.2 and some factors concerning the alignment of the system in Sec. 5.1.

*This equation is the normalized version of that appearing in Sec. 1.4, and is obtained from it by division by the constant term, a_0 . Thus, $A_2 = a_2/a_0$ and $A_4 = a_4/a_0$.

†Although the A_4 terms are not very sensitive, the observation of values near zero frequently precludes possible solutions for high admixture ratios which generally require a significant A_4 term.

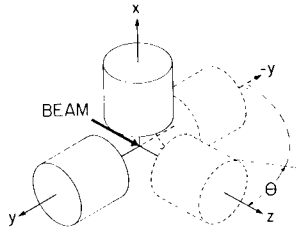


Fig. 10 - The relationship of the three detectors used in the present experiment to provide the geometries defined in Table 1. The two detectors shown with solid lines are fixed in position, while the third detector moves between the two positions shown with dashed lines.

Table 1
Definition of the Geometries (Experimental Configurations) Used in the Present Experiment in Terms of the Equivalent Chalk River Geometries and the Spherical Angles θ and ϕ , Where the Subscript 2 Refers to the Primary and the Subscript 3 to the Secondary Members of the Two-Part Cascade from the Capturing Level to the Ground State

Geometry	Equivalent Geometry*	Spherical Angle (deg)		
		θ_2	θ_3	ϕ
A	I	variable†	90	180
B	II	90	variable	180
C	VI	90	variable	90
D	VII	variable	90	90

*Reference 3.

†Variable: $0 \leq \theta \leq 90$ degrees.

It should be noted that this arrangement produces the equivalent of two legs of the spherical octant sometimes used at Chalk River (3). The degree of overdetermination thus provided has proved adequate, at least in the present experiment, which is restricted to the case of zero-spin ground state for the target nucleus, as this case removes the possibility of admixture in the entrance channel.

3. EXPERIMENTAL APPARATUS

3.1 Accelerator and Beam Optics System

The accelerator used in this experiment to provide a beam of protons is a horizontal 2-MV Van de Graaff obtained from the High Voltage Engineering Corporation in 1953 as an electron accelerator and later converted for positive-ion acceleration. At the beginning of the present project this accelerator was equipped with the original vacuum system including very slow mercury diffusion pumps and a wholly inadequate cold trap arrangement. The only provision for measurement of the energy of the proton beam was provided by a wide-gap, 25-degree-deflection magnet sector which does not provide a sufficiently homogeneous field for proton moment magnetometer measurement or control. This arrangement lacked both adequate stability and reproducibility for use with (p,γ) reactions, where (as seen in Sec. 1.3) the narrow and closely spaced nature of the resonances provides strict limitations on these performance characteristics.

Accordingly, before the present experiment could be performed, it was necessary to equip the accelerator with an auxiliary system which provides the following characteristics: (a) a beam optics system (energy analysis, beam deflection, and strong focusing)

capable of providing at a specified location on the target a well focused, high-intensity beam of protons with a very small spread in energy, and with the energy of this beam readily and reproducibly adjustable and highly stable at a given setting; (b) a vacuum system with pumping arrangements capable of handling the additional volume provided by the beam optics equipment, capable of sufficient pumping speed to allow the acceleration of high-intensity proton beams (with attendant large gas flow), and capable of maintaining the vacuum system (particularly the accelerating tube) relatively free of hydrocarbon contamination; and (c) the capability of handling high-intensity proton beams by restricting the beam from striking any but water-cooled surfaces. These requirements have been met by the present arrangements in the manner described below.

3.1.1 Beam Optics System

The energy analysis system has been built around a simple 1-m-radius electrostatic analyzer (hereafter called ESA) designed by L.W. Seagondollar. This instrument has been provided with an exceptionally stable high-voltage power supply referenced to a digitally set high-precision standard and stabilized by a chopper amplifier feedback system. Because the ESA does not provide separation of the mass components present in the proton beam, the 25-degree-deflection magnet sector has been maintained in the system for this purpose and to provide steering into the ESA. By reversing the field direction of the magnet, a less highly analyzed beam is available at an auxiliary port for irradiations and experiments with less stringent energy requirements.

Because of the well-known tendency of Van de Graaff accelerators to shift the position and angle of the output beam in the course of time, and because the narrow spacing of the plates of the ESA will tolerate little change in either angle or position of the beam at the input, a double-slit, double-deflector system has been provided for the input of the ESA. In addition to the input deflector system a set of deflectors has been provided on the output of the ESA to allow positioning of the beam accurately on target (see Sec. 3.2). Astigmatic strong-focusing sections have been provided for both the input and output of the ESA, which itself provides focusing in only one plane. The two strong focusing sections are independently adjustable: that in the input section to provide a vertical line object for the input slits of the ESA (this condition may also be affected by the rotatable shims of the magnet sector) and that in the output section to convert the vertical line image at the output slit of the ESA to a point focus, or at least a circular focus, at the target. These elements are all shown in Fig. 11, which illustrates schematically the layout of the beam optics system.

To avoid providing separate high-voltage supplies for the sixteen separate plates (electrodes) of the deflector and strong focusing system, a single high-capacity (5-kV, 100-mA) supply is used such that the individual voltages required are provided by a dropping resistor and high-voltage triode for each voltage. The voltages are then adjusted by varying the grid voltages oppositely in pairs so that each two-unit element works about a midvoltage of 2.5 kV. That is, to achieve a net deflection, the voltage of one plate of a deflector pair is raised above and that of the opposite plate lowered below 2.5 kV by equal amounts. As the output strong focusing section requires a greater range of high voltage than that provided for the other units, separate supplies are provided for it. The control circuitry for the deflector and strong focusing system provides in addition to the voltage controls, indicator circuits showing the current balance on the input slits and the current intercepted on the aperture formed by the target slit edges (see Sec. 3.2), as well as high-voltage run-up controls and safety shutdown of high voltage in the event of bias or vacuum failure or when manually initiated.

Because both the magnet and ESA are energy dispersive, the magnet must be maintained at a setting consistent with that of the ESA. For this reason, the magnet current supply circuit has been stabilized to provide a constant current. This stabilization allows

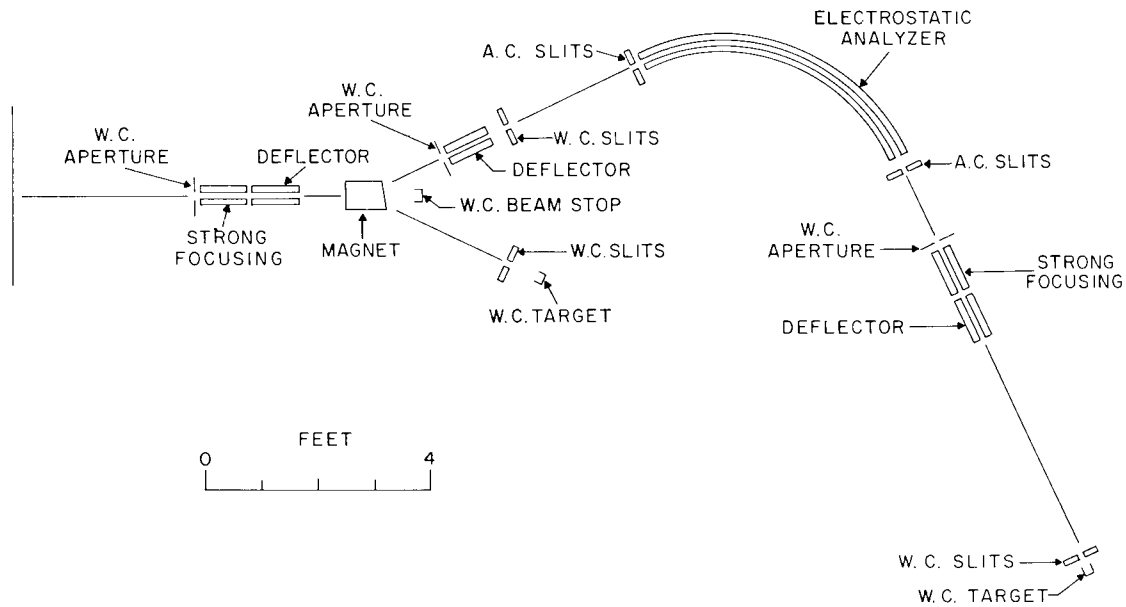


Fig. 11 - A schematic representation of the elements of the beam optics system used in the present arrangements. The scale applies only to the distance along the beam path. The initials W.C. or A.C. indicate whether a possible point of beam contact is water or air cooled.

minimum readjustment to maintain the beam for the ESA during long runs. The magnet control circuit has also been provided with precision nulling circuits which allow the presetting of the magnet current close to that required by the ESA and with switching arrangements which allow the magnet to be brought into adjustment with the ESA and which allow the choice of control slits for the corona feedback stabilization of the Van de Graaff voltage to be transferred from the magnet output slit to the ESA output slit without losing control of the beam. The control of pneumatically driven beam blockers is also contained in the magnet control circuit with provision that they automatically be driven in or out as required in the switching arrangements. An electron repeller voltage which allows accurate beam current measurements at the beam stoppers and the target is supplied from the magnet control. An interlock which prevents the passing of the beam to the target by interposing the last beam blocker is also provided in this circuit. The interlock is activated by failure of the repeller voltage (by accidental short) or by the absence of coolant to the target.

The stability and reproducibility of the energy analysis system have proved to be quite satisfactory in the present experiment, where the closeness in spacing of some of the resonances used have required the use of targets as thin as 2 keV, this condition requiring that the beam energy be maintained constant to within approximately 0.5 keV (~ 0.03 percent) to provide peak yield for the resonance. Only occasional adjustments throughout a working day have proved necessary to maintain this condition in the present experiments. In the use of the ESA, however, difficulty has occasionally been experienced in transmitting the beam through the ESA without it striking the plates, despite the double deflection arrangement on the input. These difficulties are believed to arise in cases where the changes in beam positions are large enough to cause distortions of the beam when it passes through the deflectors or strong focusing sections sufficiently off axis or to the distorted fields which result when the average potential of a pair of plates deviates too greatly from the midvoltage.

3.1.2 Vacuum System

The old pumping arrangements have been replaced by a low-back-streaming, high-efficiency oil diffusion pump and a long-lived liquid nitrogen cold trap of the Butler design (7). The main pump is a 6-in. pump backed by a 2-in. booster and roughed by a 5-cfm compound mechanical pump. A smaller auxiliary pump (4 in.) and cold trap have been supplied near the ESA output to provide low-impedance pumping to these areas remote from the main pumps. High-vacuum gauges have been provided at the openings to the system of both the main and auxiliary pumping arrangements, and gauges have also been provided to monitor the fore vacuum conditions. The system is equipped with pneumatically driven valves which may isolate the diffusion pumps and traps from the system or from the fore pumps. In addition failure indicators are provided for water pressure, water flow (temperature of efflux), and liquid nitrogen level of the main cold trap (temperature of evolved gases).

The control of the whole system is contained in a circuit which provides interlock and indicator arrangements to provide the following emergency actions: (1) If the pressure as determined by the main high-vacuum gauge reaches a predetermined level, the accelerator high voltage is interrupted; similarly for the auxiliary system, the high voltage of the ESA and deflector and strong focusing systems are interrupted. (2) If the pressure in the fore line of the main system reaches a set (low) level, indicating disruption of the vacuum, the main pumps and trap are isolated from the system by the gate valves. (3) If the pressure in the fore line of the main system continues to increase after the action of (2) to a set (higher) level, indicating the failure is within pump or trap, the diffusion pump heater power is interrupted. (4) If the pressure in the fore line of the auxiliary system reaches a set level the diffusion pump and trap are isolated and the power interrupted to the heater. (5) If the liquid nitrogen of the main trap is exhausted, the trap and pumps are isolated from the system by the gate valves. (6) If there is an outage of water pressure or if the flow is seriously restricted, the diffusion pump power is interrupted and the pumps and traps isolated from the system. (7) If an electric power outage occurs, all pneumatic valves are closed, and the valves remain closed and the power to the diffusion pumps remains off upon resumption of service. These interlocks must be manually reset, except that a switch is provided which allows unattended operation (out of hours) which permits the following automatic restart procedure for the main system in the case of the resumption of power: The fore pump is started; and, if liquid nitrogen is still present in the trap, the fore line valve is opened and power applied to the diffusion pump heaters. The main valves remain closed, isolating the pumps and trap from the system, until manually reset. If the trap were to warm up, the contaminants would be released into the pumping system. However, in those cases where the power outage is not so long as to boil away all of the remaining liquid nitrogen of the trap the restart prevents this release. The auxiliary system is normally isolated from the system except in accelerator operation, and no automatic restart is provided for it.

An unusual feature of the system is the arrangement of lights for indicating interlock failure or shorted condition, the latter being permitted by a front panel switch. As seen in Fig. 12, an external failure indication opens the relay, interrupting the contact closure provided for the load and causing the lighting of the red interlock failure indication. If interlock failure is removed, the relay closes, providing continuity to the load and causing the lighting of the green interlock condition indicator. If it is necessary to operate the system while interlock failure is occurring, this may be accomplished by the switch which closes the relay and causes the lighting of a yellow interlock condition indication. Thus, this arrangement not only provides facility in achieving interlock short but it also provides a prominent indication of the shorted condition, which remains until the situation is corrected. These arrangements were designed to overcome a common difficulty in interlocked systems, that is, the necessity at some point of shorting the interlock because of sensing circuit malfunction or unusual restart conditions. Unfortunately common practice under such conditions is to short out the interlock with clip lead or jumper and to provide

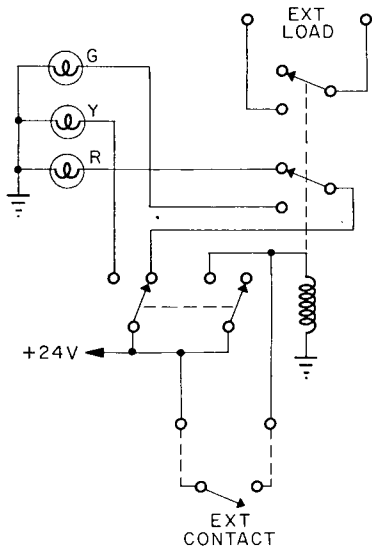


Fig. 12 - An interlock shorting arrangement and condition indicator used in the vacuum control and other systems in this Laboratory. The switch allows facility in achieving interlock short and provides indication of this short or of the interlock condition. (The labels G, Y, and R stand for green, yellow, and red.)

no indication of this condition. Because of the lack of indication, the presence of the short may be forgotten and an interlock condition which is not present relied upon. The present arrangements obviate this problem.

3.1.3 High-Intensity-Beam Capabilities

The adaptation of the system to withstand high-intensity (up to 150 microamperes unanalyzed) proton beams has required a complete redesign of the magnet box to provide water cooled arrangements to stop the unwanted mass components of the Van de Graaff beam. To restrict the beam at the input of the deflector and strong focusing sections, water cooled baffles have been provided of a design which allows reasonable pumping throughput while remaining optically dense to the beam except through the acceptance aperture. The pneumatically driven beam stops following the output slits of both the magnet and the electrostatic analyzers have also been provided with water cooling, allowing prolonged interruptions of the beam at either point. These beam stops are electrically isolated and are provided with electron repeller electrodes to allow beam current measurements at these points. The isolated output slit edges for the magnet, which form the first member of the double slit input for the ESA, are water cooled; however, it has not been found necessary to provide water cooling for the second isolated set of slit edges or for the isolated output slit edges of the ESA, as both sets of slit edges normally accept only a small amount of current from the edges of the beam. The arrangements for handling the high-intensity beam in the vicinity of the target are described in the next section.

3.2 Experimental Equipment

In the design of the present experiment the primary concern has been one of intensity, because the yield from the reaction is very low, the proton energy range available being well below the Coulomb barrier height. An additional concern is that, by the use of separated isotopes and careful attention to the control of contaminants, an experimental situation must be provided in which the vast preponderance of coincident radiation present is that sought. Even with the multiplicity gained by the sum-coincidence method, it is essential that as large a solid angle as possible be provided for the detectors and that the reaction yield be enhanced by utilizing large proton beam currents. The necessity of providing high detection efficiency for the weak reaction and some of the requirements of

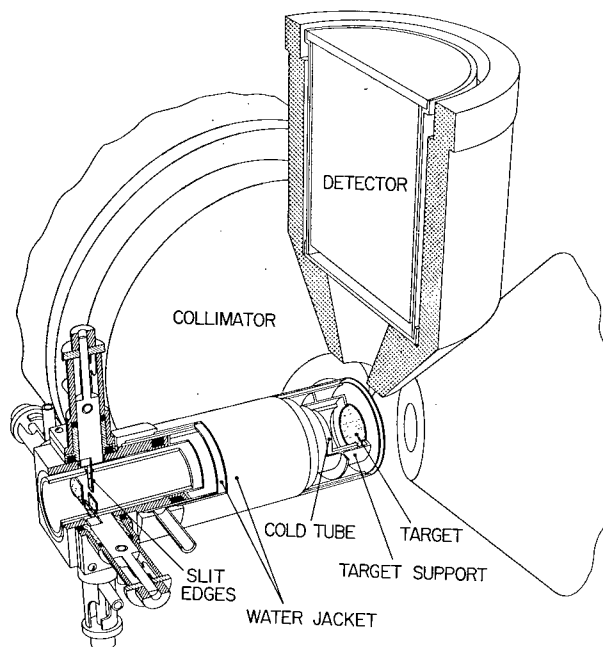


Fig. 13 - A cutaway perspective drawing of the apparatus in the vicinity of the target showing the relationship of the main elements of the system with respect to the target. (The collimators are shown partially withdrawn for clarity.) The beam of protons enters from the left, passes through the slit edges (shown partially cut away) and strikes the center of the target.

the double sum-coincidence systems have led to deviations from normal arrangements and procedures. These departures and their effect on the results are discussed in this and succeeding sections as they arise.

The main elements of the physical apparatus are shown in Fig. 13, which is a cutaway drawing of the materials in the vicinity of the target. Three detectors, each a 3 in. diam \times 3 in. long NaI(Tl) crystal, are contained within the three conical collimators. A section of the vertical member is shown; the configuration of the other two collimators is identical except that their horizontal mounting permits a greater thickness of shielding around the sides of the detectors. The arrangement is designed to place the front face of the crystals 6.0 cm from the source of the radiation, which is the 1/8-in.-diam circle illuminated by the proton beam at the center of the target. This source-to-crystal-face distance was chosen as the smallest consistent with providing the collimation requirements while permitting the detectors to be placed as close as 90 degrees to each other. The apex of the inner cone of the collimator (half angle, 26.5 degrees) is displaced from the target toward the detector such that no portion of the source directly illuminates the inner wall of the collimator. An additional graded absorber is placed over the front face of each crystal container to restrict acceptance of Pb x-rays from the collimators and the large flux of Coulomb-excited gamma rays from the target backing.

The correlation table which supports the detectors is shown in Fig. 14a. All three detectors are capable of radial motion toward the target and the two in the horizontal plane are capable as well of angular motion between the beam direction and 90 degrees to either side. For both the radial and angular movements the carriages supporting the

collimators and shields roll on precision bearings. The large diameter of the angular scale provided on the table and the care with which this scale was laid out provide an accuracy far greater than that necessary for correlation work. This scale and a fine micrometer screw supplied for one of the detector carriages were provided to permit possible resonance fluorescence experiments with this goniometer. The radial positions of all of the collimators are determined by 0.001-in.-division dial indicators. These indicators permit the collimators to be readily withdrawn and reinserted with considerable precision. In addition microswitch contacts provide signals for visual indication that the collimators are in position. The radial positions of the detectors are shown farther out than normal in Fig. 13 for purposes of clarity. In operation the front face of a collimator, when placed at 90 degrees, extends to within 1/32 in. of the outer wall of the target chamber, as seen in Fig. 14b.

In Fig. 13 the beam of protons enters coaxially with the target chamber from the left foreground, passes between the slit edges (shown partially cut away) and strikes the center of the target. The target consists of a surface layer, approximately 2 keV thick to 1.5-MeV protons, of isotopically enriched ^{60}Ni electrodeposited from very pure solutions (as described in Ref. 1) on a 3/4 in. diam \times 0.025 in. thick Au backing. The target backing and the last set of beam defining slits are of high-purity (99.97%) Au, heavily etched to remove surface contamination. It was found that unetched disks showed evidence of the presence of aluminum, presumably due to Al_2O_3 used as a polishing agent in the preparation of the necessarily flat (for heat conduction purposes) surfaces of the disk. Aluminum is a particularly bad contaminant for sum-coincidence work in that the Q-value is very high, allowing the possibility that energy-degraded quanta may meet the sum condition, and that unlike the common $^{19}\text{F}(p,\alpha\gamma)^{16}\text{O}$ contaminant reaction, the $^{27}\text{Al}(p,\gamma\gamma)^{28}\text{Si}$ reaction provides cascades of coincident gamma rays. Surface etching completely eliminates the Al contamination, leaving the disks free of contamination except for minute contributions from base metals, presumably residual volume contaminants of the Au. The use of Au rather than the higher thermal conductivity metal Ag, was based on the much lower Coulomb excitation cross sections for Au at the proton energies used. Other materials more acceptable from this point of view were not available in a form sufficiently free of contaminants, or were of too low a thermal conductivity, or were of too low a melting point.

The target backing is positioned within the evacuated chamber by a lightweight Al support and forced against the end of the target chamber by atmospheric pressure on the cup-shaped chamber. This chamber is a double-walled water jacket which provides, by means of spacers (not shown), that the water be restricted to flow between the flat walls directly behind the target backing at the end of the chamber. The innermost of these walls, which is in contact with the target disk, is machined flat from pure Cu to provide efficient transfer to the coolant of the heat liberated in the stopping of the proton beam in the target backing. While the interface between the Au disk and the Cu wall restricts the efficiency of the cooling arrangements, the convenience afforded by this method in the changing of targets recommends this approach, particularly in that the 50- μA analyzed proton beam which this system will sustain is near the capacity of the accelerator used in the present experiment.

The use of a cylindrical rather than spherical geometry in the vicinity of the target is not standard in correlation work; however, its use here is based upon the necessity of simultaneously providing water cooling to the target, a large solid angle to the detectors, and a small opening to the conical collimators. The placing of the target normal to the beam, rather than at 45 degrees, also allows the measurement of the correlation to either side in the horizontal plane (as described in Sec. 5.2). The materials in the vicinity of the target are as light as possible, providing individual wall thicknesses of no greater than 1/32 in., except for the cold tube which has a 1/16-in.-thick wall, but which is placed so as to not intervene between the target and detectors. The cup of the target chamber is over 3 in. deep to allow the placement of the necessarily heavier materials concerned

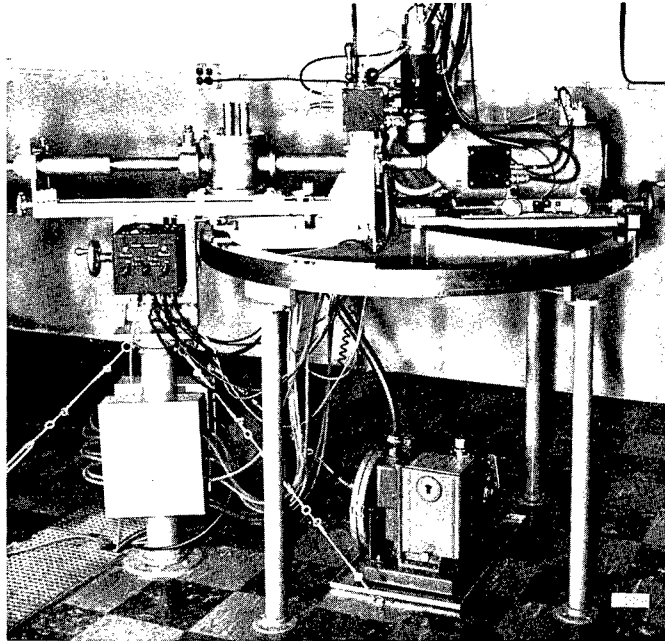


Fig. 14a - A general view of the correlation table, target protection cold trap, and target chamber

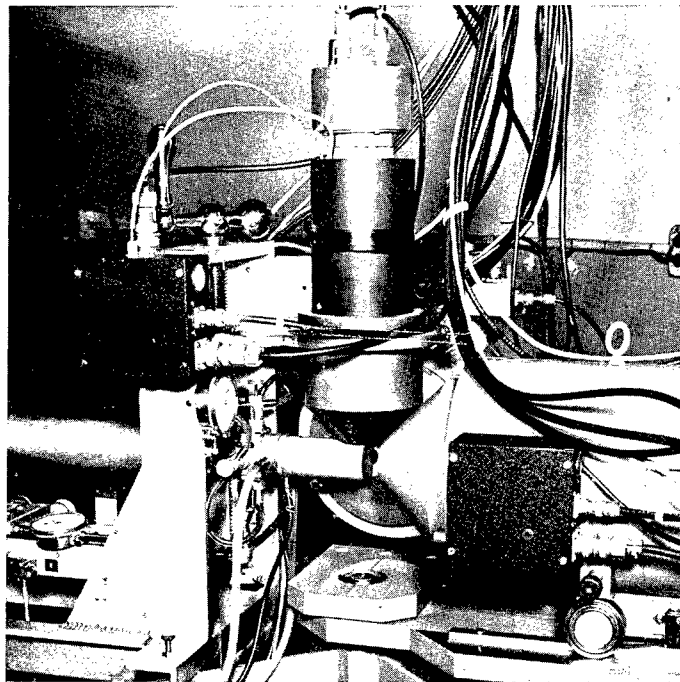


Fig. 14b - A closer view in the vicinity of the target chamber

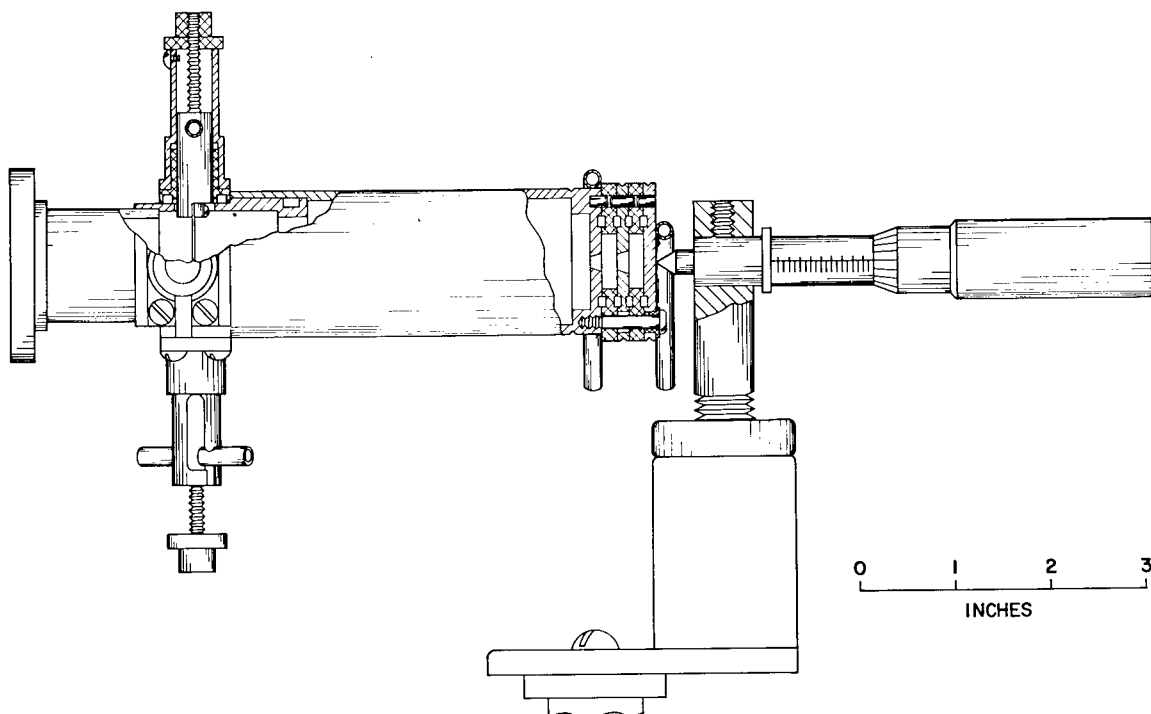


Fig. 15 - A plane cutaway view of the target slits, beam-finder device, and alignment micrometer. The beam finder consists of a 1/8-in.-diam aperture and Faraday cup (both water cooled) which is positioned with respect to the center of the correlation table by means of the micrometer device.

with the O-ring seal and water cooling arrangements at a sufficient distance that they will not significantly serve as a scatterer for gamma rays from the target to the detectors. The surfaces of the Cu cold tube and the Al target support near the target are Ag plated to prevent reactions induced by scattered beam. Correction factors to account for the unequal absorption of gamma rays from the target by the anisotropic distribution of materials in the vicinity of the target have been calculated as a function of the angle of the detector, as described in Sec. 5.3.

The source position for the correlations is determined by the momentary position of the beam on the face of the target. The problem of locating and maintaining this position is intensified over that encountered in normal uncollimated arrangements (even those subtending large solid angles) by the closeness of the front face of the collimators, the apertures of which provide the definitive elements of solid angle for the detectors. In order to provide sufficiently accurate positioning and stability of the beam position at the target, it has been found necessary to place a set of beam defining slit edges fairly close to the target, at a distance of approximately 4-1/2 in. In the present experimental arrangement the beam is aligned over the fixed center of rotation of the correlation table, the slit edges are adjusted to define the beam, and the beam is maintained in this position at the target by adjustment to keep the beam centered within these slit edges. To achieve initial alignment, a beam positioning device, shown in Fig. 15, replaces the target chamber of Fig. 13 such that a 1/8-in.-diam aperture followed by a Faraday cup (both water cooled) is in the position of the target plane and is aligned with respect to the center of the table by the use of the micrometer device. The beam, at the full intensity used in the experiment, is then directed by means of electrostatic deflectors and strong focusing elements to provide minimum current intercepted by the aperture with maximum current transmitted to the Faraday cup, and the slit edges radially adjusted to define this position.

The use of the beam positioning device provides a difficulty with regard to the cold tube shown in Fig. 13. This cold tube, maintained at liquid nitrogen temperature, serves to protect the target and the slit edges while under bombardment from the accumulation of contaminants (as described in Ref. 1). When in position, the end of the tube extends to 3/16 in. from the target, this position placing the cold tube outside of the cone of acceptance of the collimators. To prevent the icing of the cold tube which would occur upon exposure to the atmosphere when the beam positioning device is replaced with the target chamber, a means is provided to isolate the cold surfaces to prevent the disruption of the vacuum in which they are maintained. This isolation is achieved by translation of the cold tube and its supporting reservoir along the beam axis away from the target to a position before the last valve in the system. This translation is by means of a carriage and sliding-seal arrangement, shown in Fig. 14a, where the relationship of the cold trap, valve, and target chamber is evident.

The cold tube also serves as an electrode to provide an electron repeller voltage of -200 V to permit accurate measurements of the beam current intercepted by both the slit edges and the target. The slit edges and housings are electrically insulated from the target chamber by the use of nylon elements and the target chamber itself insulated from ground by a glass sleeve which is the last element of the system before those parts shown in Fig. 13. The whole of the cold trap and carriage arrangement of Fig. 14a is insulated from ground to provide the repeller voltage.

The cold trap-target chamber arrangement is supported, as may be seen in Fig. 14a, on a milling vice which with the flexibility provided by a syphon bellows permits the alignment of the beam finder over the table as well as the withdrawal of the target chamber back along the beam direction. The target chamber is reinserted to the same axial position with the aid of a dial indicator similar to those used to determine the radial positions of the detectors. Likewise, the position of the cold tube with respect to the target is determined by a dial indicator from the position of the carriage supporting the cold trap. Both motions are also supplied with microswitches which provide for visual indication that these members are appropriately in position. The black box mounted on the cold trap support in Fig. 14a provides metering and switching arrangements between the beam finder and target chambers, as well as control and indicators for the repeller voltage and coolant flow arrangements.

Because in use the slit edges are introduced through narrow slots in the wall of the cold tube, as seen in Fig. 13, it is necessary that these slit edges be capable of being withdrawn outside the cold tube and later reinserted to the identical position determined in the beam alignment procedure. This capability is provided in a reasonably small and lightweight manner by the slit housing arrangements shown cutaway in Fig. 13. Here, the position of a slit edge is defined by the limiting action against atmospheric pressure provided by the innermost of the two knobs seen at the outer end of each slit housing. The knobs are threaded (threads not shown) to the rod extending from the water-cooled heat sink which supports the slit edge. The outermost knob provides a means of locking the limiting knob to the threaded shaft once initial adjustment has been achieved. The slit edge may then be withdrawn by outward motion, guided by the water-cooling tubing within the slots provided in the housing, and the withdrawn position secured by a 1/8-turn twist. Then, after the target chamber has been installed and evacuated and the cold tube repositioned, the slit edges are reinserted to allow the positioning of the beam on target at the position which has been defined by the beam positioning device.

Although the measures described above permit the alignment of the beam positioning at the target as defined by the edges of the beam within an acceptable accuracy of approximately 0.005 in., the effective source for the correlations is defined not by the geometric center relative to the edges of the beam but by the center of current density at the target. Because the shape of the beam profile is not necessarily symmetric, these two centers unfortunately do not necessarily coincide, and further, their relationship may change

throughout the day depending upon changes in the focusing conditions of the accelerator. This uncertainty in the position of the center of current density at the target remains the largest single source of systematic error identified in the present experiment. These effects, however, may be somewhat minimized by the procedures of data accumulation (see Sec. 5.2).

4. EXPERIMENTAL ELECTRONICS

4.1 General Arrangement and Data Control

The main element in any instrumentation based upon scintillation detectors is the multichannel pulse-height analyzer (hereafter called PHA), which converts the information in analog form of the amplified pulses from the photomultiplier to a digital form and cumulatively stores this information for presentation on demand. The ability of the PHA to analyze only those pulses which are selected, or gated, by external circuitry provides great experimental flexibility, as in the present experiment where complex amplitude and timing requirements are used to select only the small number of events of interest from the total spectrum of pulses from the detector.

Thus, the second major element in the electronic instrumentation is the circuitry used to determine whether a given event meets these special requirements. The arrangements used in the present experiment to accomplish this selection are illustrated in the simplified functional block diagram of Fig. 16. Here, the two separate spectra evolved in the double sum-coincidence arrangement (see Sec. 2.3) are accommodated by use of the split-memory feature of the PHA, which allows the routing of the storage of selected pulses from the moving detector (shown here as Det. 2) into one or the other halves of the memory, according to which of the fixed detectors the event in the moving detector is in coincidence. Thus, the sum condition is applied by the Sum Disc. (gate) to the adjusted and stabilized outputs of all three detectors; a gate pulse allowing the analysis of the associated pulse from the moving detector is produced by a slow coincidence of a sum condition and a fast-coincidence condition between the moving detector and either of the

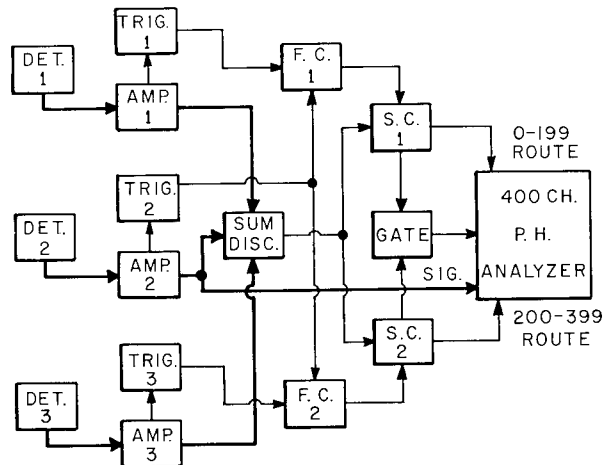


Fig. 16 - Simplified functional block diagram of the electronics illustrating the manner in which the two spectra from the double sum-coincidence arrangement are stored in the two halves of the pulse-height-analyzer memory according to the coincidence condition

fixed detectors; and the event is stored in the appropriate half of the memory as routed by the particular fast-slow coincidence condition. The special circuitry, called the sum-coincidence circuit, which applies the amplitude and timing restrictions to generate the gating and routing pulses was designed in this Laboratory to meet these special requirements, and is described in detail in Sec. 4.2. The essential gain stabilization system, not shown in Fig. 16, is described in detail in Sec. 4.3.

The detectors used in the present experiment are 3 in. diam \times 3 in. long NaI(Tl) crystals in Type A, Low Mass Mounting, provided by the Harshaw Chemical Company. These are mounted through a light pipe (see Sec. 4.3) to RCA Type 8054 photomultiplier tubes. Conventional stabilized high-voltage power supplies, Hamner Model N-401 and Atomic Model 312, are used, but the voltage distribution arrangements at the phototube base are modified (see Sec. 4.3) to allow change in the effective high voltage across the photomultiplier structure to achieve gain stabilization. Hamner N-361 high-performance preamplifiers and N-308 series double-delay-line amplifiers are used to amplify and shape the photomultiplier pulses. The Hamner N-670 pulse crossover pick-off gates, mounted integrally with each amplifier, are used to provide trigger signals for the fast coincidence circuits. The amplifier associated with the fixed crystal out of the horizontal plane is a Hamner N-328 amplifier, which additionally contains an integrally mounted single-channel pulse-height analyzer (differential discriminator) used in the present experiment as a monitor gate.

Double-delay-line amplifiers and the associated pulse-crossover-pickoff circuits have been used in order to provide minimum walk (change in time delay with pulse amplitude) in the trigger pulses for the wide range of the pulse heights which may be selected by the sum condition. The property of the double-delay-line principle which provides that the pulses, independent of pulse height, will cross over the zero level at the same time after the initiation of the event is illustrated in Fig. 17(b), where two different pulse heights are shown. Another feature is that, because the areas of the positive and negative portions of the wave form are equal, capacitors throughout the circuits are left with no net accumulation of charge; therefore, this type amplifier also provides the fast recovery and low distortion features necessary for use at high counting rates or for high-precision use at lower rates.

In the early part of this project a 100-channel PHA, designed and built at NRL by the Nuclear Instrumentation Branch of the Radiation Division was used, as in the spectra of Sec. 2.1. However, that used since September 1963, including use in the reaction experiment reported here, has been an RIDL 400-channel PHA, Model 34-12B, which provides the split-memory feature mentioned above, while providing a more adequate resolution

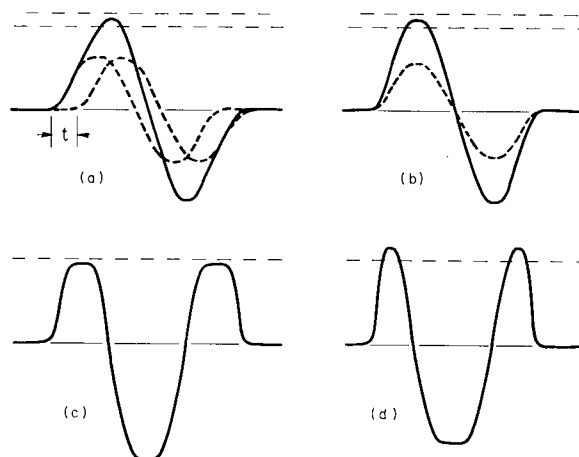


Fig. 17 - Pulse shapes from the double delay line amplifiers for various combinations of pulses. In (a) two smaller pulses (dashed curves) separated by a time interval t are added (solid curve), and in (b) two similar pulses with no time separation are added. The differentiated wave forms for the summed pulses are shown in (c) and (d), respectively, illustrating the operation of the slope discriminator to distinguish the two cases. Discriminator levels are indicated by the horizontal dashed lines.

(200 channels) for each spectrum. This instrument is provided with a punched-paper-tape readout, and in the present arrangement a typed copy of the data is produced from the tape by a Flexowriter electric typewriter and, when required, a plotted graph of the spectra is obtained from the tape by a tape reader and Moseley Model 50A tape translator driving a standard Moseley X-Y plotter. The use of a punched tape output and "off-line" recording or plotting provides much shorter readout times (approx. 1 min for 400 channels) than otherwise. The punched paper tape code used is compatible with the NAREC computer at this Laboratory, and it is intended that these tapes be fed directly to the computer for analysis as soon as programs being written are completed for this purpose. However, these were not available for use with the data of the present report.

In addition to the instruments associated directly with the detector systems, several commercial instruments have been provided to measure other parameters pertinent to the present experiment, as follows: (a) true time interval, the total time interval during which data are being accumulated, as measured by an Atomic Model 930 precision timer; (b) live time interval, that portion of the total interval during which the circuitry allows the acceptance of a new pulse for analysis, as determined by signals indicating the normal analysis and storage dead time of the PHA and additionally the dead time due to a blocker signal of the sum-coincidence circuit (see Sec. 4.2), as measured by an RIDL Model 54-1 live timer; (c) total charge, due to the proton beam accumulated on target during the time interval, as measured by an Eldorado Model CI-110 current integrator; and (d) several scalars, monitoring the outputs of the monitor gate and routing gate generators during the time interval.

It is of course essential that the above instruments and the PHA work in synchronization, and a master data control circuit has been built in this Laboratory for that purpose. The data control allows: manual start and stop of the counting interval, automatic stop at a preset signal provided by any of the above instruments, reset of all instruments including the PHA, initiation of the readout cycle of the PHA, and certain automatic cycling operations. In addition a data interlock circuit is provided which, when selected, prevents the accumulation of data when a proton beam current within certain specified limits is not present at the target. Also, a restart and alarm circuit has been provided which, when selected, allows restart of data accumulation under certain conditions after beam interruption and provides two tone levels of audio alarm indicating either completion of a preset counting interval or of data interruption due to beam failure. Further, two additional levels of audio alarm are provided to indicate vacuum failure or radiation hazard as indicated by external circuitry.

4.2 Sum-Coincidence Circuit

A block diagram of the sum-coincidence circuit is shown in Fig. 18. This circuit provides three amplitude discriminators: two of these, designated upper and lower discriminators and each working off of the sums of pulses from the three amplifiers, together form the sum-gate; and a third discriminator, designated the slope discriminator, working off the differentiated sum of the amplifier outputs, provides an auxiliary fast-discriminator condition. Two fast-coincidence circuits work from the crossover pickoff pulses from the three amplifiers and are capable by means of the switching arrangements of responding to various coincidence combinations. Two slow-coincidence and output driver circuits each accept the switch-selectable outputs of the three amplitude discriminators as well as an external gate and one of the fast coincidence circuits. A blocker circuit is activated by a pulse from any of the crossover pickoff circuits or a trigger pulse from the gain-stabilizer circuitry and provides an output which blocks the inputs of the amplitude and fast coincidence discriminators for a prescribed period and provides a corresponding dead time signal to the external live time circuit.

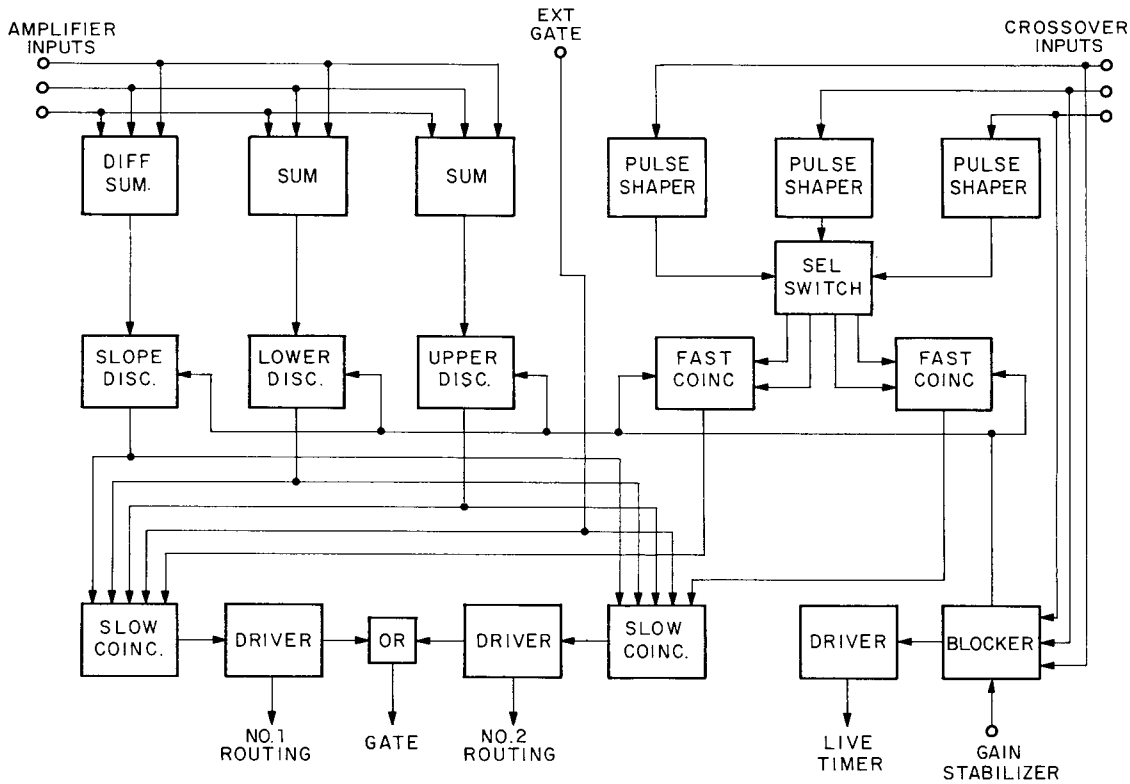


Fig. 18 - Principal elements of the sum-coincidence circuit

The slope discriminator is intended to provide a degree of double pulse rejection for closely spaced pulses and to provide an improved resolving time for the summing procedure when the fast-coincidence circuitry is not used. The principal of operation is indicated in Fig. 17 where two instances of addition of the amplitude of two smaller but equal pulses are shown; the two separated by a short time interval t (each indicated by a dashed curve and the sum of the two by the solid curve) is shown in (a), and the two occurring simultaneously (each indicated by the single dashed curve and the sum of the two by the solid curve) is shown in (b). Although the two pulses displaced in time are not true sum-coincidence events, they produce a pulse which lies within the sum gate discriminators (here indicated by the horizontal dashed lines). Such events may be distinguished from true coincidence, at least when not too great a disparity exists between the two pulses, by a measure of the slope of the leading edge of the summed pulse. Thus, since all single pulses from the amplifier have the same rise time, the slope from the addition of two smaller pulses displaced in time will never be as great as that produced by a single pulse or the sum of two coincident smaller pulses which yield the same amplitude for the summed pulse. This is illustrated in (c) and (d) of Fig. 17, where the derivatives of the summed pulses indicate that the differentiated pulse reaches a greater amplitude in the time coincidence case, and that a discriminator level applied to such a differentiated pulse at the level shown by the horizontal dashed line can differentiate between the coincident and time displaced cases.

Figure 19 shows (a) the sum and bias elements for the upper and lower discriminators, (b) the differential sum and bias elements for the slope discriminator, and (c) the discriminator circuit used for all three amplitude gates as well as elsewhere within the sum-coincidence circuit. Because thermionic amplifiers with a 100-V-maximum linear output are used, and because the tunnel diodes (used to provide exceptional stability for

UNCLASSIFIED

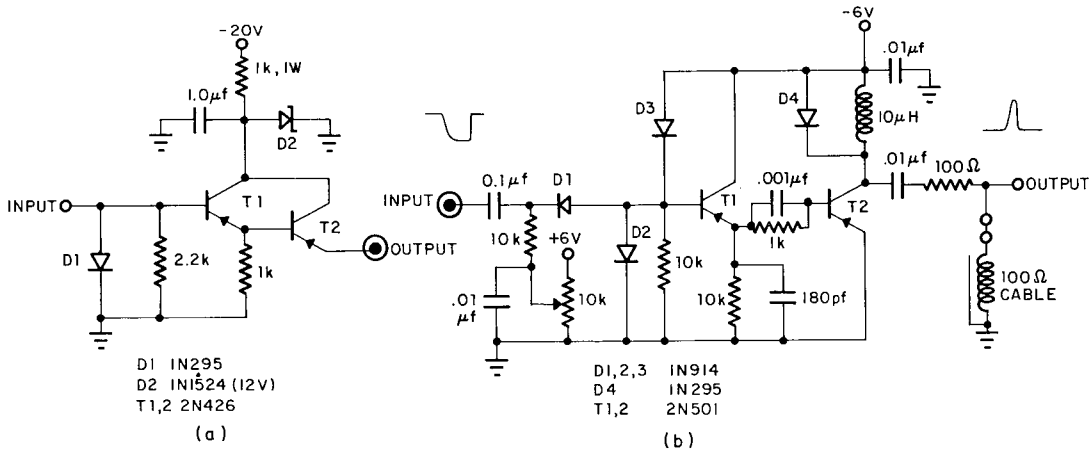


Fig. 20 - Elements of the sum-coincidence circuit: (a) output driver used with the pulse crossover pickoff circuit, and (b) pulse-shaping circuit used for the fast-coincidence arrangements

slow-coincidence circuit for events which should have been excluded because the pulse exceeded the upper discriminator level. This possibility is avoided in the present circuit by the blocker circuit to be described below, but fast recovery of the discriminators is necessary to prevent excessive dead time for the blocker.

Because the variable delay arrangements positioned between the crossover pickoff circuits and the sum-coincidence circuit require the use of 50-Ω cable, and because the output of the N-670 circuit is inadequate to drive this cable, the transistorized crossover output driver shown in part (a) of Fig. 20 is provided and mounted in each amplifier. The -20 V required for these circuits is supplied by a separate external power supply to avoid overloading the already marginal negative power supply of the amplifiers. The variable delay unit provides for the insertion of different lengths of RG 11/U cable by coaxial switch selection to provide changes in increments of 1 nsec over a range of 80 nsec. Arrangements providing coarser changes are provided in the other two lines. The output pulses of the crossover pickoff circuit, which have a rise time of greater than 100 nsec, are not directly suitable for the fast-coincidence arrangements, and the pulse shaper shown in part (b) of Fig. 20 is provided. The discrimination of the input of this circuit provides a means of making small adjustments in the delay by means of the 10-kΩ trim pot.* The two transistors form a univibrator providing a fast-rising saturated pulse which is then clipped by the shorted 93-Ω cable on the output. The length of this cable of course determines the width of the output pulse. Those currently used in the present experiment are 15 feet long.

The same discriminator unit shown in Fig. 19(c) is used in the fast-coincidence arrangement shown in Fig. 21, where by means of current discrimination it determines if the trigger pulses have occurred close enough in time to add to provide a current pulse sufficient to trigger the discriminator. The current bias for the two discriminators are provided by a dual 5-kΩ helipot which affords control over a limited range of the resolving time of the coincidence circuit by affecting the degree of overlap of the trigger pulses necessary to exceed the discrimination level. At the inputs of the discriminators, 1-kΩ trim pots are provided to permit adjustments allowing equal response from the two discriminator units.

*The full range of adjustment is not available, as the discriminator must be set sufficiently below the maximum pulse height to provide saturation of the output transistor in order to provide the necessary constant pulse height for the shaped pulses.

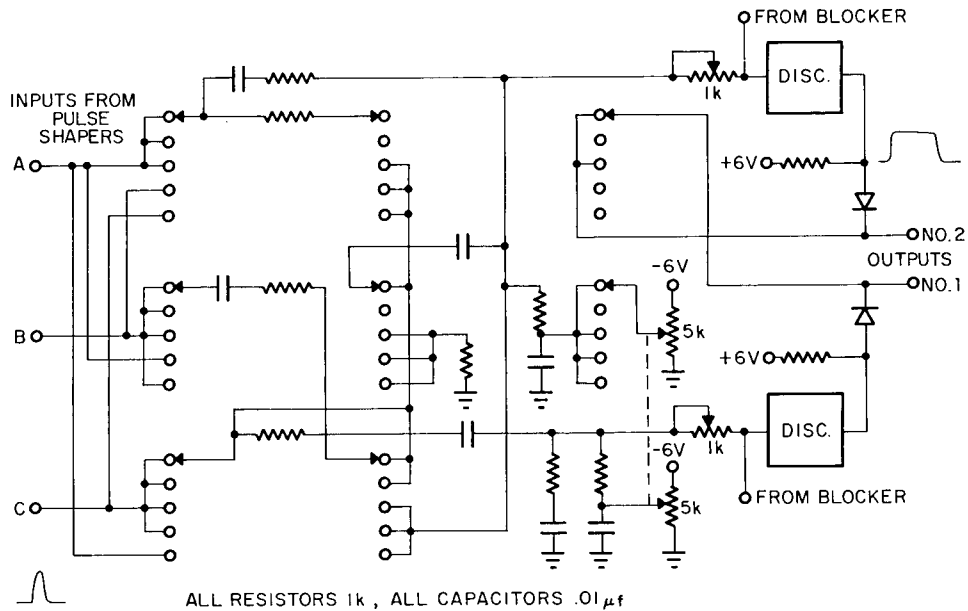
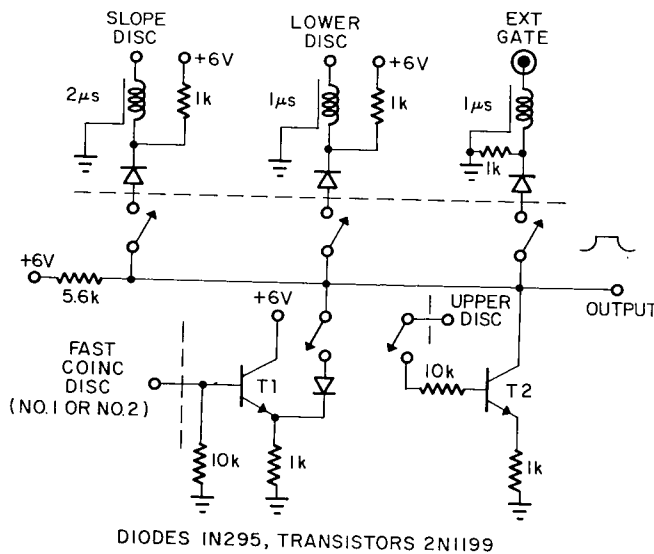


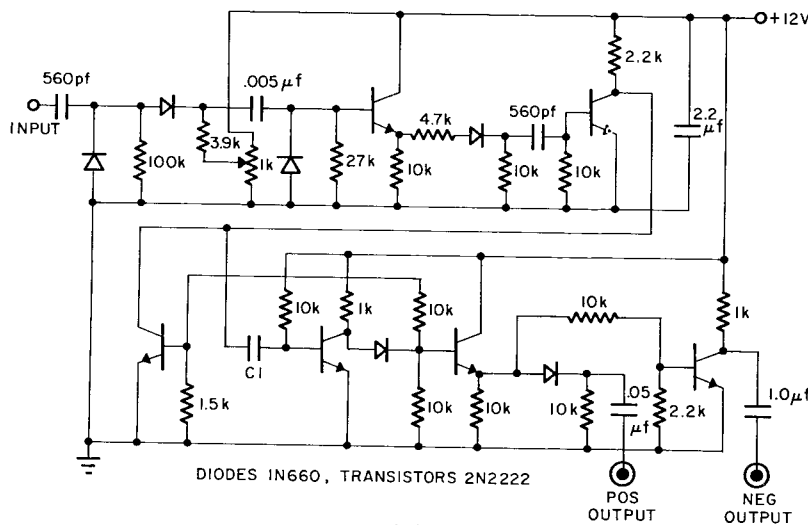
Fig. 21 - Element of the sum-coincidence circuit: the fast-coincidence circuit and switching arrangements

The switching arrangements shown in Fig. 21 allow the achievement of various coincident conditions among the three detectors as follows (in order from the top position of the switch): (a) ABC, a triple coincidence between all three detectors, the output appearing on both No. 1 and No. 2; (b) BC, a double coincidence between Det. 2 and Det. 3, appearing on output No. 1 only; (c) -BC, a double coincidence either between Det. 1 and Det. 3, appearing on output No. 1, or a double coincidence between Det. 1 and Det. 2, appearing on output No. 2, but no output produced for a double coincidence between Det. 2 and Det. 3; (d) -AB, and (e) -AC, cyclical permutations of (c), obtained by switching the input signals. The last two positions provide the arrangements used in the present experiment to allow either Det. 2 or Det. 3 of Fig. 16 to be the moving detector (see Sec. 2.3). This substitution also requires a switching of the input of the PHA from amplifier No. 2 to amplifier No. 3. This switching is accomplished by a circuit (not shown) consisting of three coaxial relays, which permits the selection of any of the three amplifiers for the input to the PHA and the appropriate termination of the two amplifier outputs not selected. The terminations each include a trim pot which allow the adjustment to match the $1\text{-k}\Omega$ impedance provided at the input of the PHA as required by the RG 65/U cable used to transmit and delay the signals to the PHA. The desirability of being able to select either of the detectors in the horizontal plane as the moving detector is discussed in Sec. 5.2.

Two slow-coincidence circuits are provided, each as shown in Fig. 22(a), allowing the switch selection of the various possible coincidence conditions by means of a separate toggle switch for each condition. Thus, the 6 V is dropped across the $5.6\text{k}\Omega$ resistor and the output point held near zero by the conduction of any of the selected diodes of the slope discriminator, lower discriminator, fast coincidence, or external gate. If all of the selected diodes are simultaneously back-biased by output pulses from each of these circuits, then the output point of the slow-coincidence circuit will rise to 6 V, provided that an output pulse from the upper discriminator, if selected, does not cause conduction of the transistor T2. The output of the slope, lower, and upper discriminators and external gate are common through separate switches to the two slow-coincidence circuits, but the two outputs from the fast-coincidence circuits are each routed to a separate slow-coincidence circuit. Because of the forward voltage drop of the diodes, back-biasing of some (but not



(a)

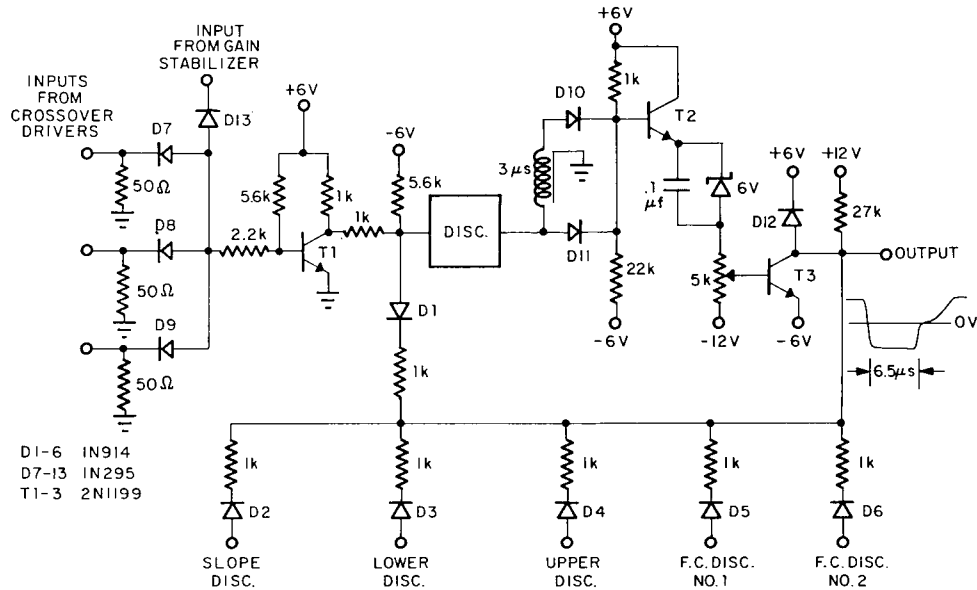


(b)

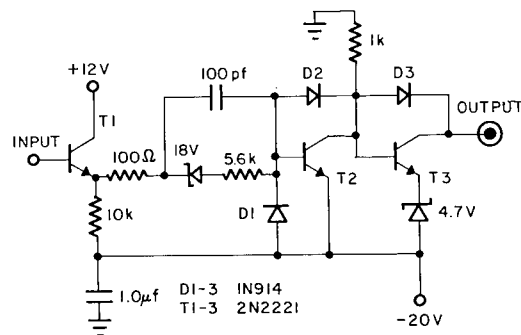
Fig. 22 - Elements of the sum-coincidence circuit: (a) the slow-coincidence circuit including selector toggle switches and (b) output driver circuit

all) selected diodes produces partial amplitude output pulses which must be discriminated against by the output driver by adjustment of the potentiometer near the input, as shown in Fig. 22(b). Each slow-coincidence circuit is provided with such an output driver to produce both the +10-V and -10-V pulses of appropriate lengths required by the gating and routing conditions of the RIDL 34-12B PHA. An "or" gate allows the gating of the analyzer when either output circuit fires.

The outputs of the crossover pickoff circuits associated with each amplifier, which are used to trigger the fast-coincidence circuits, also provide a convenient trigger for the



(a) The blocker circuit



(b) The live-timer driver circuit

Fig. 23 - Elements of the sum-coincidence circuit

blocker circuit for the sum-coincidence arrangement, shown in Fig. 23(a), in that they do not block the consideration of the event with which they are associated, because of the inherent (approx. $1 \mu\text{sec}$) delay in their generation by this event, and in that a trigger pulse occurs whenever a significant event is detected by the amplifiers, as the threshold level of the crossover pickoff circuits are set quite low (about 2 to 3 percent of the sum energy). The presence of a trigger pulse on any of the three inputs (or a trigger signal from the gain stabilizer circuit) is detected by the fixed level discriminator, and an output pulse of approximately a $3.5\text{-}\mu\text{sec}$ duration generated. Both the direct output and a version of the output delayed by $3.0 \mu\text{sec}$ are mixed and presented to the output transistor T3. The bias adjustment* afforded by the $5\text{-k}\Omega$ pot on the base of this transistor allow adjustment to permit the overlap of these two pulses to provide a single long

*Care should be taken in the adjustment of this bias to prevent biasing of the transistor into a steady conduction state, which will destroy the transistor.

pulse of the form shown. The output of the blocker system is applied through 1-kΩ resistors and high-quality diodes to the input of the discriminator circuits used in the amplitude-discrimination and fast-coincidence circuits. This output is also applied to the discriminator of the blocker system itself, thereby permitting recovery of the blocker discriminator during the last 3 μsec of the blocker output pulse. The shape of the trailing edge of the blocker output pulse, which changes slope as it crosses the zero voltage line, is designed to minimize the possibility of inducing small positive pulses at the input of the various discriminator circuits by capacitive coupling through the diodes.

The blocker system incorporated in the sum-coincidence circuits provides more positive action than one which would only prevent output pulses from the sum-coincidence circuit during the blocker time. This is because the positive blocking of the inputs in the present case provides the necessary recovery time for the univibrator outputs of the discriminator circuits as previously described. While the use of such a blocker is essential at high counting rates where a relatively larger number of events are apt to occur within the pertinent time interval, even at the somewhat lower rates encountered in the present experiment some events will occur within this time interval, and the rejection of the false gating conditions which can occur under such circumstances is desirable because the restrictions of the sum-coincident circuit are so severe that only a very small number of the input pulses are selected and the acceptance of even small numbers of false gating pulses could cause serious difficulties.

Because the sum coincidence circuit is positively locked out or "dead" during the time the blocker pulse is negative, this factor should be considered in the live-time measurement (see Sec. 4.1) when the PHA is used in a gated condition. To this end a signal corresponding to the dead time induced by the blocker is sent by low-impedance cable, RG 62/U, to the live-time circuits. A high current driver, shown in Fig. 23(b) has been provided to drive this cable. The signal to the live timer is passed through a gate which causes the interruption of the signal when the PHA is operated in an ungated condition as set by the master data control circuit.

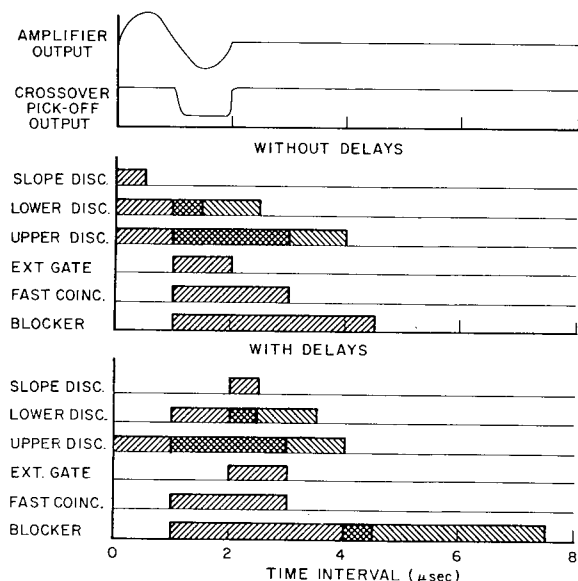


Fig. 24 - Timing diagram for the sum-coincidence circuit showing the pulse widths and delays provided to produce coincidence conditions between 2.0 and 2.5 μsec from the initiation of the event

The effective operation of the slow-coincidence circuits require that the output pulses from the various discriminator circuits be of appropriate widths and appropriately delayed such that any event truly meeting the conditions will cause all affected circuits to back-bias their diodes at the same time. The timing arrangements are shown in Fig. 24, where both the undelayed pulses and the delayed pulses are shown. Because the initiation of the output pulses from the upper and lower discriminators depend upon the setting of the discriminator level, allowance must be made for the range of delays which may occur. Possible extremes of this range are indicated in Fig. 24 by the left- and right-hand hatchings. Thus, although the slope discriminator will fire early because it depends upon the leading edge of the pulse, the upper and lower discriminators would fire later if set near the rounded top of the pulse from the amplifier, and a full microsecond has been allowed for this eventuality. The fast-coincidence and blocker signals, on the other hand, always appear approximately 1 μsec after the

initiation of the pulse at the time the amplifier pulse crosses over the base line. The external gate circuit which is designed to work with the single-channel pulse height analyzer of the N-328 amplifier also has an inherent delay of approximately $1 \mu\text{sec}$.

The widths of the pulses and the delays supplied for them are then determined for each coincident condition on the basis that if the condition is met, the circuit will produce, when delayed, a pulse occurring within the interval 2.0 to $2.5 \mu\text{sec}$ from time zero, corresponding to initiation of the event in the detector. Thus, the lower discriminator must be of a $1.5\text{-}\mu\text{sec}$ duration and delayed $1 \mu\text{sec}$ to cover the full range of possibilities. The slope discriminator, and the external gate are also appropriately delayed to bring them within the time interval, and the fast coincidence output is not further delayed but is provided with sufficient length to cover this interval. The time extent of these various signals determines the requirements for the upper discriminator, which, because it is in anticoincidence, must cover the full range within which any other pulse may occur. The length of $3 \mu\text{sec}$ is seen to be adequate to cover the extreme possibilities. The blocker signal meanwhile covers the region from 1 to $7.5 \mu\text{sec}$. It of course does not prevent an output for acceptable events occurring at time zero, since it only blocks the input of the discriminators at a time of $1 \mu\text{sec}$. It does, however, prevent the consideration of any pulse arriving between 1 and $7.5 \mu\text{sec}$ from the initiation of any significant event in any of the three detectors.

Most of the circuits elements described in this section have been developed on printed circuit boards, and the total sum-coincident circuitry is packaged in a single unit providing the switch and helipot controls on the front panel. Commercial power supplies in small modular units have been used to provide the voltages of ± 6 , ± 12 and -20 V required. All voltages should be well stabilized, particularly the -12 V required for the amplitude bias. In the present application the transistorized sum-coincidence and gain stabilizer circuits are separately placed in a thermally isolated part of the containing cabinet and provided with an independent air flow.

4.3 Gain-Stabilizer System

A block diagram of the gain stabilizer system is shown in Fig. 25. The main elements of the system (listed in the order in which they are discussed in this section) are: the light source; the mounting by which the light pulses are introduced into the photomultiplier; the electrical system for the pulsing and stabilization of the light source, including the stabilized power supply, flash driver unit, and source of trigger signals; and the stabilization system, which includes the tunnel-diode-discriminator arrangements and the stabilizer, which achieves regulation of the gain through the modification of the effective high voltage experienced by the photomultiplier.

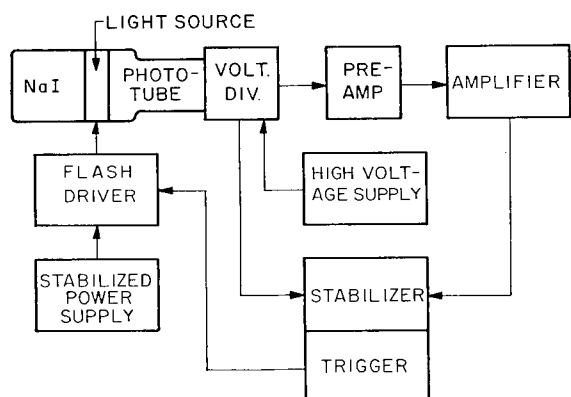


Fig. 25 - Main elements of the gain-stabilization system

The 6977 tube is an indicator tube designed for use with transistorized circuits. Packaged in a subminiature envelope, it consists of a filamentary cathode, a grid, and a helically wound plate coated with phosphor. Electrically, the tube is a triode and as such may be operated by control of either the grid (e.g., cutoff at -3 V, full conduction at zero volts) or by pulsing the plate from ground to a maximum of 50 V. The latter choice has been made in the present case, on the theory that the larger voltage may be regulated to greater relative precision than the smaller voltage required for the grid. The use of a higher voltage, however, could produce radiation of the electrical signal, particularly into the high-impedance system of the photomultiplier structure, and special care has been taken to shield against this possibility.

The phosphor of the 6977 tube is regrettably slower than that of NaI. Although this phosphor is listed as P-15, which should have a fast ultraviolet component, the ultraviolet radiation was not observed in tests in this Laboratory. Queries to the factory resulted in the information that the processing of this tube eliminates this property of the phosphor, it not having been thought necessary to maintain it for the expected use of the tube as an indicator in the visible region. Thus, two courses are possible: either pulsing with a sufficiently short pulse to simulate NaI radiation, or pulsing with a longer pulse and depending upon the clipping within the amplifier. The latter course has been chosen due largely to the difficulty in providing the necessary precision in the width of a short pulse, particularly since the inevitable and sometimes variable stray capacitances may affect the necessarily sharp rise and fall times of the electrical pulse.

Because of the space limitations within the Pb shielding in the present experiment, the light source has been introduced directly in a light pipe interposed between the scintillation crystal and the photomultiplier tube. Although this method has the disadvantages that the light source intercepts some of the light from the scintillator to the phototube (~ 7 percent) and that the additional interfaces and mismatched indices of reflection cause some loss of transmission, these effects are generally small, and it has otherwise been attempted in design of the light pipe to obtain optimum transmission of the scintillator signal in order to preserve the best resolution possible. The light output from the 6977 tube is directional and in the present arrangement has been directed toward the scintillator in order to diffuse the light signal and cause exposure of the whole photocathode rather than a limited area.

The light output level of the 6977 tube when pulsed to full amplitude is generally larger than that obtained from the NaI scintillator. In the present arrangement this level has been attenuated by the use of gelatin-based neutral-density filters rather than by a small aperture, because the plate of the tube is of questionable mechanical stability, and because motion across a small aperture would result in an apparent instability. In order to keep the electrical signal as near maximum as possible a filter has been fitted to each individual tube, since it has been observed that light output under maximum plate voltage may vary by a factor of two or better from tube to tube. It should be cautioned that before irrevocable decision is made on the amount of filter to be used, either the tubes should be allowed to stabilize under dark conditions or an appropriate safety factor allowed to account for the initial drift which has been observed in this application.

The light-source-mounting housing used in the present arrangement is shown in Fig. 26(a). The $3/8$ -in.-thick light pipe is beveled to accommodate the photocathode diameter ($\sim 2-5/8$ in.) and the larger diameter (~ 3 in.) of the glass window of the scintillation crystal mounting. An aluminum ring, whose O.D. corresponds to that of the flange of the crystal mounting, makes contact with the light pipe only at the edges and, when cemented to the light pipe, seals the greater portion of the area of the bevel such that this polished surface, backed by air, may provide total internal reflection. A $9/32$ -in.-diam hole projects radially into the light pipe to accommodate the 6977 tube. As indicated in Fig. 26(b), a shield, fabricated from 200-mesh nickel screen to form a cylinder about $1-1/4$ in. long with an O.D. allowing a slip fit inside the $9/32$ -in. diam-hole, clears

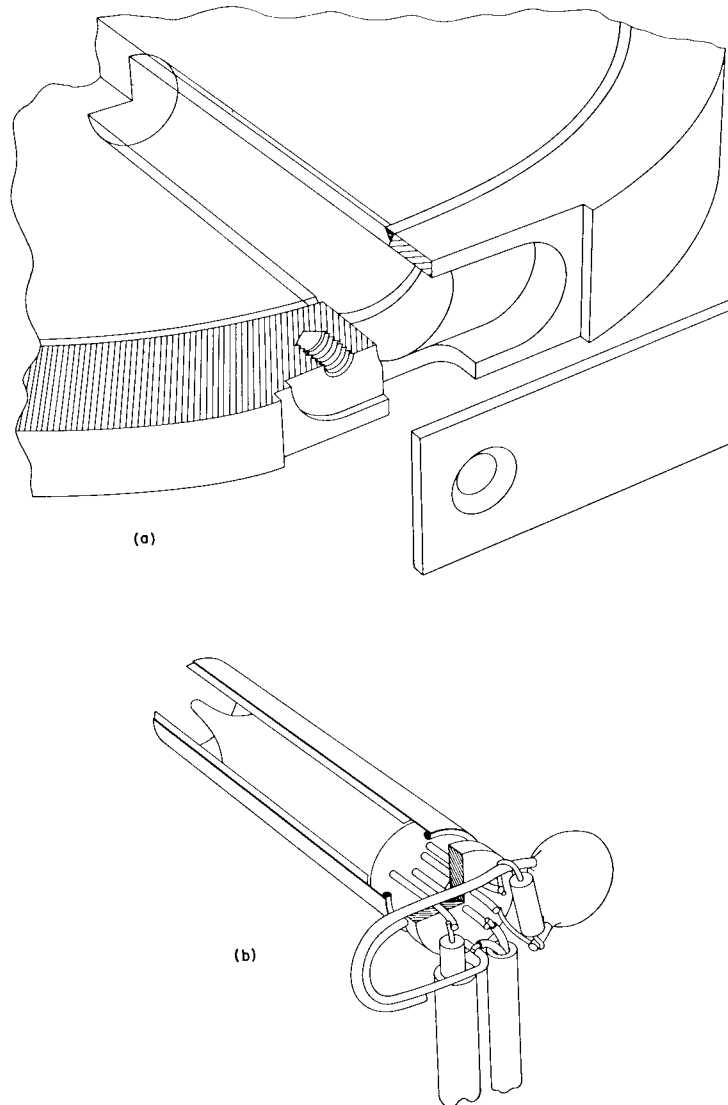


Fig. 26 - Cutaway perspective drawing showing (a) a portion of the Lucite light pipe and Al housing and (b) the light-source assembly

the body of the 6977 tube to allow insertion of the gelatin-base neutral-density filters, cut and rolled into a cylinder, between the tube and shield. A Teflon spacer, drilled to slip over the electrical leads of the tube and a ground lead from the shield, forms a plug which allows sealing off the cavity around the tube.

An outer cavity milled in the aluminum housing accommodates a $0.001\text{-}\mu\text{F}$ miniature disk capacitor and a $1/10\text{-W } 100\text{-k}\Omega$ resistor, which form the grid resistor and grid bypass capacitor of the tube. Microdot coaxial cable, type RG180/U, is used to conduct the plate pulses to the tube, and twin-lead shielded wire is used to conduct the filament voltage and ground to the housing. These cables enter the housing parallel to the axis of the phototube through a slot on the phototube side of the housing. With the leads of the tube clipped appropriately short, it is possible to make solder connection between the components,

these leads, and the incoming wires within the space allotted, as indicated in Fig. 26(b). The assembly is secured within the aluminum housing by a cover plate which provides, by means of a single screw, the pressure necessary to assure grounding of the aluminum housing. Once the appropriate filters have been fitted to the tube to provide a range of light pulses corresponding to the range of equivalent gamma-ray energies desired, the remaining space between the Teflon plug and the cover plate within the milled cavity is filled with epoxy resin, thus providing light tightness and further anchoring of the incoming cables. A drop of epoxy is also placed at the bottom of the hole in the light pipe in order to increase the mechanical stability of the tube-filter-shield assembly. The finished assembly provides a separate sealed unit which may be inserted between any mounted 3-in.-diam crystal and phototube and coupled to them by the usual arrangement of high-viscosity silicon fluid and black tape.

Because of the effect of stray capacitance upon the rise time of the plate pulse of the 6977 tube, an effort is made to keep the coaxial cable leading to this plate as short as possible. In the present application, where two of the scintillation crystals are contained within cylindrical 2-in.-thick-wall Pb shields, a back-slanted hole has been provided through this shield near the phototube to accommodate the cables for the plate pulse from the driving circuit which is placed immediately at the exit of this hole on the outside of the Pb shield. The boxes containing this circuit may be seen in Fig. 14. The flash driver circuit is shown in Fig. 27(a). Here, the positive trigger pulse described below is differentiated by the input capacitor and used to trigger the univibrator formed by the transistors T1 and T2, the width of the pulse being determined by C1 (a pulse of about 2.5- μ sec width is used in the present arrangement). The output of the univibrator drives the emitter follower, T3, into saturation, producing a constant-amplitude pulse of nearly 50 V (determined by the zener diode regulator) across the noninductive output potentiometer, R9. Adjustment of R9 allows the setting of the desired amplitude for the plate pulse for the 6977 tube. The dropping resistors, R6, R7, and R8, and the zener diodes should be placed so as to provide minimum thermal influence on the sensitive components T3 and R9. The 100 V dc at 40 mA required by each flash driver is supplied from a common power supply, which is a well-regulated commercial unit. As a commercial source for a 1-V supply was not found of the necessary stability for the filament of the 6977 tube, the regulator shown in Fig. 27(b), which itself requires well-regulated supplies of +12 and -12 V dc, has been used in the present arrangement. It should be noted that the transistors T1 and T2 and the zener diode D2 are temperature sensitive and should be placed in an environment of reasonable temperature stability. The unit shown was designed to provide 1 V dc at 90 mA adequate to supply each of three 6977 tubes with a 30-mA filament current.

In the present system of three stabilized detectors, provision against simultaneous firing or more than one 6977 tube has been made by supplying trigger signals to the flash driver circuits in a sequential fashion. This has been accomplished by driving a three-bit shift register shown in block diagram form in Fig. 28(a) with the oscillator circuit shown in 28(b). A single shift register unit is shown in 28(c). Depending on the length and type cable used between the shift register and the flash driver, it may be necessary to further attenuate the signal if the flash driver fires on other than the desired signal from the shift register. In the present three-unit system the oscillator works at approximately 3 kc/sec thus firing the pulsed light source of each detector at approximately a 1-kc/sec rate. The choice of 1 kc/sec is made between the conflicting requirements of a high pulse rate to provide a fast response time to the gain stabilization system and a low rate to provide minimum interference and dead time in the system due to the light pulses.

In the present arrangement it has been possible to prevent the sum-coincidence system from considering the photomultiplier pulses due to the light source by gating the blocker (see Sec. 4.2) of the sum-coincidence circuit by the trigger pulses from the oscillator of the gain stabilizer circuits. This arrangement makes it possible to take advantage of one of the principal benefits of using a pulsed light source rather than a random

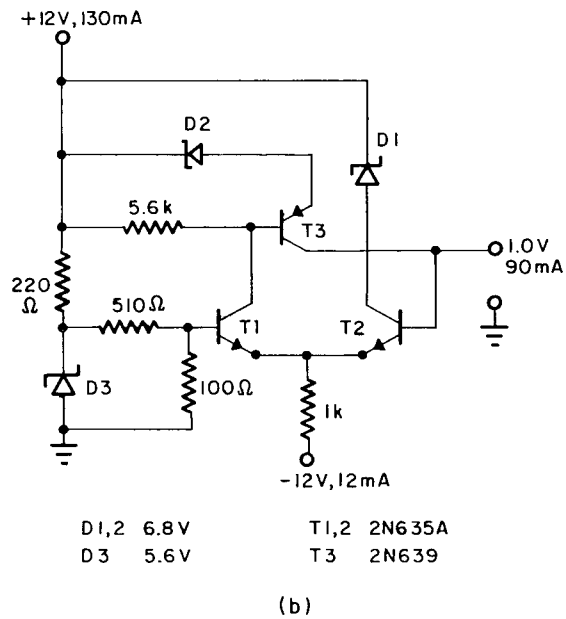
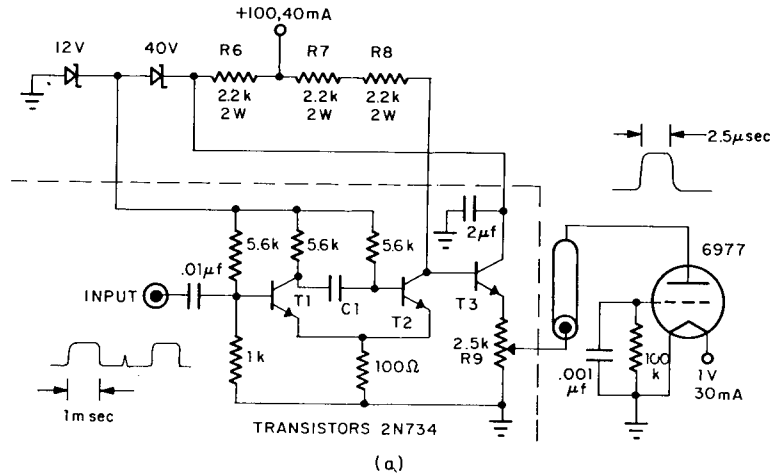


Fig. 27 - Elements of the gain-stabilizer circuit: (a) flash driver and light source and (b) the 1-V regulator to provide the current for the light-source filament

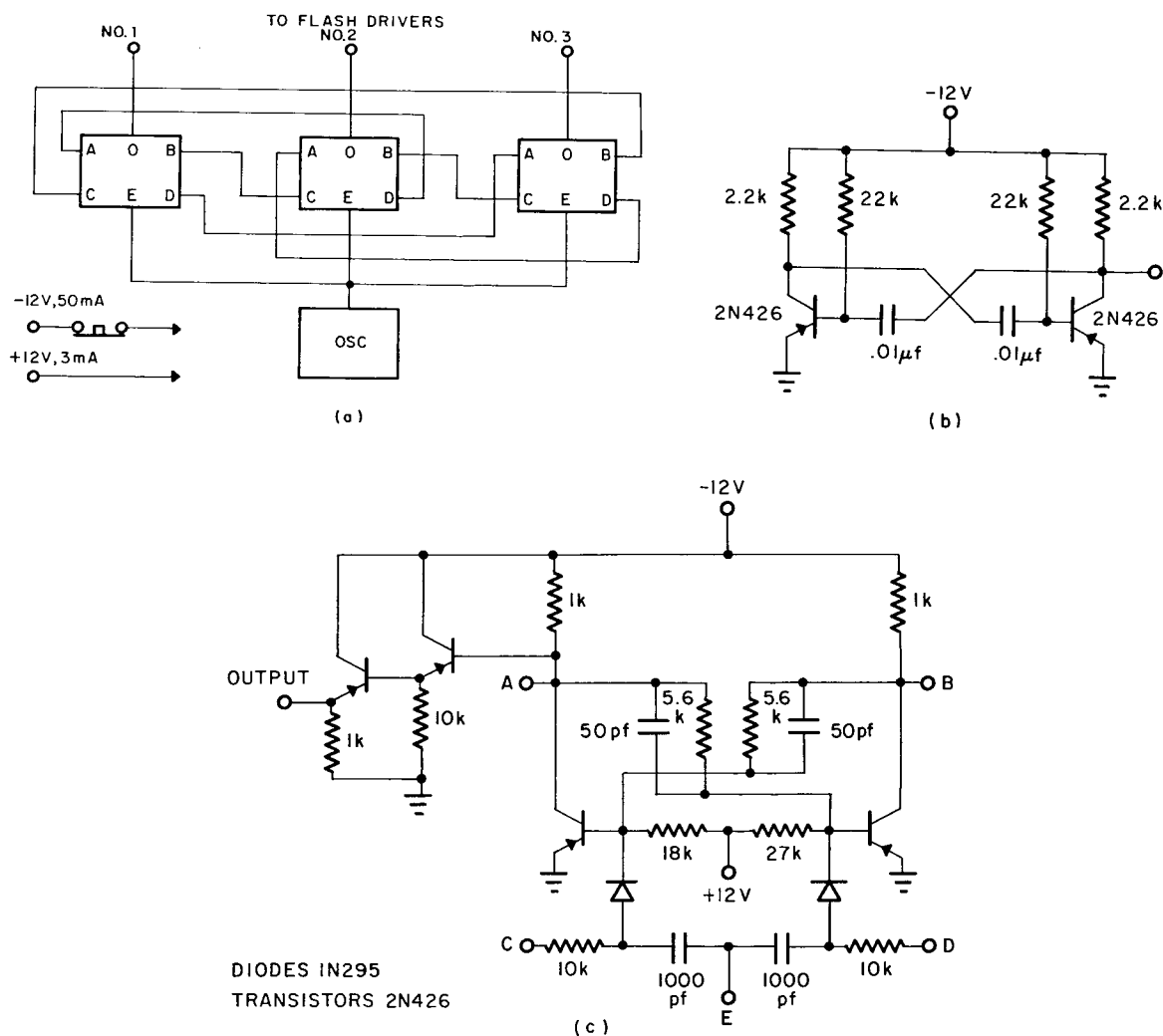


Fig. 28 - Elements of the gain-stabilizer circuit: (a) triggering circuits showing oscillator and shift register, (b) the oscillator circuit, and (c) a unit of the shift register

radiation source; namely, that the light source pulse occurs on command and that therefore the influence of the light pulse may be gated out of other circuitry when necessary. Likewise the oscillator or shift register signals could be used to gate on the discriminators of the gain stabilizer system if it were necessary to separate the light-source pulses from those due to background from a random source. Because the light source is adjusted to produce a peak which appears above all other peaks in the sum-coincidence spectra, the background on which the light peak is superimposed is negligible; therefore, no such gating is used in the present arrangement.

These light pulses produce a distribution of pulse heights from the detector system which is very highly Gaussian and of a width somewhat less than those produced by a gamma ray of equivalent energy in the NaI crystal, as expected. Because the light source does not produce pulses outside the Gaussian distribution, the light peak may be placed at any point within the spectrum without interfering with the spectrum outside its immediate area. In the present experiment the peak is placed near the top of the spectrum, where it provides the greatest sensitivity in the regulation in the gain of the system and where it is superimposed upon a small and constant background.

Because the stability of the system depends not only upon the stability of the light source but also upon the stability of the circuits which determine the centroid of the peak formed by the light pulses, a tunnel diode discrimination system has been provided in the present arrangement which results in excellent stability in the sensing of the centroid. The stabilizer discriminator circuit* used is shown in Fig. 29. This circuit includes three tunnel-diode discriminators which form two adjacent windows. The output pulse of the lower discriminator in each window is delayed and that of the upper discriminator lengthened such that the following anticoincidence circuit may determine whether the input pulse lay within the upper or lower of the two windows. The system shown works with positive pulses from a thermionic amplifier (maximum 100 V) and presents an input impedance of 10 k Ω . In the present system the current biasing of the tunnel diodes is achieved by a 10-turn helipot and three small trim pots. Some adjustment of the latter are necessary to preserve equal window widths when the helipot is changed; however, this inconvenience has been minimal in the present system, since the discriminator is nearly always placed at the same point near the top of the spectrum. Because the -12 V of the helipot is directly related to the discriminator's stability, this voltage should be well regulated. It also should be noted that this discriminator system may be set only for pulses in the upper half of the spectrum due to the properties of the tunnel diode and the circuits used.

The feedback of the discriminator system information to adjust the gain of the detector-amplifier system is achieved through the stabilizer shown in Fig. 29(e). This stabilizer consists of a bi-stable device, formed by the transistors T1 and T2, which stands by in the state into which it was driven by the last pulse received from one of the outputs of the discriminator circuit. Thus, when the discriminator system straddles the centroid of the pulse distribution from the light source, the bi-stable device will spend statistically equal times in its two states. A voltage level depending upon its state is passed through the emitter follower, T3, to the base of the regulating transistor, T4. When the regulation switch, S1, is appropriately placed, T4 is interposed between the photocathode of the photomultiplier and ground. The placement of the integrating capacitor, C1, allows the augmentation of this capacitance by the current gain of the transistor, thereby providing a suitably long time constant for the integration of the voltage level resulting from the state of the bi-stable device. Thus, in the previously mentioned case where the bi-stable device spends statistically equal times in the two states, the integrated current to the base of T4 remains steady at a preset level. If the centroid shifts, resulting in a statistically greater portion of the time being spent in one state of the bi-stable, the integrated current to the base of T4 will change accordingly, resulting in a change in the potential of the photocathode with respect to ground and therefore of the effective high voltage across the photomultiplier structure. In the present system, to provide an adequate range of correction the average working level of the photocathode has been set at approximately 25 V.

In order to prevent accidental isolation of the photocathode from ground by the interruption of the intervening wiring, a 50-V zener diode to ground has been installed directly in the phototube base circuit. The photocathode is normally connected by S1 to either a standard voltage of 25 V provided by a zener diode or to the regulating transistor. The voltage level above ground of the photocathode is also sensed by a 50- μ A meter in series with the resistances R11 and R12, the latter providing an adjustment to allow centering of the meter on the voltage provided by the \sim 25-V zener diode in the nonregulating position of S1. The setting of the current bias to the base of T4 is achieved through the adjustment of the potentiometer, which allows the level of the photocathode to be brought to the standard setting when the discriminator system straddles the centroid of the peak. With S1 in the regulation position the meter reads the photocathode potential, and once the gain of the system has been set to provide the standard voltage reading, deviations from this

*This circuit is similar to one used by K. Marlow in a gain-stabilizer system based for the most part upon the principles contained in the present report.

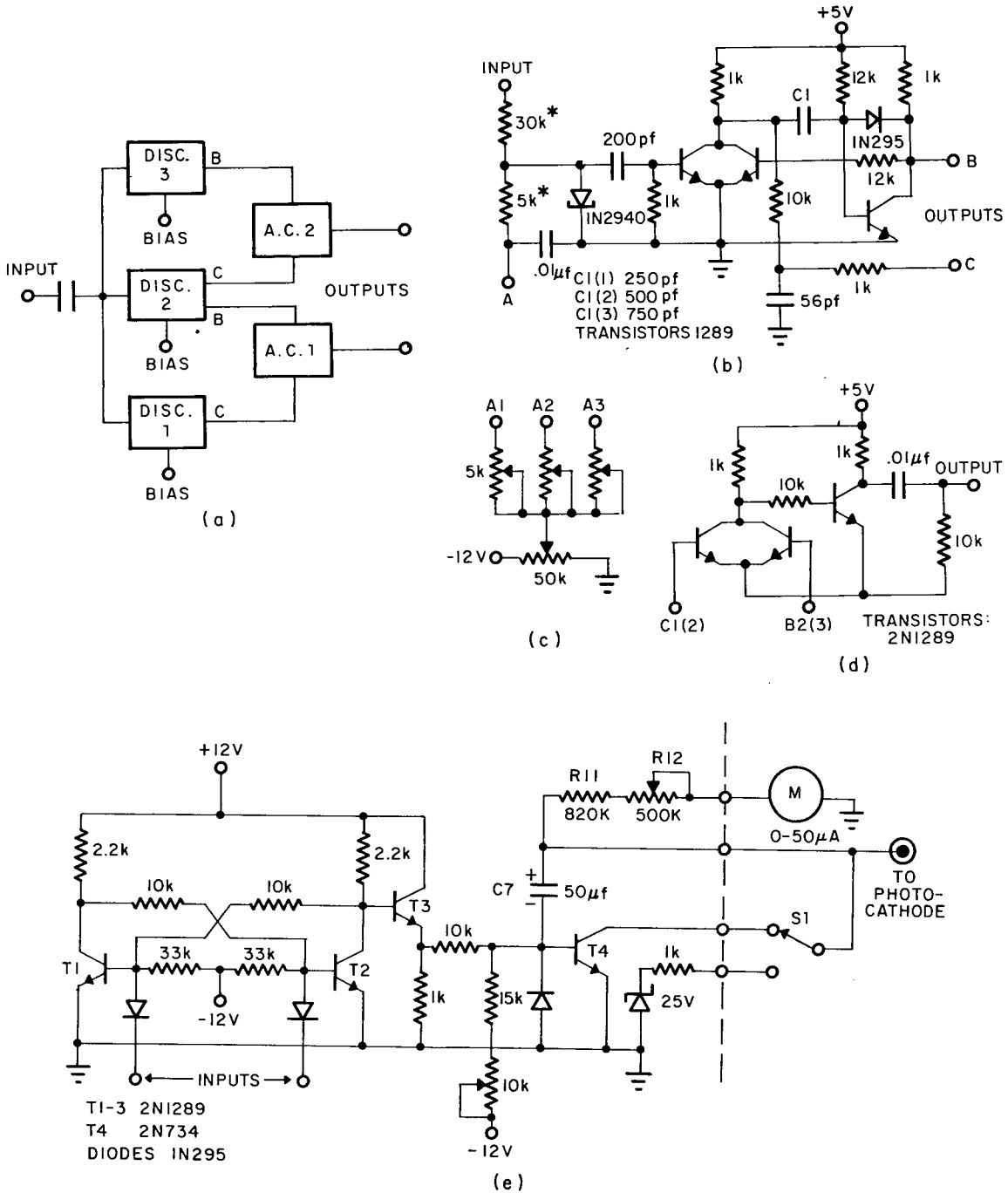


Fig. 29 - Elements of the gain-stabilizer circuit: (a) block diagram of the discriminator elements including: (b) the discriminator, univibrator, and delay elements, (c) the bias unit, and (d) the anticoincidence circuit (A.C.); and (e) the stabilizer circuit

reading represent the error signal necessary to correct the gain. This arrangement, therefore, supplies an indication of the correction being applied, and a means of determining when the system gain is properly adjusted to provide minimum error signal. In the present system, which utilizes printed circuit boards for all circuits, three discriminator-stabilizer systems are provided in one chassis along with the oscillator and shift register used to trigger the flash drivers. The meters for the error signal indication, the helipots for discriminator level adjustment, and "Regulation-Stand-By" switches, S1, are front panel located. The flash drivers are mounted near the detectors, as previously described, and the stabilized power supplies for the light-pulse system are mounted in a temperature stabilized environment not far from the detectors.

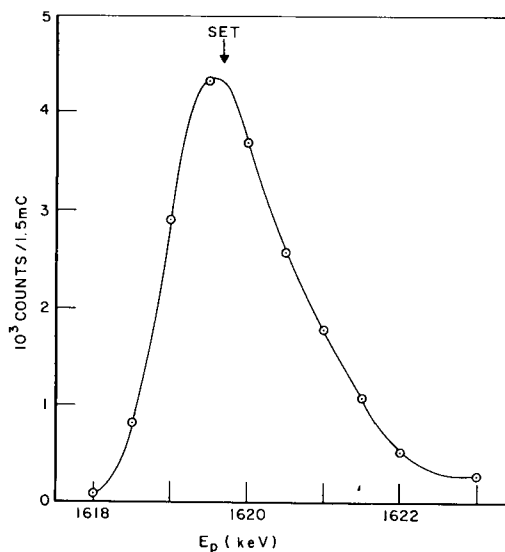
5. PROCEDURE AND DATA ANALYSIS

5.1 Alignment Procedures

The detectors and their associated collimators are aligned using the micrometer device appearing in Fig. 15. This device is positioned by and attached to the pin at the table center around which the detector carriages rotate (see Fig. 14a). The axis of a collimator is aligned with the center defined by the micrometer point using a device (not shown) which fits the front face of the collimators and defines the axis of the collimator by the aperture in the front face. The adjustment of the scale zero for the radial position indicator for each detector is set by means of a similar device which establishes the proper distance between the front face of the collimator and the center defined by the micrometer. Both the collimators themselves and the positioning devices have been machined with considerable precision which allows, even with the slight flexing of the supporting members of the correlation table under the weight of the shields, an alignment to within 0.015 in. in the positioning of the axis and to within 0.005 in. for the center-to-collimator-face distance. Although the aperture of the collimator is the chief element in the determination of the solid angle of the detectors, the source-to-crystal-face distance becomes a factor when (as in the present experiment) the efficiency of the detector for the absorption of the full energy of the gamma ray is important. The actual depth of the crystal behind the front face of the containing mounting is of course essential to this measurement and has been determined in the present case by a method described in Ref. 1, wherein a highly-plane-collimated source of gamma rays is used to define the crystal face with respect to the optically determined face of the container by observing the counting rate for photo-peak events from the crystal as it is translated on an axis normal to the plane of the incident gamma rays. The rather large front-face-of-container-to-front-face-of-crystal distance averages 0.85 cm for the detectors used in the present experiment. This distance is seen in Fig. 13, where the influence of the accompanying dead space upon the effectiveness of the shielding may be surmised. The positioning of the crystal container within the cylindrical cavity of the collimator is determined by the front face of this cavity and radial spacers (not shown). Little readjustment of the positions of collimators or detectors have been required in the present arrangements, although they are checked periodically.

The alignment of the beam with respect to the center of rotation of the detectors has been described in detail in Sec. 3.2. These procedures are performed at the beginning of each day on which correlation measurements are made. It should be emphasized that the beam is aligned with the beam finder under the identical conditions under which correlations are run with regard to the energy and intensity of the beam, such that (at least initially) the beam, as defined by its edges, is positioned with good accuracy. While the center of current density at the target may not initially coincide with the geometrical center, and while this center of current density may shift farther with respect to the geometrical center in the course of the day, the method of alignment used is not sensitive to these discrepancies; the method used defines the geometrical center with sufficient accuracy and stability that it has not been found desirable or necessary during measurements in the course of a day to redefine this geometrical center with the beam finding device.

Fig. 30 - A limited excitation curve over the 1620-keV resonance typical of those taken daily to locate the optimum settings for the proton energy



The exact setting of the ESA to provide maximum yield from the resonance under study is determined initially each day by running a limited excitation curve over the resonance, such as the one illustrated in Fig. 30, which is typical of the target thicknesses used at this resonance. The yield curves are determined by counting the number of monitor events (see below) which occur in the accumulation of a preset amount of charge on the target as a function of the proton energy setting of the ESA. Additionally, a measure of the monitor count rate is provided by an auxiliary linear count-rate meter. This meter is observed throughout the course of the experiment, and when (under constant current conditions) the meter indicates a decline in the yield from the maximum, the settings of the ESA are incremented plus and minus 0.5 keV to redefine the peak position of the resonance curve, and the settings are changed as necessary.

The various adjustments of the sum-coincidence and gain stabilizer circuits were described in Secs. 4.2 and 4.3. Most of these adjustments have required little resetting from the settings determined after the components had adequately aged. These settings are, however, periodically checked and readjusted where necessary, especially in instances where components or elements of the system have been replaced. The major attention in the daily checking of the system for the correlation runs is to the gain conditions of each of the detector systems and their relationship to the discriminators of the sum-gate. Such checking measurements are made with respect to the channel grid of the PHA. Long-term stability of the PHA is not required for this purpose, as the PHA is used only to determine the relationship of a peak position with the positions of the discriminator cutoffs. The use of the PHA for checking this relationship makes it necessary that the other discriminators of the system react identically to the pulses whether or not the amplified pulses are being viewed by the PHA. That is, because the PHA may view only one detector system at a time, the detector systems must present to the sum-coincidence and gain-stabilizer discriminators the same pulse height conditions when terminated as when they are viewed by the PHA. To assure this condition the trim pots of the terminating resistances are adjusted until switching between the PHA viewed position and the terminated position may be repeatedly accomplished without indication of correction on the error-signal-indicating meters of the gain stabilizer circuit. These adjustments are of course made for each of the three detectors, since the gain and sum conditions are checked for each detector sequentially by the PHA.

The long-term stability of the base line and the conversion gain of the PHA over the course of a working day is of course desirable to prevent shifts in the peak positions which would interfere with the summing of the data, although lack of long-term stability

will not cause the distortions of the sum-coincidence spectra which arise only for detector system gain shifts with respect to the sum-condition discriminators. Shifts of the conversion gain of the PHA from day to day are of no consequence, as they are compensated for by the daily adjustments of system gain, but base-line shifts from day to day may cause difficulty in summing the data, particularly for the lower energy peaks. This effect is not as important for higher energy peaks, since the gain adjustments compensate for the base-line shifts in proportion to the closeness of the peak position to the position of the sum gate. Although the 100-channel PHA used previously provided some difficulty in base-line stability, the RIDL 34-12B PHA used now shows a stability of this quantity nearly comparable to the system gain stability and thus has proved satisfactory for the present purposes.

To expedite the daily setting of the system gain conditions for each detector with respect to the PHA, a relatively strong PoBe source (polonium-beryllium, chiefly a neutron source but also providing a high-energy gamma ray of 4.43 MeV) is used to reset the discriminator current biases of the gain stabilizer circuits such as to place the total capture peak from the PoBe spectrum in the same predetermined channel of the PHA for each detector. The source is of sufficient strength that deviations from the desired setting by 1/2 channel or more may be determined from the live display within a few seconds, and sufficient statistics to define the peak position to approximately 0.2 channel may be obtained in 1 or 2 minutes. Thus, if, as is usually the case, no serious shifts in gain have occurred for any of the three detectors from the time of the previous setting, the gain of the detectors may be brought into acceptable agreement with the predetermined values in 15 or 20 minutes, when these checking and adjustment procedures are being conducted concurrently with other startup procedures.

After the beam has been aligned on target and the proton energy setting determined, the gain conditions for each detector are checked under operating conditions of the beam on target. In this case the total capture peak for the transition from the capturing level to the ground state is used if it is sufficiently strong to obtain reasonable statistics in approximately 5 minutes. This peak-strength condition has been met in all cases in the present experiment, but instances have been found in experiments with other nuclides where it is necessary to use other peaks, such as those associated with the transitions to the first excited state. Because the ground state transition represents the excitation energy of the capturing level for which the sum gate is set, it is most convenient to use this peak when possible.

For each of the three detectors two 200-channel spectra are obtained: one ungated in order to display the gain and base-line conditions and the other gated by only the (toggle-switch-selected) upper and lower discriminator conditions in order to determine the position of the sum gate with respect to the total capture peak. If the gain condition as represented by this peak position does not agree within a limit (usually 1/2 channel) of a predetermined value, readjustment of the gain stabilizers is made and the measurement repeated. Early in the use of the present experimental arrangement, these checking runs were repeated at the conclusion of the correlation measurements each day. However, this latter practice has been discontinued, as it has been found that any significant gain changes that might occur are reflected by shifts* in the positions of the peaks of the sum-coincidence spectra for the detector system involved. In fact it is customary now to check the positions of the two strongest peaks in each spectrum by means of the oscilloscope display before readout. Thus, in the rare instances where a shift has occurred it is detected immediately, the situation corrected, and the run repeated.

The trim pots which determine the position of the discriminators for the sum gate for each detector seldom require readjustment, but such adjustments are made on the basis

*Shifts are observed even when they occur only in one of the fixed detectors (only the moving detector is observed by the PHA), as such shifts distort the sum condition and result in peak displacements in the observed spectrum.

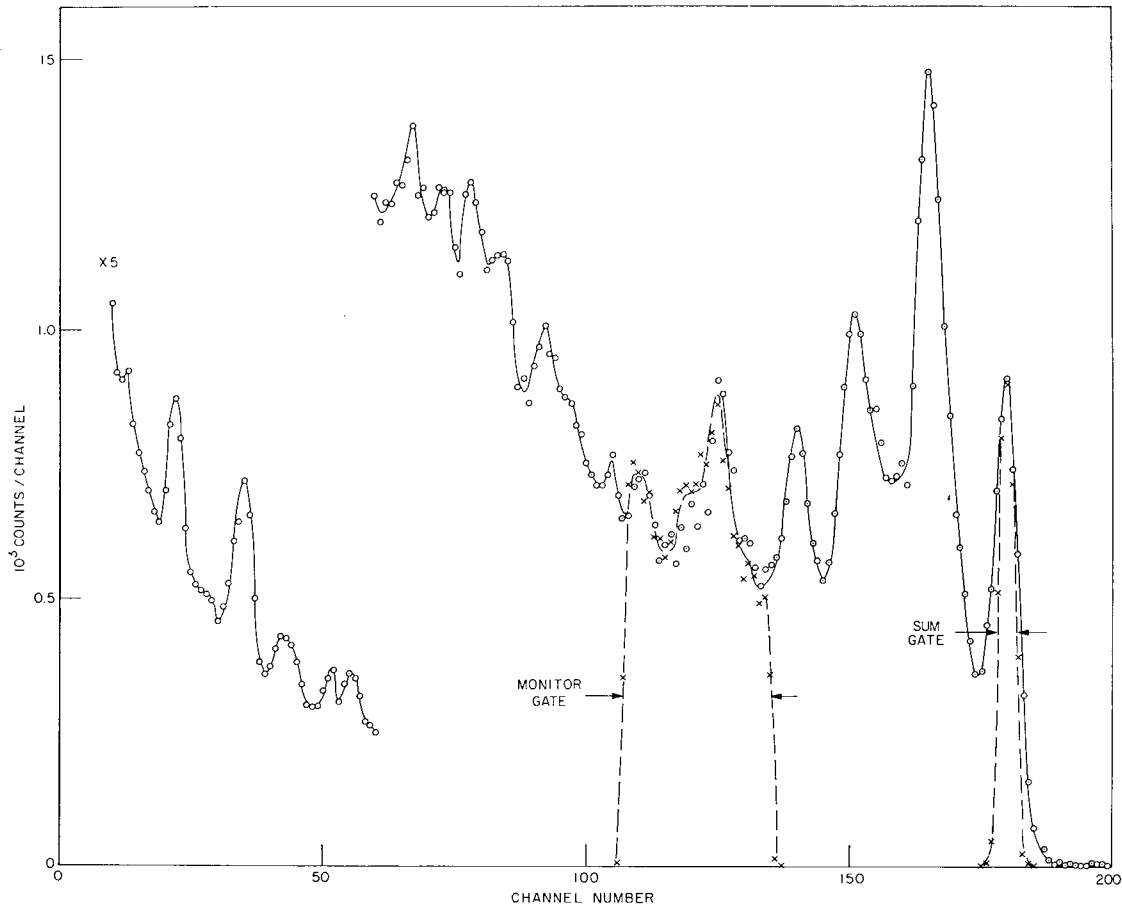


Fig. 31 - A typical ungated spectrum (circles) and gated spectra (x's) for the sum gate and monitor gate as obtained daily for each detector (except monitor gate) to check the gain and base-line conditions and the gate settings

of the preliminary checking runs when it is found that the widths of the gates for the three detectors differ or when the positions have shifted with respect to standard conditions. An example of the spectra resulting from these checking runs is shown in Fig. 31, where the ungated and sum-condition gated spectra are shown. Also shown is the monitor gate (discussed below), which is checked only periodically, as its position is less critical than the sum gate.

The timing arrangements of the fast-coincidence circuit are also checked daily by standard delay-curve techniques. Two such delay curves are run simultaneously by varying the delay in one line of the coincidence circuit with the variable delays described in Sec. 4.2. For these curves the toggle switches of the sum-coincidence circuit are set to allow monitoring of the fast-coincidence events with the crossover-condition-selector switch in the -AC position (the variable delay is associated with Det. 2, that is, in the B timing circuit). If the two curves are found to be in reasonable agreement, the variable delay is set to correspond to the middle of the curves. If the two curves are displaced, small adjustments of the delay are made by means of the discriminator trim pot of the pulse forming circuits (see Sec. 4.2) to bring the curves into conjunction. An example of this measurement is shown in Fig. 32, where it is seen that a flat top to the delay curve of at least 20 nsec is provided to allow for small shifts in the delay and primarily to accommodate the residual walk of the trigger pulses from the crossover pickoff circuit. It should be noted that the delay curves are determined with the coincident radiation from the target

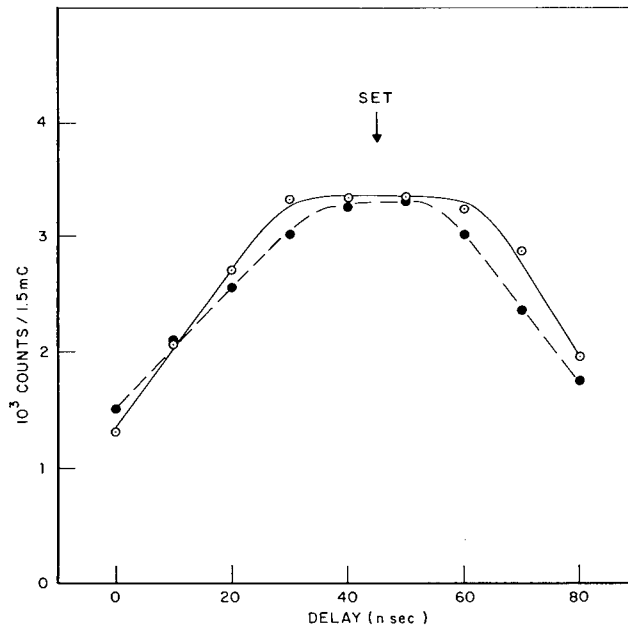


Fig. 32 - Typical delay curves for the fast-coincidence circuit obtained daily by varying the delay in one element of the fast-coincidence circuit

under bombardment and not from some radioactive source, the use of which could lead to small mis-setting of the delay conditions, because the gamma-ray energies from the source would differ so greatly from those of the reaction.

It has been found with the present arrangement that the crossover pickoff circuits provide unusual stability, seldom shifting as much as even 3 to 5 nsec in any measurement from the average maintained over extended periods of time. The positions of the thresholds for the crossover pickoff circuits have also shown good stability with time after initial aging. The initial setting of this threshold level may depend on the nuclide under study, as the threshold must be set below a pulse-height equivalent to the lowest energy gamma ray which will appear in the sum-coincidence spectra. This energy is almost always that of the first excited state due to the properties of gamma emission and the sum-coincidence method as discussed in Sec. 6.1. In the present experiment the first excited state of ^{61}Cu is known to be at 0.47 MeV, and the threshold levels in the present arrangement have been set at approximately 0.2 MeV equivalent. Any change of the threshold requires readjustment of the hysteresis control of the pickoff circuit. For this purpose a pulser and attenuator are used in conjunction with a fast oscilloscope to determine settings appropriate to produce the desired threshold level and minimum walk of the trigger pulses over the full range of pulse heights.

5.2 Correlation Measurement Procedures

An important consideration in any correlation measurement in which determinations of the yield at different angles are made nonsimultaneously is the problem of normalizing the yield at the various angles to the same criterion. One such criterion sometimes used is the number of protons striking the target as determined by the integrated beam current at the target. This criterion, however, requires greater stability of the surface layer of target materials and of the proton-beam energy than are available with the conditions

required by the present experiment. More satisfactory in the present case is the direct measurement of the reaction yield as obtained from counting the output of a monitor gate placed over a suitable portion of the high-energy region of the pulse-height spectrum of a fixed-position detector.

Positioning such a monitor detector in the present arrangement is a difficult problem in that virtually all the space surrounding the target is occupied at one time or another by one of the three detectors, the target chamber, or the supporting table. Although it would be desirable to use a detector less dependent upon beam position, it thus becomes necessary to additionally utilize one of these detectors as a monitor, the one normal to the horizontal plane being chosen for this purpose as it is the only one of the three detectors which remains fixed in position throughout. The use of one of the gain stabilized detectors does, however, minimize a common difficulty in correlation monitoring arrangement, that is, the problem of gain shifts with respect to the discriminator levels of the monitor gate. This difficulty is further minimized by the choice of the position of the discriminators in the spectrum such that any shifts that occur are apt to add as many counts on one end of the gate as are taken away on the other end. The position chosen for the monitor gate for one of the resonances used in the present experiment is shown in Fig. 31.

Because the single-channel pulse-height analyzer which forms the monitor gate provides essentially negligible dead time, the counts accumulated from the gate represent the reaction yield in the total time interval, whereas the fraction of such events which represent the actual live-time interval may vary with the live-time interval, which itself changes with the position of the detector, beam intensity, and target condition. Accordingly, the monitor counts are corrected by the ratio of the live-time interval to the true (total) time interval for each run, where the live-time measurement properly takes into account the dead time of the sum-coincidence circuit as well as that of the PHA (as described in Sec. 4.2). The yield from the reactions studied in the region covered by the monitor gate is generally sufficiently greater than the background yield in this region as to make the background contribution negligible in most cases. A determination of this quantity is afforded by the limited excitation curve (see Sec. 5.1) or the "off-resonance" measurements (see below), where the yields of the monitor gate on and off resonance are obtained and correction for the off-resonance background (in terms of beam charge accumulated) is made to the monitor count if necessary.

The reaction yield as represented by the monitor counts is used to normalize the various runs that form the correlation measurement on a given day. However, when data obtained on different days must be utilized together, the slow drifts which may have occurred from day to day in the width of both the monitor gate and sum gate may introduce unnecessary error. Accordingly the sum of the routing pulses associated with a given geometry set for all the appropriate runs on a given day are used in normalizing the results of one or more days to the same standard. The number of such events for each run are determined by counting the number of routing pulses associated with that particular geometry set. This latter normalization factor, which applies to all runs for a given set on a given day, of course contains no angular dependence, since the factor is determined from the sum of runs at different angles.

In the measurement of the correlations, the three-angle approach recently reported by Reich, Merrill, and Klema (8) has been used. That report deals with the analysis of directional correlation data which may be represented in the normalized Legendre expansion used with the present data. It is shown in that report that measurement at three particular angles, with additional weighting (a greater number of observations) for the center angle, produces an enhanced statistical precision. These authors emphasize the distinctions between statistical precision, which is independent of the values of the expansion coefficients and depends only upon statistical factors, and accuracy, which depends in addition on systematic errors; and they point out that the more common equal-angle

approach may frequently better serve the interest of the latter in the revelation of certain types of systematic error, such as alignment errors. In the present experiment, however, the three-angle approach, with slight modification, provides better control of the chief source of systematic error present, that is, the uncertainty in the position of the center of current density at the target. Thus, because the position of this center (see Sec. 3.2) may be significantly displaced from the center of the system only in the plane of the target (normal to the beam direction), a measurement of the anisotropy thus introduced and an approximate canceling of the effect is best made by repeated measurements at a small number of angles, if pairs of angles are observed to both sides of the beam axis.

Therefore, in the procedure used in the present experiment, a large number of shorter runs, each for an equal number* of monitor counts, are made, distributed among the three angles such that half of these at each angle are obtained with the fixed detector (in the horizontal plane) to one side and the other half to the other side. A fourteen-run sequence is used, distributed two, three, and two to each side at the angles 0, 43.6, and 90 degrees, respectively. The sequence is systematically arranged, as indicated in Table 2, so that any slow drifts in condition are apt to be distributed properly among the angles.

It should be noted that the system is not symmetrical in the vertical plane, as it is in the horizontal plane (that is, a detector may be placed on the vertical axis only above the target, not below it), and vertical displacements of the beam are not compensated for by the three-angle technique. However, because the monitor counts will have the same dependence upon the vertical position of the center of current density at the target as the geometry set (C and D) involving the vertical detector, the vertical displacements of the center are compensated in these geometries, but not for the geometry set (A and B) involving only the detectors in the horizontal plane. In the latter case these horizontally compensated observations may be distorted by the fluctuations in the monitor counts due to vertical displacements of the center which are not similarly reflected in the horizontal detectors.

Various possible sources of background in the sum-coincidence arrangement have been investigated. However, the amplitude and timing conditions imposed by this arrangement are so stringent that most of the usual background factors of ordinary measurements become completely negligible. One background source which was found to be of nonnegligible proportions is the occurrence of accidental time coincidences. These arise chiefly from the large numbers of small pulses corresponding mainly to low-energy gamma rays (Coulomb excitation) and X-rays from the target backing. Such low-energy events may meet the requirement of the sum condition when these events accidentally add to a pulse corresponding to a somewhat less than full-sum-energy event in the other detector.

In the sum-coincidence arrangement there are actually two resolving times involved: the usual fast-coincidence resolving time, determined by the width of the shaped pulses and the bias level of the discriminator, and a longer resolving time, corresponding to the fact that two pulses must occur within a certain period (1 to 1.5 μ sec) in order for the positive portions of the pulse (see Fig. 17(b) for pulse shape) to add. This latter factor becomes important in the choice of the delays used in the experimental determination of the accidental spectra. Thus, while the delay arrangements must be sufficiently distorted that no events truly in fast time coincidence may be recorded, the delays must not be distorted by too great an amount or the amplitude restrictions will no longer resemble those which actually pertain in the "true plus accidental" case. Accordingly, for the experimental measurement of the "accidental only" spectra, the delays were displaced by 200 nsec, added to one line, subtracted from a second line, and the third line remaining the

*Identically equal numbers are not required, as differences may be accommodated in the normalization. However, approximately equal runs are needed to provide the weighting requirements of the three-angle approach; accordingly the monitor count scaler is frequently used as the basis for presetting the counting intervals.

Table 2
Sequence of Experimental Configurations Used in the Determination
of the Triple Correlations of the Present Experiment

For each counting interval (run) the positions of the two detectors in the horizontal plane are listed in terms of the angle θ with respect to the beam axis, where the angle is positive in the sense of clockwise rotation as viewed from above. The number of the detector viewed by the PHA and the setting of the coincidence condition switch are also indicated, where the A, B, and C refer to the timing circuits associated with detectors 1, 2, and 3, respectively, and where the notation -AB indicates that the coincidence circuits will not accept double coincidences between the A and B circuits but will accept double coincidences between the two remaining permutations and will route the storage of the information accordingly.

Run No.	θ_2 (deg)	θ_3 (deg)	Detector No.	Coincident Condition
1	-90	0	3	-AB
2	-43.6	90	2	-AC
3	-90	90	2	-AC
4	-90	43.6	3	-AB
5	0	90	2	-AC
6	-43.6	90	2	-AC
7	-90	90	3	-AB
8	-90	43.6	3	-AB
9	-90	0	3	-AB
10	-43.6	90	2	-AC
11	-90	90	2	-AC
12	0	90	2	-AC
13	-90	43.6	3	-AB
14	-90	90	3	-AB

same. Even so, this arrangement results in a separation of the delays for two of the detectors of 400 nsec, which is uncomfortably large; however, examination of the data show no significant differences between the spectra from detectors whose delays were displaced by 400 and those by 200 nsec except that some pulses normally excluded by the threshold were apparently allowed in the 400-nsec displacement. These events lie outside the normal sum-coincidence pulse distributions and do not otherwise affect the measurement. To evaluate the accidental time coincidences, sum-coincidence spectra under otherwise normal conditions were run for one full day of correlations measurements with the delays distorted as above. The results are shown in Fig. 33, where the spectrum shown is the sum over all angles and geometries for the full day of correlation measurements. A spectrum obtained under normal sum-coincidence conditions is shown for comparison. It is seen that the accidental spectrum is significant largely only at the extreme low and high energy ends of the spectrum, as expected from the source, described above. In this situation, which is for the 1620-keV resonance, it was necessary to correct for the accidentals only for the lowest and highest peaks of the spectrum, corresponding respectively to the secondary and primary members of the cascade through the 0.47-MeV first-excited state. The corrections which were applied for these peaks to each

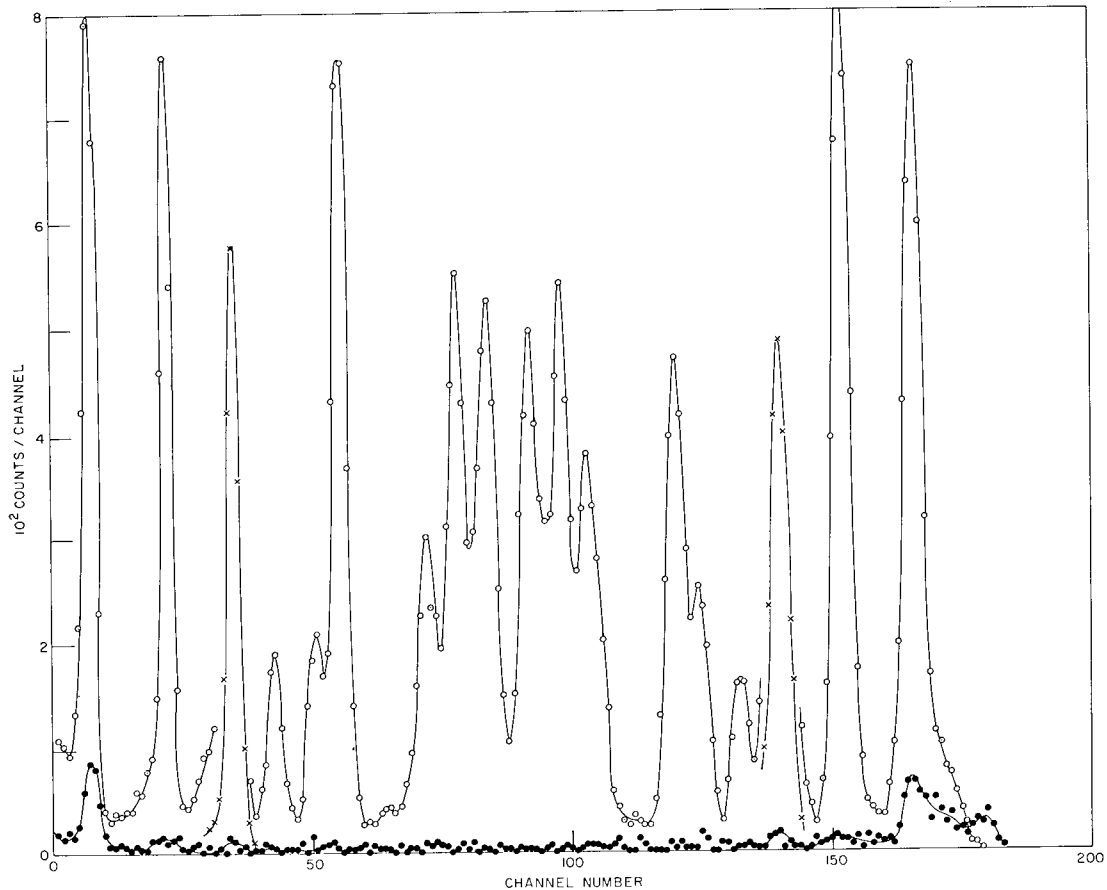


Fig. 33 - A normal sum-coincidence spectrum (open circles) and an "accidental only" spectrum (closed circles) obtained under identical conditions except that the timing was distorted to prevent acceptance of "true" fast coincidences. The spectra are normalized to approximately the same yield. The counts in the accidental spectrum appearing above the highest peak of the normal spectrum are spurious and arise from the timing distortions. The scale should be multiplied by a factor of 4 for the points marked by x's.

of the normal sum-coincidence measurements were determined from separate sums of the data for each of the six angle-and-geometry combinations.

A second source of sum-coincidence background which was found to be not quite negligible in some cases is the effect of the next-lowest-energy resonance from the Ni reaction. This effect depends upon the target thickness relative to the spacing of the resonances and upon the relative intensities of the resonances. The effect is not to be confused with coherent interference of the levels, which is negligible in this case because of the extreme narrowness of the natural width of the capturing level (see Sec. 1.3 and Ref. 1). At only the 1620-keV resonance was correction attempted for the effect of the 13-keV-lower, and nearly equally intense, resonance at 1607 keV (listed as 1605 keV in Ref. 1). For each target that was run at the 1620-keV resonance, the amount of contribution from a resonance 13 keV lower in energy was evaluated to allow correction for the different correlations observed at that resonance. For the 1620-keV resonance the next highest energy resonance is located with a separation of 18 keV, thereby allowing an evaluation of the effect of a 13-keV-lower resonance by off-resonance measurements at 1633 keV. Typical

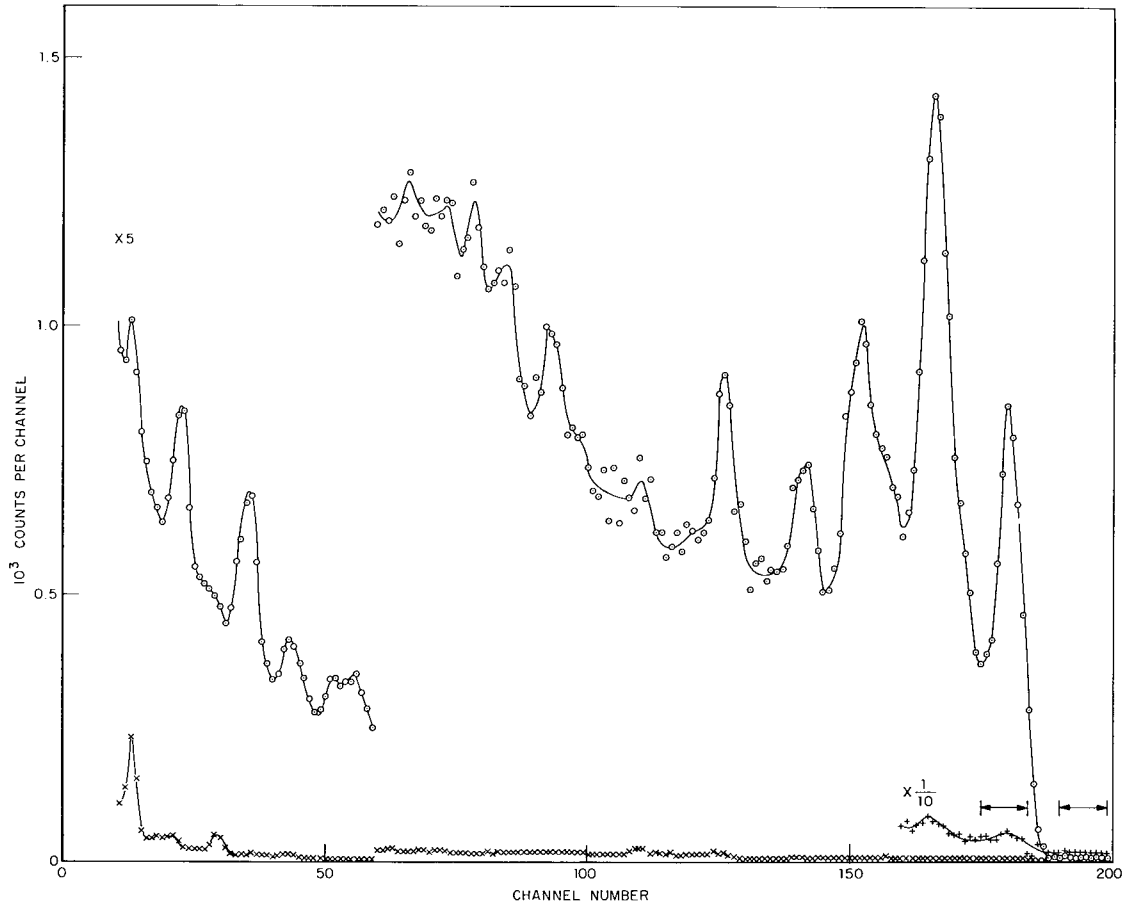


Fig. 34 - Ungated spectra obtained on resonance at 1620 keV (circles) and off resonance at 1633 keV (x's) normalized to the same number of incident protons (total beam charge accumulated). The off-resonance curve is also shown to a factor of 10 expanded scale (crosses) for some of the upper channels. Arrows indicate the two groups of channels used in evaluation of the amount of reaction due the next-lowest-energy resonance.

examples of on- and off-resonance spectra obtained at 1620 and 1633 keV, respectively, are shown in Fig. 34, where the results from the longer runs made off resonance have been normalized to the on-resonance results in terms of accumulated beam charge. Here the channels near the total capture peak for the ground state transition obtained at the higher energy are also shown to an expanded scale. The number of counts near this peak (the sum of the counts in the indicated channels) are used to determine a normalization factor for this correction for the measurements of each day. Correction for the background under the peak from other sources was necessary only for the off-resonance measurements at 1633 keV. This correction was accomplished by subtraction of the counts from an equal number of channels above the pulse-height distribution due to the Ni, as shown by the higher of the two indicated regions in Fig. 34. Correlation measurements were then run for one day only at the 1607-keV resonance, and this data, summed for the six angle-and-geometry combinations and normalized by the appropriate factors determined as described above, was used to correct the results for individual days of normal correlation measurements.

Nonresonant high-energy gamma-ray effects, due to reactions induced by the incident beam with system contaminants, and formerly a problem in these measurements, have

been measured and found to be reduced to negligible proportions by the cold-tube and target-backing-etching procedures (described in Sec. 3.2). In addition, the magnitude of the possible effects of the detection of all members of a three-part cascade were also evaluated by requiring a triple sum-coincidence for events in the three detectors. Conditions for detection of triple coincidences were met with the crossover-condition-selector switch of the sum-coincidence circuit in the ABC position (see Sec. 4.2) and with the resolution helipot set to discriminate against double coincidences. That the arrangement properly detected triple coincidences was checked with a ^{22}Na source with the two detectors in the horizontal plane each set at $\theta = \pm 90$ degrees. Thus, due to the positive 180-degree correlation of the two annihilation quanta, the spectrum of the vertical detector was purely that of the 1.27-MeV gamma ray, while those of the horizontal detectors were each the spectrum of the annihilation radiation only.

Of course, the spectra obtained in the correlation measurements of a single day for the Ni reaction under the triple-coincidence conditions do not directly represent those results which would be obtained for three-part cascades under the normal double-coincidence conditions, which require for the detection of triple coincidences that two of the three events occur in one or the other of the detectors. Fortunately, however, it was found that the triple-coincidence events are sufficiently infrequent in the present arrangement as to be relatively negligible and to require no correction. This result was not unexpected, because triple coincidences, whether occurring in either two or three detectors, involve an additional efficiency term. This efficiency term (including solid angle) varies in the present arrangement of the detectors from about 0.02 to 0.005, depending upon the energy of the gamma ray.

None of the background effects evaluated above provide an explanation for any background between the sum-coincidence peaks, at least at other than the extremes of the spectra; yet the existence of such a background is indicated by both a filling of the valleys between the peaks and a broadening of the less intense peaks as observed in statistically significant sums of sum-coincidence spectra. The origin of this background remains undetermined, although it may in part be due to weaker unresolved transitions or to instrumental errors such as false gating conditions. Whatever the cause, the correction for this background becomes an important factor when the analysis of peaks corresponding to some of the weaker two-part cascades is considered. It has been found that if a constant background is assumed and determined from those points in the spectrum representing the bottom of the valleys, then the subtraction of such a background from the weak peaks results in the observation of reasonable widths for these peaks comparable to the widths observed for the stronger peaks where the background subtraction is a negligible factor. Thus, at least to a first approximation, the subtraction of a constant background appears to be justified for the correction of the weaker peaks. Such a background, which must be separately determined for each of the six possible angle-and-geometry combinations, however, must depend upon the points with the weakest statistical significance of any points appearing in the spectrum. It is therefore to be expected that a certain amount of systematic error is apt to be introduced into the correlation measurement in direct relation to the relative magnitude of the background subtraction necessary.

5.3 Data Analysis

An example of the data obtained from the present arrangement is shown in Fig. 35, where both an ungated and a sum-coincidence-gated spectrum are shown normalized to the same yield. The sum-coincidence spectrum is a sum over angle and geometry of all data obtained in two days of correlation measurements at this resonance. Both the improvement in peak definition and the accompanying loss of intensity in the sum-coincidence gated spectrum are readily apparent. As noted in Sec. 2.1, a single peak exists for each gamma ray occurring in a two-part cascade from the capturing level to the ground state. These peaks are nearly Gaussian, although distortions on the side of the peaks away from the

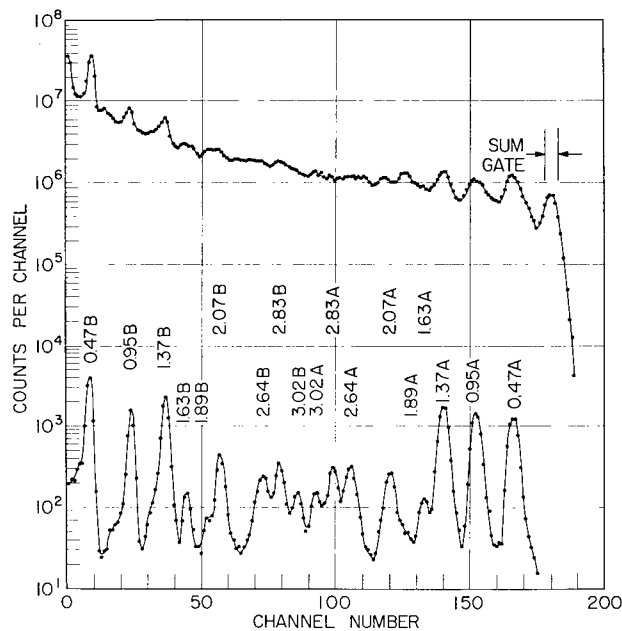


Fig. 35 - Ungated (upper) and sum-coincidence gated (lower) spectra, normalized to the same reaction yield, as obtained at the 1599-keV resonance. The peaks of the sum-coincidence spectra are labeled as to the intermediate excited state (energy in MeV), involved in the two-part cascade to the ground state, and as to whether the transition is the primary (A) or secondary (B) member of the cascade.

middle of the spectrum are apparent, particularly on the more narrow peaks in the lower portion of the spectrum. The Gaussian nature of the peaks is better illustrated in Fig. 36, where examples of both intense and weak transitions are provided by the members of the cascades associated with the 1.37- and 1.63-MeV states. Shown with the data are the parabolas fitted to the data after background subtraction. (The Gaussian distribution appears as a parabolic curve in the semilogarithmic representation.) As the sources of the distortions observed in Figs. 35 and 36 are not completely understood, the determination of the yield of gamma rays associated with a given peak has been restricted to fitting the Gaussian portions of that peak.

The yields of two-part cascades observed with the present arrangement are too weak to obtain adequate statistics for any but the strongest transitions in the course of a single day of correlation measurements. Thus, in addition to the requirement of gain stability over the course of a day, it is required that the gain condition be reproduced from day to day to allow the summing of individual spectra taken over an extended period (see Sec. 5.1 for procedures used to assure this condition). The remarkable success of the present arrangement in satisfying these reproducibility and stability requirements is illustrated in Fig. 35, and further examples are shown in Sec. 6.2.

Thus, even in cases where the statistics are so poor in an individual run (or sum of a small number of runs) as to make difficult the determination of all three of the parameters associated with a Gaussian peak, it has been possible to determine the peak-position and width parameters with greater precision from data obtained by summing the individual spectra taken under varying conditions of angle and geometry. These parameters may then

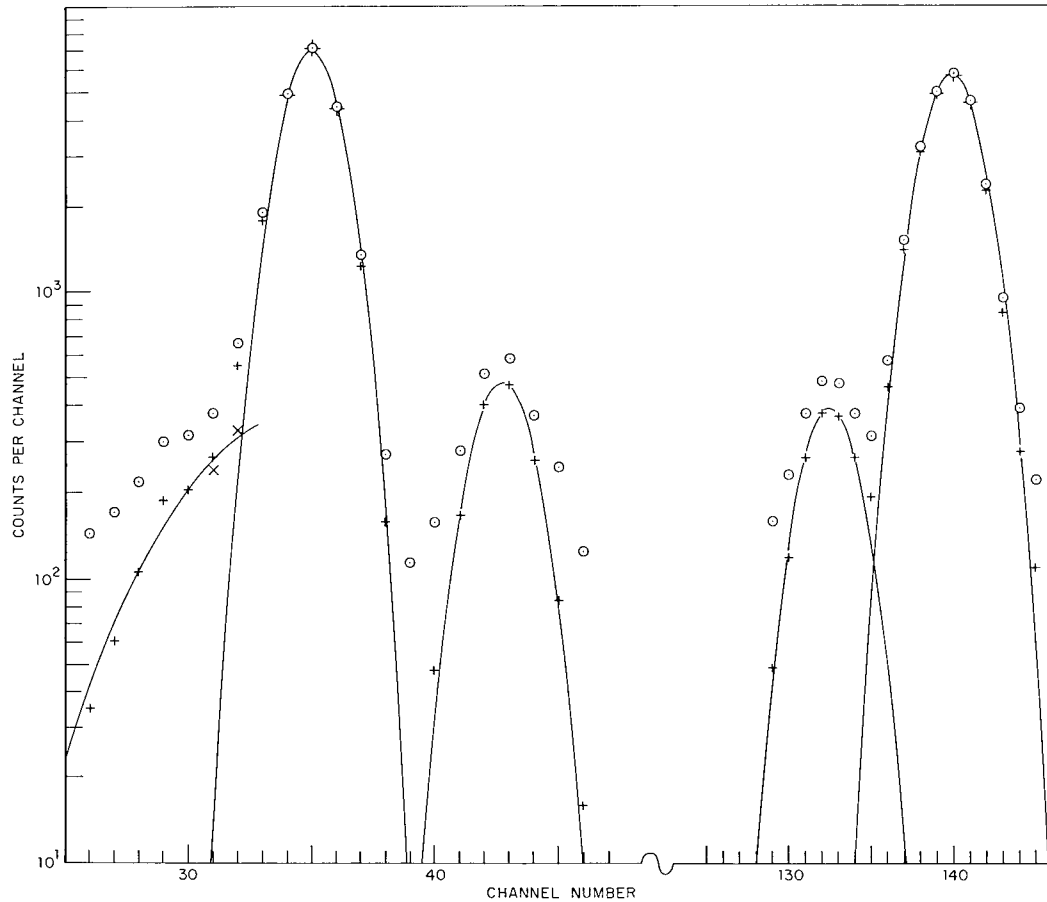


Fig. 36 - Examples of the fitting of Gaussian distributions to the peaks resulting from transitions through the 1.37-MeV and 1.63-MeV states at the 1620-keV resonance. The circles are from the summed data, and the crosses result from the subtraction of the estimated background. Parabolic curves representing the Gaussian distribution in the semi-logarithmic display are fit to these points. A distortion is observed to the low side of the lowest peak, and an attempt at fitting it is shown. Knowledge of this distribution is necessary in the iterative process used in separating incompletely-resolved peaks (not illustrated).

be applied to the fits of the peaks in individual runs in order to determine the remaining parameter, amplitude, for these individual runs. Therefore, the determination of the peak yield resolves into the determination of a weighted mean for this quantity based upon the individual points making up the peak, where the predictions for the total yield of the peak for each point is based upon the parameters determined in the fit of the summed data.

Of course, if the peaks were pure Gaussian without distortions, were completely isolated from neighboring peaks, and were not superimposed upon any background, then the determination of the yield of the peak could be made by simply summing all the points associated with the peak. That these conditions are not met in the spectra resulting from the sum-coincidence arrangement has already been shown. Therefore, the determination of the peak yield must depend either upon the consideration of only those points which are not significantly distorted by these effects, or upon consideration of most of the points but only after correction for these effects. Either approach requires a knowledge of the Gaussian distribution appropriate to the peak as determined from the summed data.

In the discussion which follows, the use of a barred value, such as \bar{x} , indicates values appropriate to the pure Gaussian distribution fitted to the sum data, and unbarred values represent values associated with the individual peak for which the yield determination is being made. The quantity x_i represents the number of counts in the i th channel, and Y represents the peak yield. Then for the fitted curve,

$$\bar{Y} = \sum_{-\infty}^{\infty} \bar{x}_i, \quad (1)$$

and the fraction of the total yield appearing in the i th channel is \bar{x}_i/\bar{Y} . This fraction may be used with the data from the individual run to predict the peak yield on the basis of the count for each channel in the peak by the relation,

$$Y_i = x_i \frac{\bar{Y}}{\bar{x}_i}. \quad (2)$$

The predicted yield could then be determined by making an appropriate mean of the values predicted from only the most suitable channels. However, purely on a statistical basis a straight mean is inappropriate and a weighted mean should be considered. Now in the semilogarithmic representation the standard deviation associated with the count in the i th channel, $\bar{\sigma}_i$, is the relative error for the point,

$$\bar{\sigma}_i = \frac{E_{\bar{x}_i}}{\bar{x}_i} = \bar{x}_i^{-1/2}, \quad (3)$$

where as usual in counting statistics, $E_{\bar{x}} = \bar{x}^{1/2}$. Thus the weighting factor, \bar{w}_i , is

$$\bar{w}_i = \frac{1}{\bar{\sigma}_i^2} = \bar{x}_i, \quad (4)$$

or to convert the mean determination into a simple cumulative product, the weighting factor is normalized,

$$\bar{W}_i = \frac{\bar{x}_i}{\bar{Y}_n}, \quad (5)$$

where

$$\bar{Y}_n = \sum_n \bar{x}_i, \quad (6)$$

where the summation over n is that over the channels chosen to be satisfactory for the peak-yield determination (relatively free of distorting effects). Then utilizing Eqs. (1) and (6), the determination of the peak yield resolves to

$$Y = \frac{\bar{Y}}{\bar{Y}_n} \sum_n x_i. \quad (7)$$

It can be seen that in the idealized case mentioned earlier, where there are no interfering effects, that $\bar{Y}_n = \bar{Y}$ and the determination of the peak yield becomes the expected simple sum. Equation (7) may of course be determined directly from Eq. (2) by substitution of the sum over n channels for the x_i and \bar{x}_i and by the use of Eq. (6). However, Eq. (7)

is not directly useful in nonidealized cases, and the weighted mean approach must be utilized in cases where other than purely statistical weighting is appropriate. Thus, it is clear that factors other than purely statistical may degrade the integrity of the points away from the center of the Gaussian, where undetected effects from background or distortions may have a relatively larger influence on the observed point. Two approaches to this problem have been used in the present work. The first approach, which was applied to the earlier work involving only the stronger peaks, allows the subtraction of background if it is thought to be significant but accounts for the presumed loss of integrity of the points away from the centers of the peaks by arbitrarily distorting the weighting factors, as follows:

$$\bar{w}'_i = \frac{\bar{x}_i^2}{\bar{Y}'_n}, \quad (8)$$

where

$$\bar{Y}'_n = \sum_n \bar{x}_i^2. \quad (9)$$

Thus the determination of the yield of the peak resolves to

$$Y = \sum_n x_i \frac{\bar{Y} \bar{x}_i^2}{x_i \bar{Y}'_n} = \sum_n \bar{a}_i x_i, \quad (10)$$

where

$$\bar{a}_i = \bar{x}_i \frac{\bar{Y}}{\bar{Y}'_n}. \quad (11)$$

The factor \bar{a}_i then may be determined solely in terms of the fitted distribution and a knowledge of which channels of this distribution are satisfactory (relatively undistorted) for the determination of the peak yield.

In the present experiment, because computer programs to handle the data analysis were not yet available, and because of the large number of peaks to be fitted, a graphical method rather than a least-squares method has been used to determine the fit to the summed data. Examples of such fits, determined by fitting parabolic templates to the summed data displayed in a semilogarithmic representation (with the background subtracted) are shown in Fig. 36. The \bar{a}_i are then obtained from the \bar{x}_i of the graphical fit for the appropriate channels, as indicated in Eqs. (11), (1), and (9). The determination of Eq. (1) may be made by simply summing all significant channels from the graphical fit or by calculation from the parameters of the parabolic fit to the data. The determination of the yield for the individual run (or sums of a small number of runs) for the peak in question may then be determined as in Eq. (10) from the data in a simple cumulative product of the $x_i f_i$ for the selected n channels.

A second approach was applied to the later data in which consideration of some rather weak transitions was made, where the effects of background, distortions, and incompletely resolved peaks necessarily had to be taken into more explicit account. In this case the weighting factors of Eq. (5) were modified to more explicitly account for these effects on the integrity of individual points by means of the factor f_i ; thus

$$\bar{w}''_i = \frac{\bar{x}_i \bar{f}_i^2}{\bar{Y}''_n}, \quad (12)$$

where

$$\bar{Y}_n'' = \sum_n \bar{x}_i \bar{f}_i^2. \tag{13}$$

The factor \bar{f}_i is defined:

$$\bar{f}_i = \frac{\text{number of counts due to Gaussian}}{\text{total number of counts for the point}}. \tag{14}$$

Of course, the \bar{f}_i , which are determined from the fitted curves, are dependent upon angle and geometry, because the various effects are themselves so dependent. Thus instead of making a fit to the sum of all data over angle and geometry, it becomes necessary to make six separate fits, one for each of the angle-and-geometry combinations. Although this involves considerably more labor, some saving is obtained in that correction by the point-by-point subtraction of the interfering effects from the individual data may be replaced by correction by multiplication by the factor \bar{f}_i , determined from the sum for the particular angle and geometry. That is, the factor \bar{f}_i is included in the cumulative product. We then define a new factor $\bar{\alpha}'_i$.

$$\bar{\alpha}'_i = \bar{f}_i^2 \frac{\bar{Y}}{\bar{Y}_n''}, \tag{15}$$

which may be used analogously with Eq. (10) except that the factor $\bar{\alpha}'_i \bar{f}_i$ be used in place of $\bar{\alpha}_i$ and that the cumulative product be applied to the uncorrected data for the individual runs (or sums).

The peak yields thus obtained must be corrected as a function of the angle of the detector for the unequal absorption of the gamma rays in the anisotropic distribution of materials surrounding the target (see Sec. 3.2). These materials provided by the target backing, target support, and water jacket (see Fig. 13) are shown in one half of a horizontal section in Fig. 37. For the purposes of the correction calculation, an angle θ with respect to the beam axis in the horizontal plane has been sampled in 5-degree intervals from 0

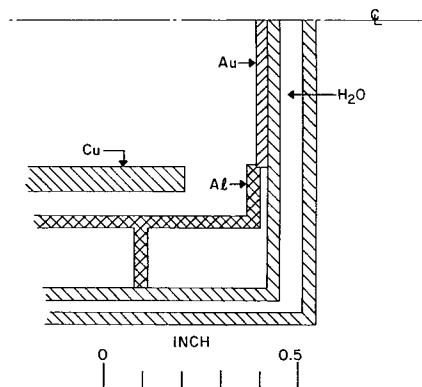


Fig. 37 - One half of a section view of the materials in the vicinity of the target. The unequal absorption of the gamma rays in these materials as a function of the angle of the detector must be corrected for in the analysis of the experimental data.

to 115 degrees and the amount of each material (path length ℓ_i) traversed by rays at each of these angles computed utilizing $\sec \theta$ and $\operatorname{cosec} \theta$ relationships. Values of the path length for those cases in which a ray traverses a corner were separately computed to yield an average value for the interval represented by the ray. Values of the linear absorption coefficient, τ , were determined for a series of gamma-ray energies, E_γ , and for each material from the mass absorption coefficients, μ , as obtained from Ref. 9 and graphically interpolated for the specific energies used. The path length and the linear absorption coefficients are used to calculate the transmission, T , for each energy at all 24 angles sampled. The standard definition of the transmission is used:

$$T_i = \exp [-\tau(E_\gamma)\ell_i]. \quad (16)$$

The total transmission is the product of the transmissions of the individual materials traversed. The case of the interval associated with a ray at $\theta = 90$ degrees is treated specially, since the Au target backing is effective in only half of this interval ($\theta \leq 90$ degrees).

Since rays which strike the crystal at large values of the angle β (angle between the ray and the axis of the crystal) are less effective in producing full-energy-absorption events in the crystal, and since the vertical bands representing the intervals of θ intercept different solid angles of the crystal face, a weighting factor, w , taking these effects explicitly into account is applied to the transmission for each interval intercepted by the crystal when placed at one of the angular positions used in the present experiment. The weighting factors are determined by subdividing the angular bands of the crystal face and determining products of the solid angles and efficiency terms, $f(\beta)$, relative to the total of such product terms for the whole crystal face. The $f(\beta)$, which are also a function of energy, are taken from the Monte Carlo results obtained in the determination of the finite geometry correction coefficients (see Sec. 5.4). The weighted transmissions for each interval involved, as appropriate to the crystal being placed at one of the three angles $\theta = 0, 45$, and 90 degrees, are calculated and the sums of these weighted transmissions for each case obtained to represent the average effective transmission of the target materials for the detector at that angle and for gamma rays of that energy. The resulting weighted transmissions, wT , as a function of gamma-ray energy are shown for the three angles in Fig. 38. As the correction factors are to be applied to sum-coincidence data, the effects of the attenuation of the other member of the two-part cascade, which is detected by a fixed detector at 90 degrees, must also be taken into account. The weighted transmission appropriate to the detection of both members of the cascade in sum-coincidence is then the product of the terms for the individual gamma rays, one in the moving crystal at that angle, θ , and the other at $\theta = 90$ degrees (with the choice of detector for the primary and secondary members of the cascade depending upon the particular geometry considered), and the multiplicative correction factor, F , is the reciprocal of this product. This factor, F , is that required to correct the raw yield to that which would have been observed had the intervening materials not been present.

The effects of some of the approximations involved in this calculation of the correction factors have been evaluated and generally found to be small (<1-2 percent). A more exact calculation which avoids most of these approximations is now being programmed for the NAREC computer. However, because the computed correction factors are relatively large, chiefly due to the effect of the relatively thick Au target backing, an experimental test was devised to determine the reliability of the computed factors. For this test it was possible to duplicate the conditions existing in the angular correlation measurements by providing a source of low-energy gamma rays with isotropic spatial distributions. For this purpose a thick* (~ 7 mg/cm²) target of natural Zn was plated on a standard Au target backing, and

*Thick in the sense of the energy loss of the incident protons, which lose a sizable fraction of their energy in traversing the layer, but negligibly thin as far as the gamma-ray transmission is concerned.

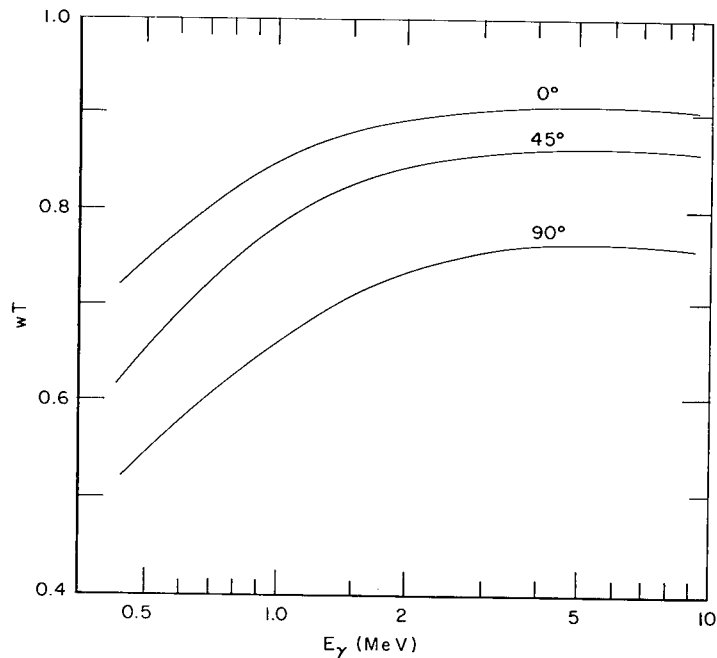


Fig. 38 - The calculated weighted transmissions, wT , of the gamma rays through the materials in the vicinity of the target for the three angles used for the detector as a function of the gamma-ray energy E_γ .

the target was bombarded for 7 hours with 1.77-MeV protons. After decay overnight to allow the disappearance of shorter half-lived activities, the gamma rays following the 78-h half-life electron-capture decay of ^{67}Ga were observed. An electron-capture decay was chosen to assure that the source of the gamma rays was in the bombarded area of the target. The use of the annihilation radiation from a positron decay (which usually results from (p, γ) reactions) would be improper since the positrons may have flown from the immediate area of the nuclear decay before annihilating. Even if the annihilation radiation was not itself used, it would contribute significant background because of its Compton distribution upon which lower energy gamma rays would be superimposed. The resulting ^{67}Ga source provides a number of low-energy gamma-ray peaks including those at 296 and 388 keV which were used in this test. Distributions of these gamma rays were determined in a manner similar to that used in the correlation case (except that ungated spectra were obtained) by measurements at the three angles to both sides in the horizontal plane. The resulting spectra were corrected for background and decay of the source and the peaks fitted with Gaussian distributions. Because the same beam alignment procedures were used for the irradiation of the Zn target, and because the resulting Ga source was not moved before the distribution measurements, these measurements identically represent the conditions encountered in correlation measurements and provide in addition to a test of the absorption correction factors a measure of the possible experimental anisotropies of the system. The results of the ^{67}Ga measurements in the present experimental arrangement expressed as a ratio of the 43 degree to 0 degree yields and the 90 degree to 0 degree yields are listed in Table 3 for each of the detectors (to the left and right sides, respectively) as well as the average value for the two detectors for comparison to the ratios from the correction factors, F , calculated for the indicated gamma-ray energies. It is noted that the fluctuations of the values appear to be random and largely statistical. It is thus concluded that the calculated results are probably accurate to at least 2 percent at the higher gamma-ray energies. The results for energies used in the

Table 3

Results of the Experimental Test of the Correction Factors Calculated to Account for the Different Absorption of the Gamma Rays by the Anisotropic Distribution of Matter in the Vicinity of the Target as a Function of the Angular Position of the Detectors

A ^{67}Ga source produced by proton bombardment of a Zn target provides isotropic distributions of gamma rays of the indicated energy E_γ . The ratio of the yield of these gamma rays observed with the indicated detector at the angle θ to the yield at $\theta = 0$ degrees is given for both $\theta = 43.6$ degrees and $\theta = 90$ degrees. Detectors 2 and 3 represent measurements to the left and right sides, respectively, of the beam direction in the horizontal plane. The average of the ratios for the two detectors is also given for comparison for the ratio determined from the calculated correction factors.

θ	E_γ (keV)	Yield Ratio (Det. 2)	Yield Ratio (Det. 3)	Yield Ratio (Av)	Yield Ratio (Calc.)
43.6	296	0.769±0.011	0.788±0.011	0.799±0.008	0.764
	388	0.855±0.020	0.827±0.020	0.841±0.014	0.839
90.0	296	0.765±0.011	0.772±0.011	0.769±0.008	0.814*
	388	0.732±0.020	0.798±0.020	0.765±0.014	0.743

*The increase in the ratio of the yield at 90 degrees to that at 0 degrees, observed at 296 keV, arises from the fact that at 90 degrees only half of the solid angle subtended by the detector requires transmission through the Au backing. Thus at lower energies where the Au becomes increasingly opaque to the radiation the trend existing at higher energies is reversed.

present experiment presumably produce higher accuracy, both because of the relative improvement in accuracy of the absorption coefficients toward higher energies and because the correction factors themselves provide smaller corrections to the data for higher gamma-ray energies.

In addition to the correction for the unequal absorption as a function of angle, the peak yields are normalized by a factor which is a product of the normalization of runs within a given day as determined from the monitor counts and the normalization for the results from one day to another as determined from the routing pulses. The generation of the normalization factors and the corrections thereto are described in Sec. 5.2. The resulting corrected and normalized yields for the three angles of measurement then represent the experimentally observed information yielding correlation function for the particular transition involved. Four such correlation functions, each corresponding to a different geometry, result for each intermediate excited state studied.

As described in Secs. 1.4 and 2.3, the correlations may be expressed in terms of the limited normalized Legendre expansion

$$W(\theta) = 1 + A_2 P_2(\cos \theta) + A_4 P_4(\cos \theta). \quad (17)$$

However, in some of the predicted correlation functions the A_4 term is required to vanish, and in these cases the correlation should be fit with the first two terms of Eq. (17) only.

Accordingly, the least-squares fit for both the first two and the first three terms are made to the normalized and corrected yields for each geometry and intermediate state. A computer routine which accomplishes these fits has been written for this purpose. This routine accepts input data in a convenient form, where in decimal notation the angle of detection in degrees, the number of counts observed for the point (normalized only to powers of ten), and a weighting factor represented by a single digit from 0 to 9 are compounded into a single word. The routine will fit correlations involving any number of input points between three and twenty four. The routine contains built-in checks on each stage of the calculation and produces as output values of the a_0 , A_2 , and A_4 coefficients as appropriate for the two- and three-term fits and the associated values of the errors for these quantities based upon the goodness of fit of the required function with the experimental points provided.

The manner in which the fourteen runs obtained on each day of correlation measurements are summed to provide the input data for the least-squares fit is somewhat arbitrary. Since even for very strong transitions more than one day of correlation measurements is generally involved, the sums of individual runs are seldom made up of less than the four or six runs made at a given angle in one day of correlation measurements. When a number of days of measurements are to be included in the same set, further summing of the data from more than one day is frequently made prior to the peak fitting procedures (described above) in order to restrict the peak fitting computations to more manageable proportions. Thus, generally the least-squares fits are provided for a nine-point sequence with three points at each angle.

Another possible approach, at least for the three-term fit of the Legendre expansion, is to sum all data for each angle and make an exact fit of the correlation function to the resulting three data points by the solution of simultaneous equations. If in the least-squares fit the weighting factors, which may be different for each angle, are made the same for all points for a given angle, as determined for the average yield of the points at that angle (see below), then the results for the values of the coefficients of the three-term least-squares fit is identical to that of the exact fit, and the two calculated values provide a check for each other. Purely statistical, or statistical plus systematic, errors can be assigned to the sums of points at a given angle for the exact fit, and these errors can be propagated by standard techniques to determine the errors associated with the coefficients of the expansion on the basis of the errors of the individual points. On the other hand, the least-squares fits yield error estimates based upon the goodness of fit to the Legendre expansion form. The error estimates from the least-squares and exact fits are generally comparable, at least for the intense well-resolved peaks, where the error estimates for the exact fit are chiefly statistical. In any event, the larger of the two errors is used in the comparison with the predicted correlation functions.

For both the weighting factors for the least-squares fit and the error estimates in the yield for the exact fit, not only the counting statistics, $E_N = N^{1/2}$, but also an estimate of the error introduced in the consideration of distortion, background, and incompletely resolved peak effects are included for those peaks where correction for these effects was necessary. This has been achieved for each peak, so affected, by multiplication of the statistical error, E_N , by a factor, f_E , proportional to the inverse of the average \bar{f}_i over the peak; thus

$$f_E = \left(\frac{1}{\bar{f}^2} \right)^{1/2} = \left(\frac{\bar{Y}}{\bar{Y}_n} \right)^{1/2}. \quad (18)$$

The use of such error estimates allows a more reasonable estimation of the expected error in the expansion coefficients for those weak transitions involving relatively large contributions from constant background or incompletely resolved peaks. These error estimates also prevent overemphasis of the low-yield points in extremely anisotropic

correlations by providing an estimation of the systematic errors which are more apt to influence such points.

The coefficients of the Legendre expansion fit to the observed correlation yields and the error estimates associated with these coefficients are the basis of the comparison of the experiment with the predicted correlation functions, as described in the next section.

5.4 Predicted Correlation Functions

The interpretation of the experimental results of triple correlations in (p,γ) reactions in terms of predicted correlation functions has been greatly facilitated by the efforts of the group at the Chalk River Laboratories of Atomic Energy of Canada, Limited, who have developed the geometry concept and provided convenient tabulations of the coefficients necessary to predict the correlation functions for this reaction. From this tabulation (3) the predictions may be generated in terms of the quantum numbers defined in Sec. 1.4 and Fig. 6 and of the four indices k_1 , k_2 , k_3 and κ , which may take only a limited number of combinations of values within the restrictions imposed by the selection of the geometries used. Then for each geometry the coefficient a_k of the Legendre expansion, where k is the index of the expansion, is given by

$$a_k = N \sum' (-1)^{L_3 - L_3'} \alpha_{k_1 k_2 k_3 k} \delta_2^{r_2} \delta_3^{r_3} Q_{k_2} Q_{k_3} D_{k_2 k_3}^{\kappa} (a, d, b, c, \ell_1, \ell_2', L_2, L_2', L_3, L_3'), \quad (19)$$

where the summation is over the indices, the α 's represent the geometry and are tabulated for each geometry as a function of the indices, the δ 's are the admixture ratios of the next highest multipole (where allowed), the r 's are exponents having the values 0, 1, or 2 depending on whether the term is of the type $L_2 L_2$, $L_2 L_2'$ ($L_2' L_2$), or $L_2' L_2'$ respectively, the Q 's are the finite geometry correction coefficients described below, and the D coefficients, which are a function of all quantum numbers and the indices, represent the correlation and are the principal content of the tabulation. The form shown here is specific to the present experiment both to the absence of the possibility of admixtures in the entrance channel (because of the zero spin of the target nucleus) and as to the absence of certain other terms which are not appropriate for the present choice of geometries.

The prediction for the coefficients of the Legendre expansion therefore resolves to a sum over a limited number of possible combinations of the indices of terms from the tabulated values of α and D and the appropriate Q factors. The resultant expressions are then in the general case a double-quadratic equation in terms of the admixture ratios, δ_2 and δ_3 for the primary and secondary transitions. The experimentally meaningful coefficients, A_k , of the normalized Legendre expansion (see Eq. (17)) are the ratio of two such complex terms. The degree of complexity of the resulting predictions for the correlations functions are therefore a function of whether or not admixtures are allowed. Four cases may be distinguished: (a) the pure-pure case, where an admixture in neither transition is allowed, and where the theoretical prediction for the A_2 coefficient for each geometry is merely a number; (b) a pure-mixed case, where an admixture is not allowed in the primary transition but is allowed in the secondary transition, and where the theoretical prediction is a function of the single variable of the secondary admixture ratio, δ_3 ; (c) the mixed-pure case, which is similar to the pure-mixed case except that the primary ratio, δ_2 , is involved instead of δ_3 ; and (d) the mixed-mixed case, where admixtures in both primary and secondary transitions are allowed, and where the prediction is a function of the two variables δ_2 and δ_3 . Cases (b) and (c) are simply represented by a curve of the value of the expansion coefficient as a function of the independent admixture ratio. However, the representation of case (d) is more difficult, as the expansion coefficients are here a function of two independent variables. For this case a contour plot represents the best approach to this problem for search and display purposes.

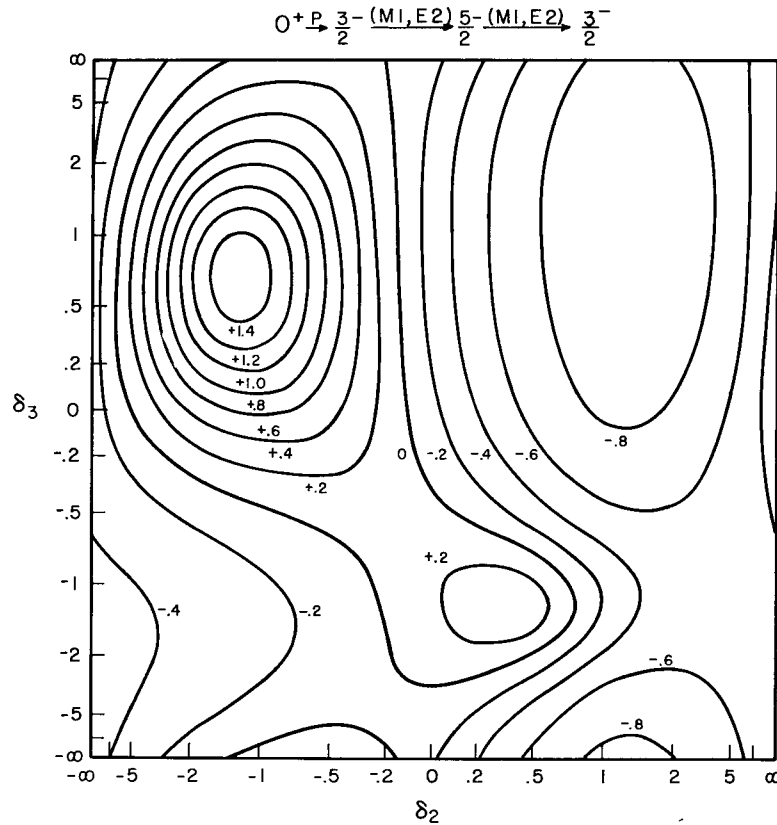


Fig. 39 - A sample contour plot representation of a predicted correlation function. The curves represent constant values of the A_2 coefficient of the Legendre expansion as a function of the two multipole admixture ratios, δ_2 and δ_3 , for the A geometry only and for the indicated spin sequence. Such plots (each uniquely different) exist for each geometry for every possible spin sequence allowing admixtures in both transitions.

Such a contour plot is shown for a particular set of quantum numbers in Fig. 39, where the two independent variables, the admixture ratios δ_3 and δ_2 , form the axes and the curves represent the loci of constant values of the A_2 expansion coefficient incremented over the range of possible values. The admixture ratio for each of the transitions has of course a unique value for a given transition found in nature, but this value may lie anywhere within the range from $-\infty$ to $+\infty$, this range including the cases of pure quadrupole ($\delta = \pm\infty$) and pure dipole ($\delta = 0$). For this reason an arctangent representation of the variable is used for the axes to allow the full range of possibilities.

While the performance of the summations involved in the determination of the predicted correlation functions, as in Eq. (19), is not overly laborious, the handling of the quadratic expressions may be, particularly the ratio of double-quadratic equations in the mixed-mixed case. Accordingly, the generation of the predicted correlations functions has been programmed for the NAREC computer, and the availability of a high-quality x-y recorder capable of working with the computer-generated output tapes has been utilized to automate the preparation of the results for either the ordinary curves or contour plots. For this routine portions of the tables of Ferguson and Rutledge (3) are read into the computer memory and functions representing the energy dependence of the q

factors are supplied. Then upon appropriate instructions, including specifications of the energies of both transitions, specification of the quantum numbers for the case to be considered, and the specification of the type case involved and output form desired, the program produces the required output.

The mechanism of the actual comparison of the experimental value of the expansion coefficient, A_2 , with the predicted values of course depends upon the type case under consideration. Thus, in the pure-pure case the comparison resolves to a determination of whether the single predicted value for each geometry lies within the range of experimentally observed quantities for the geometry, that is, whether the value lies between the values $A_2 - E_{A_2}$ and $A_2 + E_{A_2}$, where E_{A_2} is the experimental error in the value of A_2 determined as described in Sec. 5.3. In this case all four values for the different geometries must agree or nearly agree for the spin sequence upon which the predictions are based to be considered appropriate. In a similar manner in the pure-mixed or mixed-pure cases, where the predicted values of the expansion coefficient is represented by a curve as a function of the admixture ratio (again in an arctangent representation), the range of the experimental value of the expansion coefficient may be represented by a horizontal band whose extremes are again $A_2 - E_{A_2}$ and $A_2 + E_{A_2}$. An example of such a comparison for a single geometry is illustrated in Fig. 40. The regions where the curve intercepts the hatched band define allowable ranges of the admixture ratio for this particular geometry. In the general case each geometry will produce a unique and different curve for the same spin sequence, and a different experimental value will be observed in each geometry measured. Satisfactory agreement of a proposed spin sequence with experiment is then indicated by agreement of all the geometries measured for a specific value (or a range of values) of the admixture ratio. That is to say, in nature each transition has a specific admixture ratio, and the values for this ratio determined by comparison of the experimentally measured coefficient of the expansion and that predicted for the correlation function for each geometry in the case of the appropriate spin sequence must agree. Thus, if the wrong spin sequence is assumed, it is expected that no agreement on a value for the admixture ratio will be obtained provided that a sufficient number of geometries are measured. As discussed in Sec. 2.3, the A_4 coefficients of the Legendre expansion, for which a similar comparison of experiment and predicted correlation functions may be made, are generally insensitive, although they may be of some assistance in excluding some cases of possible agreement. However, in the present arrangement the use of four geometries providing a sensitive comparison for the A_2 coefficients of the expansion are generally sufficient to provide such an agreement of experiment and predicted

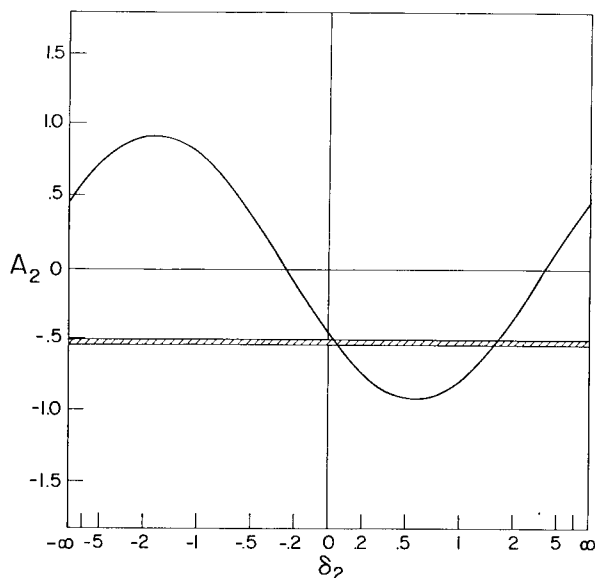
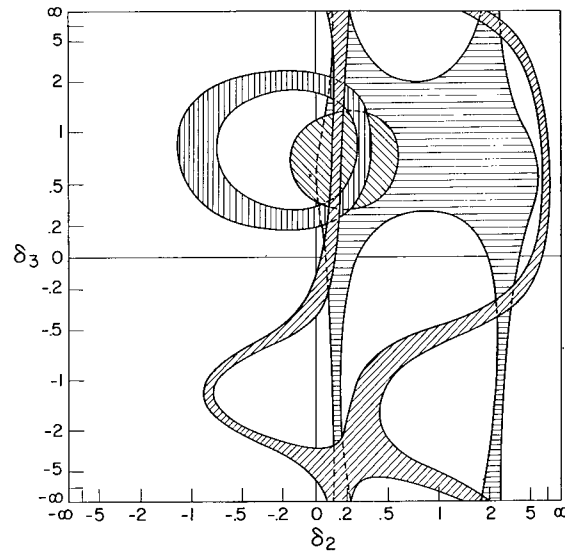


Fig. 40 - An example of the comparison of an experimental value (hatched band) and a predicted correlation function (curve) for a given spin sequence in a mixed-pure case. Shown are the value of the A_2 coefficient of the Legendre expansion as a function of the admixture ratio of the primary transition for one geometry only. The interception of the band and the curve represents values of δ_2 allowed by this observation. A similar comparison can be made for each geometry. Agreement of all observed geometries on an allowed value is necessary for the assignment of a particular spin sequence.

Fig. 41 - An example of the comparison of experiment and the predicted correlation functions in a mixed-mixed case. The experimental values result in the hatched bands for each geometry representing allowed values of the admixture ratios. The agreement of all observed geometries on an allowed value is evidenced by overlap of all bands. Such agreement is necessary for the assignment of the spin sequence.



correlation functions for only one of the possible spin sequences and thus to make an unambiguous assignment of these spin sequences and multipole admixtures, except in certain degenerate cases.

In the case of mixed-mixed transitions the comparison is more complex but is still based upon the question of agreement of all measurements of a specific value of the admixture ratios. In this case the range of an experimental value for the coefficient of the expansion is defined by interpolating* the values of $A_2 - EA_2$ and $A_2 + EA_2$ from the contour plots (such as that shown in Fig. 39). In general each geometry for a particular spin sequence produces a unique and different contour plot, and the band of allowed values of the admixture ratio defined by the experimental values of the expansion coefficient for each geometry usually are radically different, as shown in Fig. 41. Here, each hatched band represents the range of allowed values of the admixture ratios for a different geometry. In this case, of course, agreement between the geometries on specific values for these admixture ratios is indicated by overlap of all bands, as occurs in Fig. 41 in only one small area. Again in the general case, the A_4 values are generally rather insensitive and are not ordinarily used except to exclude certain possible overlaps (corresponding to large admixtures); but the four geometries provided generally allow only one such overlap for all the spin possibilities, thereby uniquely assigning the spin sequence and defining the admixture ratios for both transitions, except in certain degenerate cases.

In experiments of the type described in this report it is not always possible to make measurements under idealized conditions. Under these circumstances the deviations from the ideal situation must be compensated for by correction to the data. One such major correction to the data has been described in Sec. 5.3 with regard to unequal absorption of gamma rays from the target as a function of the angle of the detector. A second major correction factor which must be applied concerns the large acceptance angle of the detectors. The fact that the detectors are not idealized point detectors causes an effective smearing of the observed correlations. In the present experiment, because of the unusually large solid angles used the corrections necessary to account for this effect are quite significant and must be made with care. The formulation of correction factors, Q_k (which appear in Eq. (19)), for the case of cylindrical detectors was originally reported by Rose (10). He derives for the correction factor the expression $Q_k = J_k/J_0$, where

*In the computer routine the double-quadratic equations are solved for one of the variables while the other value is incremented throughout the range.

$$J_k = \int_0^\gamma w(\beta) P_k(\cos \beta) \sin \beta d\beta. \quad (20)$$

In this integral β is the angle between the axis of the crystal and a ray from the point source of radiation, and the integration is carried out between the limits of $\beta = 0$ degrees (along the axis) and $\beta = \gamma$ (the maximum half-angle subtended by the front face of the crystal). In Eq. (20), $w(\beta)$ represents the probability of interaction of the gamma ray (for the particular interaction considered) as a function of the angle β , $P_k(\cos \beta)$ is the Legendre polynomial term representing the effect of the distribution, and $\sin \beta$ is the term representing the effect of solid angle. In Rose's report and subsequent tabulations the integral of Eq. (20) has been evaluated using for the probability term the analytic expression, $w(\beta) = 1 - \exp[-\tau x(\beta)]$, where τ is the linear absorption coefficient and $x(\beta)$ is the path length within the crystal (readily determined from geometrical considerations) traversed by a ray at angle β .

While the use of this expression for $w(\beta)$ makes Eq. (20) readily tractable, it does not in the present experiment correspond to physical reality, because it represents the effect of "any interaction" of the gamma ray with the crystal and requires that all such interactions be detected. However, in the present experiment, the sum-coincidence condition restricts experimental consideration to only those events which deposit the full energy of the gamma ray in the detector. Under these circumstances the values calculated on the basis of "any interaction" with the detector may serve only as a lower limit for Q_k . This situation arises because events which interact near the walls of the detector are less likely to deposit the full energy of the gamma ray in the detector, and the finite acceptance angle subtended by the detectors are less effective in smearing the observed distribution. This effect may be seen in Fig. 42 which shows for a specific gamma-ray energy a comparison of the $w(\beta)$ for "any interaction" and for the "full energy absorption" interactions.

Because of the complexity of the mechanisms of interactions of gamma rays with the crystal, the $w(\beta)$ corresponding to the full absorption of the gamma-ray energy are not subject to analytical calculation, or indeed to reasonable approximation. It has therefore been necessary to adapt the methods of Monte Carlo calculation, or statistical simulation of the gamma-ray interaction with the NaI crystal, to determine the $w(\beta)$ corresponding to this case. For this purpose computer programs prepared by Dr. Charlotte M. Davisson of this Laboratory were used. In this program: (a) the photoelectric effect was treated as a simple absorption, (b) all the scattering processes were considered to be Compton scattering from a free electron, where the energy imparted to the electron was considered absorbed, and (c) the two pair-production electrons were assumed to be completely absorbed, except for the two annihilation photons which were assumed to be formed at the point of the pair-production interaction from the annihilation of a positron at rest. All secondary effects except annihilation radiation were neglected. At low energies (i.e., less than about 4 MeV), the effects neglected are small and probably less than the statistical error of the Monte Carlo method. As the energy increases, some of the secondary effects, in particular the escape from the crystal of the bremsstrahlung from the secondary electrons, become increasingly more important. Although these simplifying assumptions in the Monte Carlo program lead to some error in Q_k above this energy, the "true" values must show an even greater deviation from the "any interaction" curve than the Monte Carlo results. This situation arises from the fact that losses due to the secondary processes will occur with greater probability near the boundaries of the detector, thus occurring in general at larger angles and leading to an even sharper angular dependence than that calculated. In this respect the Monte Carlo results at higher energies again represent only a lower limit to the values of Q_k , but this new limit should represent a much closer approximation to the true situation than that previously available.

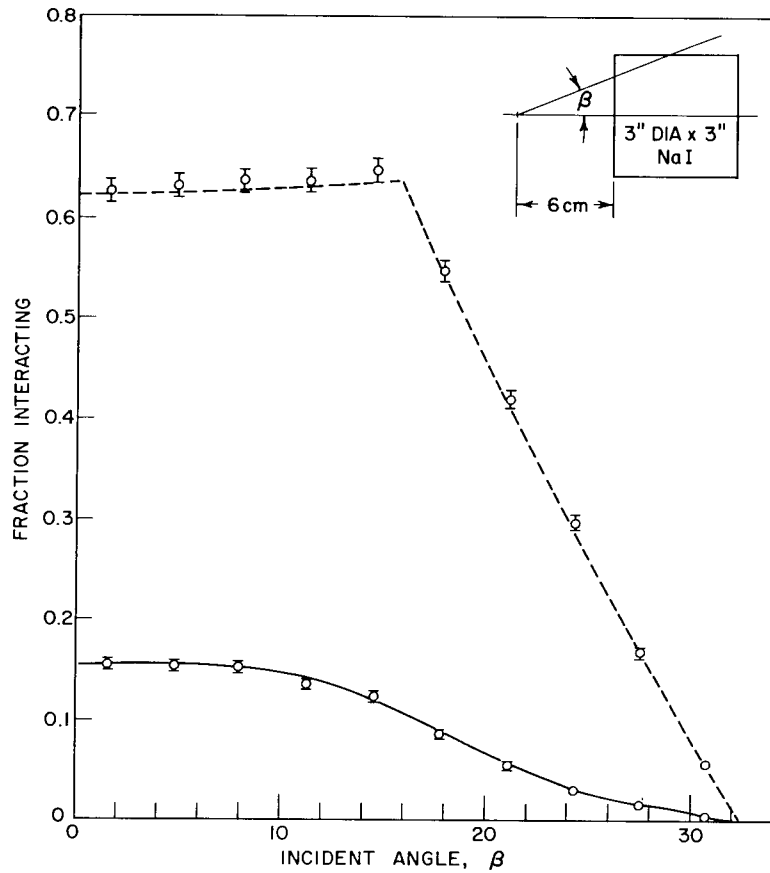


Fig. 42 - The fraction of gamma rays interacting with a scintillation crystal as a function of the incident angle, β , for an incident gamma-ray energy of 7 MeV. The dashed curve represents "any interaction" of the gamma rays with the crystal, while the solid curve represents the "full energy absorption" interaction. The insert shows the geometry defining the angle β . From Ref. 11.

The fraction of incident photons whose energy was completely absorbed was determined from the Monte Carlo calculations carried out on the NAREC digital computer as a function of the incident energy of the photon, E_γ , and the angle β to the crystal axes. The angular samplings were made at ten equally spaced angles, β_n , between 0 degrees and γ , where the β_n were determined according to the relation $\beta_n = [n - (1/2)](\gamma/10)$. For each angle at each energy 5000 photons histories were followed. The results for a crystal in the arrangement of the present experiment (except that no collimation was considered) are shown in Fig. 43 for each of the energies sampled. Because the Monte Carlo data necessarily contains statistical uncertainties, a method of smoothing the data was provided by a least-squares fitting of the points with a polynomial in powers of $\cos \beta$, i.e., $w(\beta) = \sum_i a_i \cos^i \beta$. The curves shown in the figure are the results of such fits obtained with a least-squares fitting routine due to Falvey (12). The use of a series in $\cos \beta$ allowed the evaluation of Eq. (20) in terms of the readily integrable expression

$$\int_0^\gamma \cos^n \beta \sin \beta d\beta .$$

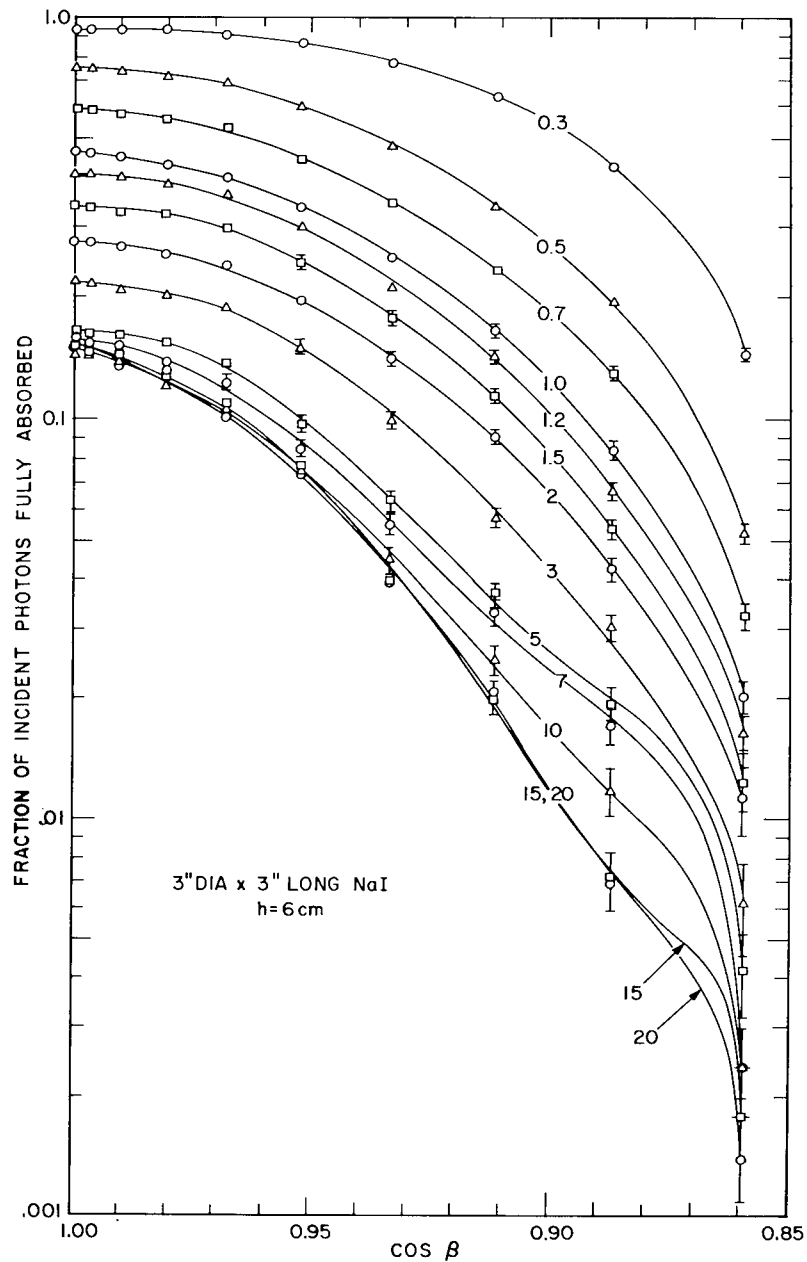


Fig. 43 - Fraction of incident photons fully absorbed as a function of $\cos \beta$. The labels on the curves give the incident photon energy in MeV. The curves result from smoothing calculation to the Monte Carlo produced data points. From Ref. 11.

Substitution of the series expansion of $w(\beta)$ in powers of $\cos \beta$ and of expressions of $P_k(\cos \beta)$ in Eq. (20) results in expressions for the J_k containing terms only in the coefficients of the cosine series, a_i , and powers of $\cos \gamma$. The use of γ (the maximum half-angle subtended by the front face of the crystal) as the limit of integration in Eq. (20) produces results corresponding to the uncollimated case, but the use of a limit β_{\max} , where $\beta_{\max} < \gamma$, corresponding to a collimated case is equally allowable. The use of collimation was specifically forbidden for the case of "any interaction" of the gamma

rays with the detector. The removal of the collimation restriction is possible in the present arrangement because the experimental acceptance of only those events depositing the full energy of the gamma rays in the crystal precludes the experimental acceptance of gamma rays scattered into the crystal by the collimator, since these events are no longer of full energy.* In practice the finite width of the sum gate necessitated by the finite energy resolution of the detectors allows the acceptance of events which have suffered slight energy degradation and hence permits the acceptance of gamma rays scattered through small angles, leading to some diffuseness of the cutoff angle, β_{\max} . In the present arrangement an effort is made at restricting such scattered events by preventing the direct illumination of the inner wall of the collimator, as described in Sec. 3.2. A probably more serious but fortunately readily calculable effect is the diffuseness of the cutoff angle, β_{\max} , occasioned by the transmission of the edges of the collimator. Because the transmission of the Pb is a strong function of the energy of the gamma ray, the effective size of the collimator aperture varies with gamma-ray energy to produce a radical effect on the Q_k factors. To account for this effect, the region just beyond the geometrical cutoff angle was divided into small angular increments and the average transmission of each increment calculated as a function of gamma-ray energy. The influence of each increment upon the value of Q_k was determined for full (uncollimated) transmission from the Monte Carlo results, and the effective fractions of this value as determined from the transmission calculations were added to the Q_k factors. Thus, the finite geometry correction coefficients used in the analysis of the data of the present experiment include not only the effects of the collimators (necessary in the sum-coincidence arrangement) but also the transmission of the edges of these collimators, and these correction coefficients neglect only the effect of acceptance of some small-angle scattered events calculated to be excluded by the collimator. The results for the present arrangements are shown in Fig. 44, which show for the two pertinent cases, $k = 2$ and 4, the results for the collimated case, the uncollimated case, and the uncollimated case as calculated on an "any interaction" basis.

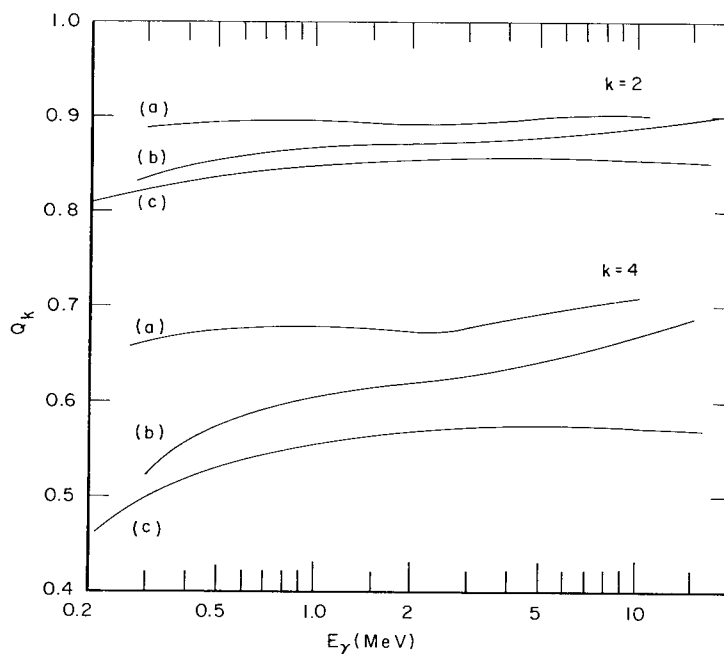


Fig. 44 - The finite geometry correction coefficient, Q_k vs incident gamma-ray energy, E_γ , for $k = 2$ and 4. The curves represent (a) the collimated case of the present arrangement for full energy absorption, (b) the uncollimated case in the same geometry for full energy absorption, and (c) the uncollimated case for "any interaction."

*The absence of a full-energy criterion, as in the "any interaction" case, would allow the experimental acceptance of events initially at an angle greater than β_{\max} but scattered into the crystal by the collimator; the acceptance of such events would require greater correction than that calculated.

6. EXPERIMENTAL RESULTS

6.1 Identification of States

The enhanced sensitivity for the detection of weak two-part cascades in the presence of stronger transitions, as evidenced in Fig. 35, permits the identification of states not readily identified from ungated spectra or, in most cases, from normal fast-slow coincidence work. Thus, all of the low-lying states reported in Ref. 1 have been identified in the present experiment as well as several additional states. However, the effect of the enhanced sensitivity of the sum-coincidence method is somewhat diluted for states above the first few in that the possibility of further cascade through some of the lower-lying states increases with increasing excitation energy. The efficiency for the detection of such three-part or four-part cascades is considerably reduced from that for a two-part cascade (see Sec. 5.2), and multiple (in excess of two-part) cascades are not normally observed in the present arrangement. As a consequence, the observation of states with spins differing by more than two units of spin from that of the capturing level is improbable in this experiment, as such states could be populated only by a cascade of at least three parts if it is assumed that octupole transitions from the capturing level will not be observed to compete.

The measurement of branching ratios, the percentage of the total transitions from a given level which populate the various possible lower levels, are frequently made in normal (p, γ) experiments (see Ref. 1, for instance). In the sum-coincidence arrangement, however, the observed intensities for two-part cascades to the ground state are not a measure of branching of the primary transitions from the capturing level, as these intensities reflect not only this branching but also that of the intermediate state. That is, two-part cascades are observed only for that part of the transitions to a given intermediate state which are followed by a transition direct to the ground state, and those which are followed by further cascading through lower levels are preferentially excluded in the sum-coincidence measurements. As a consequence, intensity measurements from the sum-coincidence arrangements are of limited usefulness and have not been pursued in this experiment.

Although necessary to the determination of some of the transitions, the sum-coincidence method does not lend itself to as great precision in the measurement of the energy of gamma rays as can be obtained for the more intense transitions under ungated but gain stabilized condition, because in the protracted period during which the sum-coincidence spectra are accumulated the average gain conditions may not be precisely identical with those at the time of calibration. Nevertheless, the stability of the present system is such that it appears reasonable to assign a probable error of ± 30 keV to each of the gamma-ray energy measurements of this report, and thus to the energy of each of the excited states reported. This assigned error value does not vary with gamma-ray energy in the manner of ordinary measurements, for the following reasons: (a) When measured under sum-coincidence conditions, the gain condition for the lower energy regions cannot be expanded as in normal ungated measurements. (b) The location of high-energy peaks can be measured with the comparable precision to the low-energy peaks under these conditions because of the properties of the sum-coincidence spectra. (c) The errors arise from partially compensating gain and base-line shifts with respect to conditions at the time of calibration; these shifts may affect the low-energy peaks as much as (or more than) the high-energy peaks (see Sec. 5.2). For the energy calibration, energies (in MeV) of the gamma rays and the sources used were: 0.511, ^{22}Na ; 0.662, ^{137}Cs ; 1.274, ^{22}Na ; 2.614, ThC' ; 4.432, PoBe ; and 6.135, $^{19}\text{F}(p, \alpha\gamma)^{16}\text{O}$ reaction at the 1372-keV resonance. The gain stabilization system prevents the shifts with counting rate for different sources which frequently plague such calibration measurements under unstabilized conditions. The energy values quoted in this report may differ slightly from, but are in good agreement with, those reported in Ref. 1; however, in order to provide a uniform energy scale for the additional states, not identified in Ref. 1, the values of the present experiment have been

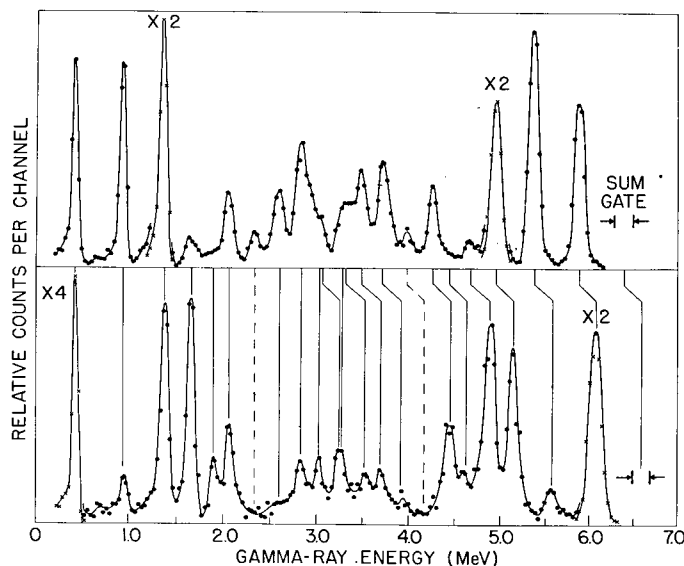


Fig. 45 - Sum-coincidence spectra obtained at the 1588-keV (upper) and the 1770-keV (lower) resonances, plotted to the same energy scale. These spectra illustrate the shift in the energy of the primary gamma rays corresponding to the difference in the excitation energy of the capturing levels and hence serve to identify the secondary gamma rays and the corresponding intermediate excited states. The scale for data points represented by x's should be multiplied by the listed factor.

uniformly used in this report. No confusion should exist on the identification of a particular level in the two reports, however, because the differences in the quoted values are small compared to the separation of neighboring states.

The identification of the energy of an intermediate state involved in a two-part cascade of course requires the establishment of the causal relationship, that is, the establishment of which gamma ray is the primary transition populating the level and which is the secondary transition de-exciting level. Such an identification is possible in the (p, γ) reactions, where capturing resonances at different excitation energies may be studied. Thus, as observed from resonances sufficiently separated in excitation energy, and for two-part cascades through the same intermediate state, the energy of the secondary transition must remain constant, as it represents the energy difference between the same intermediate level and the ground state in each case, and the energy of the primary transition must change by the same amount as the energy difference in excitation of the capturing levels. This effect is illustrated in Fig. 45 where sum-coincidence spectra obtained at the 1588-keV and 1770-keV resonances are displayed to the same energy scale. The 1588-keV resonance was used for correlation measurements (see Sec. 6.2) and the spectrum shown is a sum of spectra obtained under varying conditions of angle and geometry. The 1770-keV resonance, on the other hand, was not suitable for correlation work because of the presence of other strong resonances at too small an energy separation to the low-energy side. That resonance was accordingly run only for the present purposes and was obtained with the moving detector at $\theta = 45$ degrees to assure detection of transitions involving strongly anisotropic correlation functions. The sum-gate for the 1770-keV resonance is displaced by an amount equal to the difference in excitation energy of the two resonances, as indicated by the bent vertical line. Thus, secondary transitions are

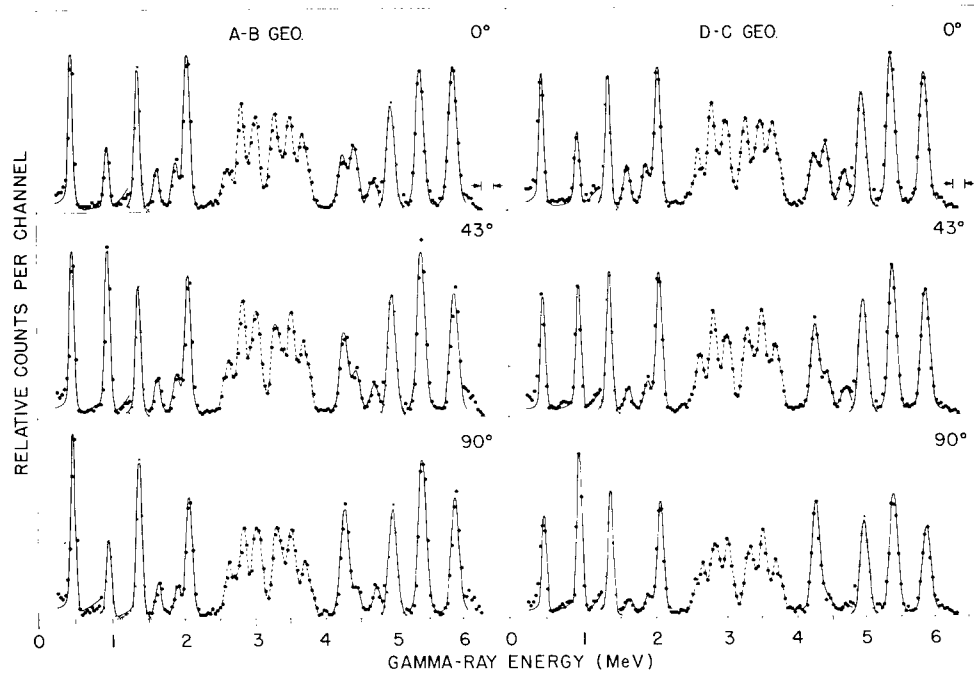


Fig. 46 - Sum-coincidence spectra obtained at the 1620-keV resonance for the two sets of geometries simultaneously measured at each of three angles by the double sum-coincidence arrangement. The data have been normalized to equal reaction yield but have not been corrected for the effects of unequal absorption of the gamma rays at the different angular positions of the detector. The solid curves are the sums of the calculated Gaussian fits made to the peaks and an estimation of the distortion and background effects. The dashed curves merely connect the points for purposes of clarity. The scale for data points represented by x's (principally the peaks at 1.37 and 4.97 MeV) should be multiplied by a factor of 3.

identified by straight vertical lines (no energy change), while primary transitions are identified by the bent vertical lines (energy change).

From Fig. 45, it is quite clear that states exist at energies of 0.47, 0.95, 1.37, 1.63, and 2.07 MeV. The existence of a state at 1.89 MeV, clearly seen at the 1770-keV resonance but barely discernible at the 1588-keV resonance, is more clearly seen at the 1620-keV resonance. The two members of a cascade observed at about 2.4 and 4.2 MeV in the 1588-keV resonance spectrum were not observed at any of the other resonances studied; therefore, positive identification of the primary and secondary members of the cascade is impossible. The vertical lines for these transitions are shown dashed to indicate the possible existence of a state corresponding to the lower of these energies, since all transitions observed below this energy proved to be secondary transitions. The three peaks, corresponding to transitions involving states at 2.64, 2.83, and 3.02 MeV, appear immediately to each side of the median energy (half of the excitation energy of the capturing level) at the 1599-keV and the 1620-keV resonances (see Figs. 35 and 46). These peaks are not as simple as might be supposed, for analysis indicates that at least those corresponding to states at 2.64 and 3.02 MeV are too wide for single peaks and that the structure in this region is surely complex. Further evidence of this is the apparent filling of the valley between the peaks corresponding to states at 2.83 and 3.02 MeV in the 1588-keV resonance spectrum and the appearance of a closely spaced doublet at the median energy in the 1770-keV spectrum. The latter peaks correspond to a state which would produce transitions unresolved from those for the 3.02 MeV state when observed

at the lower energy resonances due to the inversion of the positions of the primary and secondary transitions. The existence of transitions unresolved from those corresponding to the probable state at 2.64 MeV is also clear, although it has not been possible to determine further information on these transitions.

The congestion of peaks which appears to be occurring near the median energy is perhaps not surprising, since both an increase in level density and an inversion of the position of the primary and secondary transitions occur near this energy. It is quite likely that at least some of the weaker unresolved transitions noted above are due to states above the median energy for which such an inversion occurs. It is of course expected that states at higher excitations will not generally be as strongly excited by two-part cascade as lower energy states, both because of the previously mentioned tendency for multiple cascades and because of the strong energy dependence in the transition probability for gamma emission. These factors probably account for the apparent absence of any inversion in the transitions observed in regions other than those near the median energy.

6.2 Correlation Results

Chronologically, correlations have been run at the three resonances in the order 1599, 1588, and 1620 keV. The strong 1599-keV resonance produced adequate statistics for spin assignment only for the three strongest two-part cascades observed, namely, those involving the first three excited states. The weaker 1588-keV resonance was then run with poorer statistics as a confirmation of the unusual results obtained for the 1.37-MeV state from the 1599-keV resonance data for purposes of the report presented at a meeting of the American Physical Society (13). The 1620-keV resonance, which was chosen because it provided the most intense two-part cascade through the 1.63-MeV state of any of the usable resonances available, was subsequently given a long run in an attempt to provide adequate statistics for assignments to this and other weakly excited states. With these results, it has been possible to make assignments to this state and to the incompletely resolved pair of states at 1.89 and 2.07 MeV in addition to the previously determined first three excited states. No attempt has been made to obtain assignments for any higher excited state contained within the complex structure near the median energy, although some of these peaks provide adequate statistics, because even those peaks which appear best resolved almost surely contain contributions in unknown quantities from other transitions which may have quite different correlation functions. It would thus appear that with the resolution restrictions imposed by NaI detectors, this complexity of structure which appears here near the median energy may place a limitation on the height in excitation energy of states for which assignments may be expected with the techniques described in this report.

The sum-coincidence spectra obtained at the 1620-keV resonance are shown in Fig. 46 for the three angles in each of the two geometry sets. The results shown are appropriate sums from the 14-run sequences obtained for each of the 11 days of correlation measurement; the quality of the resultant spectra indicates the effectiveness of the means taken to achieve stability and reproducibility over such an extended period. The solid curves are the sums of the computed Gaussian distributions fit to the peaks and the estimated distortion and background effects. The peaks at 0.47 MeV in the D-C geometry (see Table 1 and Sec. 2.3) spectra and those at 2.07 MeV in all spectra are due to transitions for which the correlations are believed to be isotropic; thus, the magnitude of the correction factor for the unequal absorption of the gamma rays in the anisotropic distribution of materials in the vicinity of the target may be inferred from the degree of anisotropy observed for these peaks (see also Sec. 5.3). In addition to these instrumental effects, it may be noted that rather large but opposite anisotropies are present in peaks at 0.95 MeV in the A-B geometry and at 1.63 MeV in the D-C geometry spectra, and also in the incompletely resolved pair at 4.28 and 4.44 MeV in all spectra.

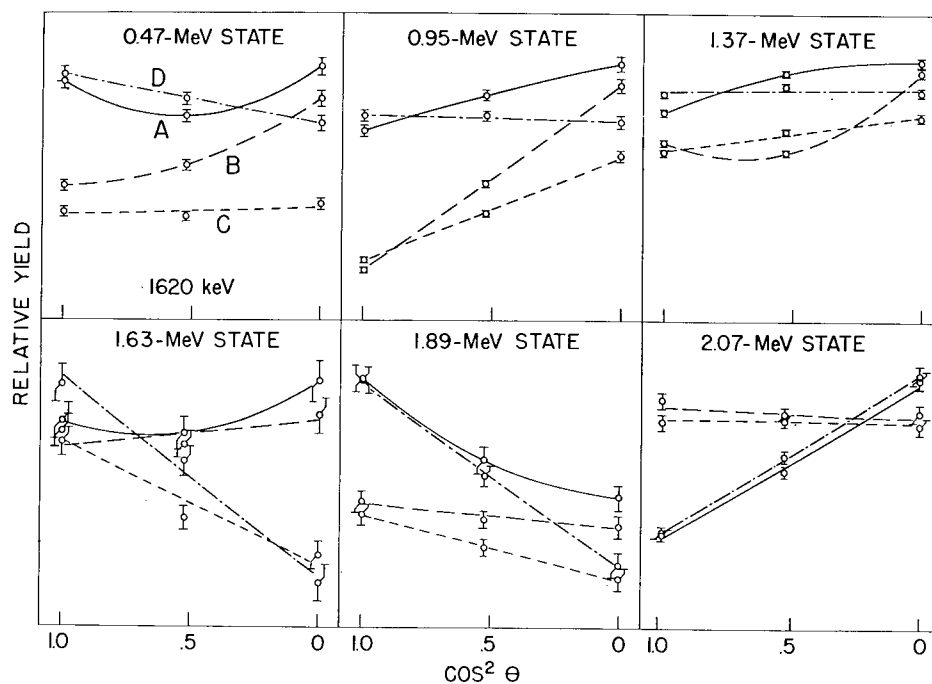


Fig. 47 - Corrected and normalized yield vs $\cos^2 \theta$ for the 24 correlation functions simultaneously measured at the 1620-keV resonance. The correlations are grouped according to the indicated intermediate excited state, and the four geometries for each state are designated by the pattern of the curves (the key is shown for the group in the upper-left-hand corner). The points are the sum of all data appropriate to that angle and geometry for each state, and the associated error bars include both purely statistical effects and an estimation of the error introduced in the correction for background, distortions, and incompletely resolved groups. The curves are calculated from the results of the least-squares fits to the normalized Legendre expansion for either the first two or first three terms, as appropriate to the theoretical predictions in agreement with the results for that state. The values of the coefficients of the normalized Legendre expansion obtained from the least-squares fit are listed in Table 4. The correlations for the A and B geometries for the 0.47-MeV state are instrumentally distorted.

The corrected and normalized yields for the 24 correlations measured at the 1620-keV resonance are shown in Fig. 47. The points shown are sums of the individual groups of runs used in the least-squares analysis, and the curves are calculated from the results of that fit for each correlation (see Sec. 5.3). The results of the fits for the coefficients of the Legendre expansion are listed in Table 4. Both the curves and the A_2 listings are for fits of two or three terms in the Legendre expansion, as required by the predicted correlation functions (see Sec. 5.4) which specify these geometries for which the A_4 must vanish. The curves reflect the vanishing A_4 requirement in such cases by appearing as straight lines in the plot against $\cos^2 \theta$, while enclosure in parentheses of entries for A_4 in Table 4 indicates those values required to vanish, the values being included to indicate the extent to which this requirement is met. The occurrence of a number of instances of exceptions to the vanishing requirement by amounts greater than the listed errors is in part statistical, but at least in some cases is probably partially due to systematic error, either that associated with the beam alignment problem or, in the case of the weaker transitions, that associated with the background subtraction. The beam-alignment effect should equally affect all transitions in that particular set, although the evidence for such

Table 4

Results of the Least-Squares Fit to the Normalized Legendre Expansion for the 24 Triple Correlations Measured Simultaneously at the 1620-keV Resonance

The correlations are identified as to the intermediate state and geometry, and the coefficients of the expansion, A_2 and A_4 , are listed. The value of A_2 is that determined from either a two-term or three-term fit as appropriate to the theoretical prediction for the assignment ultimately made to the state. Values of A_2 or A_4 enclosed in parentheses are for quantities required to vanish by these predictions, and are included to indicate the extent to which this requirement is met. Values enclosed in brackets are instrumentally distorted.

State (MeV)	Geometry	A_2	A_4
0.47	A	[-0.043±0.044]	[(0.170±0.036)]
	B	[(-0.314±0.036)]	[(0.106±0.036)]
	C	(-0.048±0.036)	(0.074±0.037)
	D	0.153±0.036	(0.007±0.036)
0.95	A	-0.184±0.028	-0.016±0.026
	B	-0.720±0.028	0.009±0.027
	C	-0.543±0.035	(0.022±0.033)
	D	0.020±0.031	(-0.012±0.029)
1.37	A	-0.112±0.018	-0.058±0.017
	B	-0.318±0.020	0.195±0.018
	C	-0.124±0.020	(-0.021±0.019)
	D	-0.006±0.019	(-0.030±0.018)
1.63	A	-0.17 ±0.09	0.13 ±0.09
	B	-0.09 ±0.08	(0.07 ±0.08)
	C	0.79 ±0.18	(0.25 ±0.15)
	D	1.12 ±0.21	(-0.14 ±0.15)
1.89	A	0.43 ±0.09	0.14 ±0.08
	B	0.15 ±0.11	(0.05 ±0.10)
	C	0.62 ±0.19	(0.04 ±0.15)
	D	0.99 ±0.13	(0.05 ±0.10)
2.07	A	-0.526±0.037	(0.044±0.036)
	B	(0.033±0.038)	(0.060±0.036)
	C	(0.008±0.038)	(-0.045±0.036)
	D	-0.517±0.036	(-0.012±0.036)

effects may itself be obscured by the statistical fluctuations. The background-subtraction effect, however, depends upon the particular transitions. However, it will be noted that large values of the A_4 coefficient relative to the probable error do not generally occur, even where they are allowed, with the notable exception of the B geometry for the 1.37-MeV state, which will be discussed below.

The predictions for the degenerate case of a 1/2-unit spin intermediate state, are isotropy for the secondary transitions in the B and C geometries, and identical anisotropies for the primary transitions in the A and D geometries. These predictions for the 0.47-MeV state are met at the 1599-keV resonance, as will be shown; but they clearly are not met by the A and B geometries at the 1620-keV resonance. This effect is due to crosstalk between detectors (see Sec. 2.2). The effect does not significantly appear in the C and D geometries, where the two detectors are always at 90 degrees from each other (and thus present no unshielded path for the transfer of an annihilation quantum from one detector to the other), or for $\theta = 0$ degrees for the A and B geometries, where the relevant detectors are again at 90 degrees to each other; but it does occur for the A and B geometries at $\theta = 43$ degrees and to an even greater extent at $\theta = 90$ degrees, as the relative opening between the detectors presented by the collimators increases to its maximum at $\theta = 90$, where the two detectors in the horizontal plane are directly opposite each other.

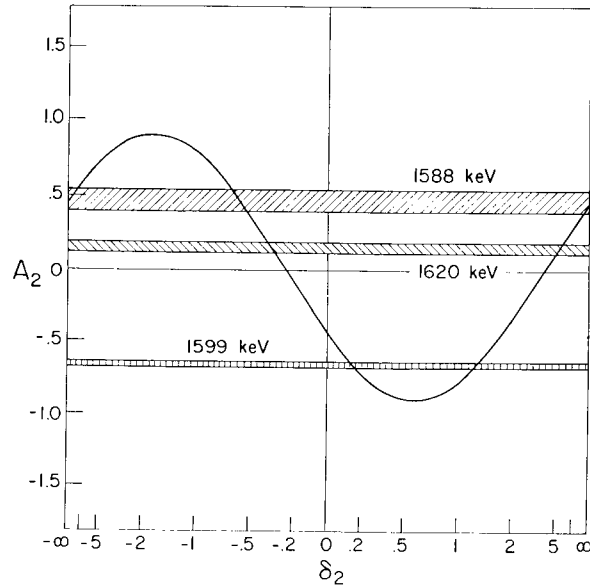
The collimators used in the present experiment are apparently sufficiently effective that such a crosstalk problem exists only with relation to the total capture peak for the ground state transitions from the capturing level. This is so because transfer of an annihilation quantum may occur for events involving a single gamma ray; that is, events which should be in this peak and which meet the sum condition but which require only a single detector-efficiency term (the fast-coincidence condition being supplied by the transfer event itself) rather than the two detector-efficiency terms normally required in sum-coincidence. The resulting increase in efficiency may be on the order of 10^2 . The satellite peaks associated with this particular transfer event mimic a state at the energy of the annihilation quantum and provide difficulty in the present experiment because such events are experimentally indistinguishable* from true two-part cascades involving the first excited state at 0.47 MeV. Even so, the effect is not appreciable unless the first excited state is rather weakly excited relative to the ground state transition in the branching of the capturing level, as occurs for the 1588-keV and 1620-keV resonances.

It is quite clear that the deviations from the predictions for a 1/2 spin assignment (listed above), observed in the A and B geometries at both the 1620-keV and 1588-keV resonances, and attributed to instrumental effects, do not contradict the 1/2 assignment. Thus, whether the isotropy observed in the secondary transitions (B and C geometries) at the 1599-keV resonance is due to a 1/2 spin assignment or to a higher spin assignment, this isotropy should be observed for these two geometries at any other resonance. This is true because even for higher spin assignments the isotropy is due to the particular quadrupole admixture for the secondary transition, and this admixture is the property of the intermediate and final states only and does not depend upon the particular capturing resonance from which the state is excited.

It is an unfortunate consequence of angular correlation theory that degeneracies are associated with low-valued spin states. One such degeneracy associated with a 1/2 spin assignment for the intermediate state is the impossibility by means of angular correlations alone, no matter how many geometries are measured, of differentiating uniquely between a 1/2 spin state and higher spin possibilities, because higher spin assignments can always be made to show agreement with the data for some particular values of the

*This is true of individual events; however, in the aggregate there is a noticeable trend for distortion of the 0.47-MeV peak toward higher energy in the spectra for $\theta = 43$ degrees and $\theta = 90$ degrees for the A-B geometry in Fig. 46.

Fig. 48 - The theoretical predictions for a $1/2$ spin assignment to the first excited state at 0.47 MeV, where the coefficient of the normalized Legendre expansion, A_2 , is shown as a function of the quadrupole amplitude ratio, δ_2 , for the primary transitions (A and D geometries). The sign convention for the admixture ratio is that of Devons and Goldfarb (2). This prediction requires isotropy for the secondary transitions (B and C geometries). The range of the experimental values for A_2 at each of the indicated resonances is shown by the hatched band. The resulting predictions for the primary quadrupole admixture are listed in Table 6.



admixture ratios. Nevertheless, the $1/2$ assignment is the most probable, when the conditions required by this assignment are met by the data, as this assignment does not require the accidental presence of a particular admixture ratio to fit the data. Another consequence of the degeneracies associated with the $1/2$ assignment is that, although the possibility of quadrupole admixture exists in both transitions, the admixture of the secondary transition is completely indeterminate. Therefore, the comparison of theory and experiment resolves to the representation of Fig. 48, where the predictions for the A_2 of the primary transitions (A and D geometries) are given as a function of the primary admixture only. As a consequence of a further degeneracy associated with the $1/2$ assignment, it is not possible to distinguish between the two predicted values of the primary admixture purely on the basis of the correlation measurements alone.

The results for the 0.47-MeV state from all three resonances at which correlations were run are shown in Fig. 48, the ranges of the experimentally observed values of A_2 being represented by the hatched horizontal bands. The experimental values used are from only the undistorted C and D geometries in those cases where distortions are evident in the A and B geometries. The 2.07-MeV state, for which correlations are observed only at the 1620-keV resonance, produces results which are also consistent with the predictions for a $1/2$ assignment. The prediction for this state is shown in Fig. 49, where the energy dependence of the finite-geometry-correction coefficients provides a very slight difference in scale from the predictions for the 0.47-MeV state.

The 0.95-MeV state, which shows large anisotropies in the B and C geometries, is consistent only with a $5/2$ assignment for the spin of the intermediate state. Here admixtures in both the primary and secondary transitions are allowed, and the predicted correlation functions corresponding to the experimental values of A_2 obtained at the 1620-keV resonance are shown in Fig. 50 in a contour plot representation. In this instance the overlap of the bands is not ideal, and it is also impossible to distinguish which of the two possible regions is appropriate. However, the results at the 1599-keV and 1588-keV resonances show that only the region associated with the lower valued possibility of the secondary admixture ratio is proper.

The 1.37-MeV state is also found to be consistent only with a $5/2$ assignment, but it produces quite a different aspect, as shown in Fig. 51. Here, better statistics were available for the transitions involving this state, and this fact is reflected in the generally more

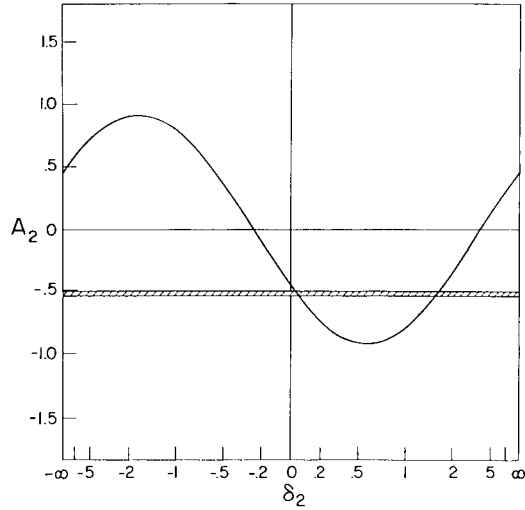


Fig. 49 - Theoretical predictions for a $1/2$ assignment to the 2.07-MeV state as observed at the 1620-keV resonance only. See Fig. 48 for details of the representation. The A_2 scale for this figure differs very slightly from that of Fig. 48 because of the effect of the finite geometry correction coefficients for the different energies of the transitions involved for the two states.

Fig. 50 - Contour plot for a $5/2$ assignment to the 0.95-MeV state as observed at the 1620-keV resonance, where the experimental results are shown as a function of the secondary and primary quadrupole admixture ratios, δ_3 and δ_2 respectively. Here the range of values of the admixture ratios allowed by the range of the experimental values of the A_2 coefficient of the normalized Legendre expansion is indicated by different hatching for each geometry. The admixture ratio axes are in an arctangent representation to allow display of the complete range of the variable. The sign convention for the admixture ratio is that of Devons and Goldfarb (2). Agreement of experiment and the predicted correlation functions is indicated by overlap of all four bands, and the range of the resulting allowed value(s) of the admixture ratio is listed in Table 6.

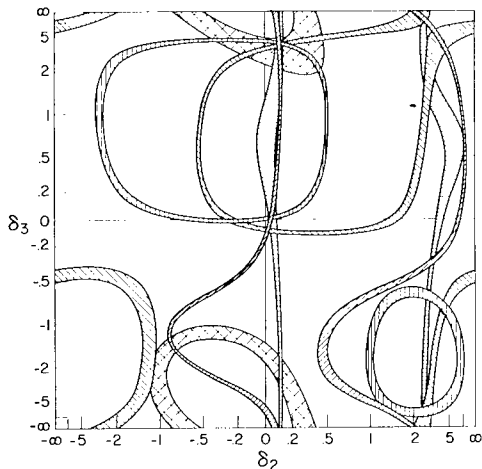
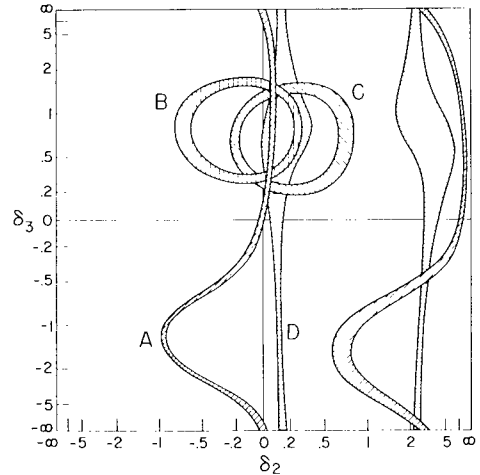


Fig. 51 - Contour plot for a $5/2$ assignment for the 1.37-MeV state as observed at the 1620-keV resonance. See Fig. 50 for the key to the hatching. Here an additional band shown by crosshatching represents the results for the significant A_4 coefficient for the B geometry. Note that the only possible overlap of all five bands occurs at an unusually high value of the secondary admixture ratio.

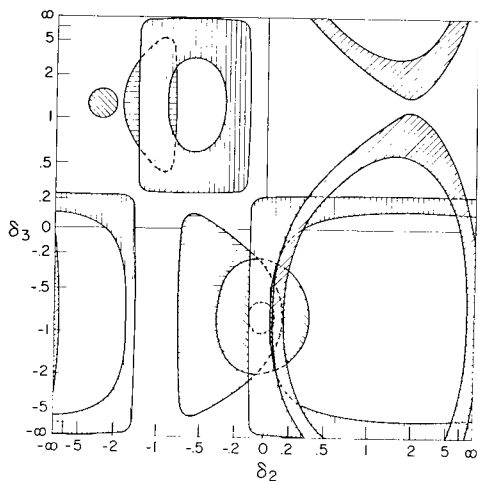


Fig. 52 - Contour plot for a possible 3/2 assignment to the 1.63-MeV state as observed at the 1620-keV resonance. See Fig. 50 for details of the representation.

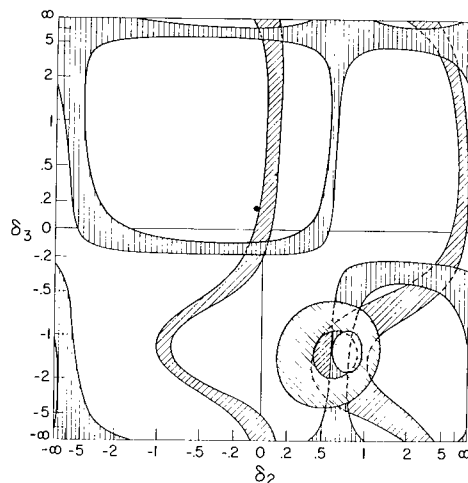


Fig. 53 - Contour plot for a possible 5/2 assignment to the 1.63-MeV state as observed at the 1620-keV resonance. See Fig. 50 for details of the representation.

narrow bands. It may be seen that the only possible overlap occurs at a surprisingly high value of the secondary admixture ratio. Such a high quadrupole admixture is generally associated with the observation of a significant A_4 value; and indeed, as previously noted, such an observation was made in this case. An additional band with crosshatching indicates the range predicted by this value, and it is seen that this band is also consistent with the observed overlap, this consistency providing conclusive evidence for the very large value of the secondary admixture ratio.

The very weak transitions through the 1.63-MeV intermediate state provide the only instance of ambiguity in the spin of the intermediate state which was observed from any of the correlations, other than those associated with the degeneracies for low-valued spin states. Probably because of the poor statistics and the greater likelihood of systematic error in connection with the background subtraction, the overlap is poor for either a possible 3/2 or 5/2 assignment, as shown in Figs. 52 and 53; therefore, it is not possible to distinguish between these two possible assignments on the basis of this comparison with the predicted correlation functions alone. There is a tendency to favor the 3/2 assignment because of the much stronger resemblance to the proved 3/2 case for the 1.89-MeV state rather than to those observed for states to which 5/2 assignments were made (see Fig. 47); but it would probably be inappropriate to make an assignment on this basis due to the present paucity of such examples.

Although the 1.89-MeV state also involved rather poor statistics and additionally involved incomplete resolution from the somewhat stronger transitions associated with the 2.07-MeV state, it does provide a clear exclusion of the 5/2 possibility and a somewhat better overlap for the allowed bands in the 3/2 prediction, as shown in Fig. 54. The case of a 3/2 assignment also provides a degeneracy, in this case only in the secondary admixture ratio, this ambiguity only recently having been reported (14). This ambiguity is evidenced by the symmetry in δ_3 , observed in Figs. 52 and 54, which is not present in the predictions for the 5/2 assignment.

The corrected and normalized yields and the fitted correlation functions are shown in Fig. 55 for the first three excited states, as observed at the 1599-keV and 1588-keV resonances. The results of the least-squares fits for the coefficients of the correlation

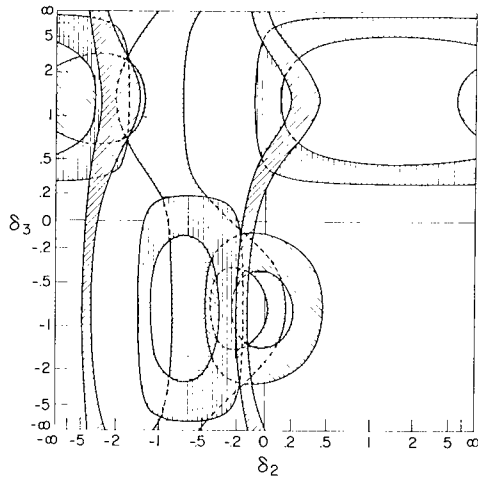


Fig. 54 - Contour plot for the 3/2 assignment to the 1.89-MeV state as observed at the 1620-keV resonance. See Fig. 50 for details of the representation. A possible overlap to the upper left is excluded by the observed A_4 coefficients (not shown).

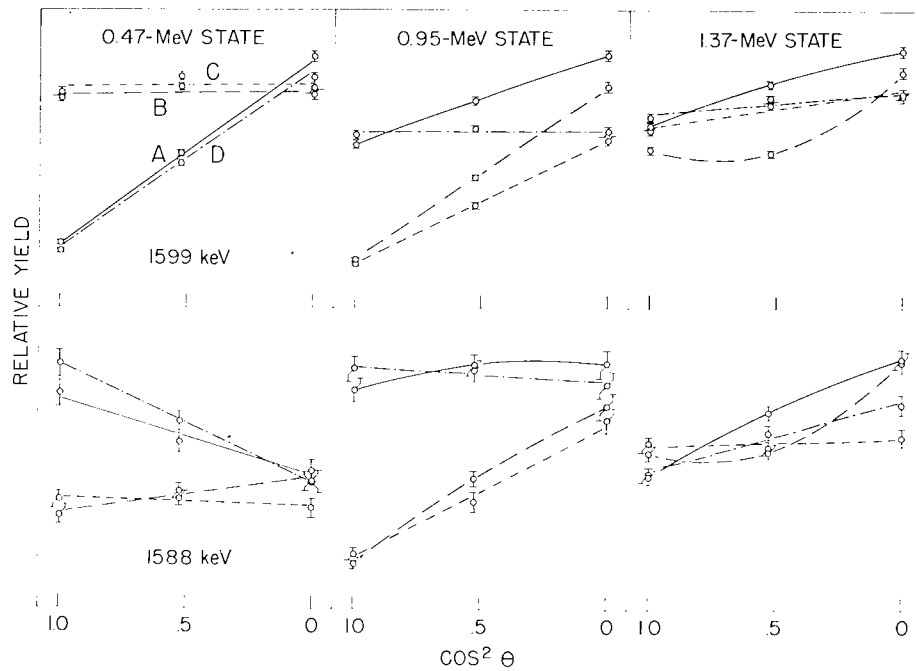


Fig. 55 - Corrected and normalized yield vs $\cos^2 \theta$ for the indicated excited states as observed at both the 1599-keV and 1588-keV resonances. See Fig. 47 for details of the representation.

functions are listed in Table 5. The previously mentioned nondistorted agreement with theory of the correlations associated with the 0.47-MeV state at the 1599-keV resonance may be noted. The comparison with theory for this state at these two resonances is shown in Fig. 48. The theoretical prediction for the 0.95-MeV state is shown for the 1599-keV resonance in Fig. 56 (that for the 1588-keV resonance was used as an example in Fig. 41); the exclusion of the higher-secondary-admixture-ratio possibility observed at the 1620-keV resonance is apparent in both. For the 1.37-MeV state, large A_4 terms are again observed in the B geometry at both resonances as indicated in Fig. 55. The

Table 5
Results of the Least-Squares Fit to the Normalized Legendre Expansion for the Twelve Triple Correlations Measured Simultaneously at Each of the Resonances at 1599 and at 1588 keV. See Table 4 for details.

Resonance (keV)	State (MeV)	Geometry	A_2	A_4
1599	0.47	A	-0.661±0.021	(0.047±0.021)
		B	(-0.010±0.021)	(-0.040±0.021)
		C	(-0.007±0.021)	(-0.057±0.031)
		D	-0.657±0.021	(-0.071±0.021)
	0.95	A	-0.267±0.023	-0.008±0.021
		B	-0.711±0.024	0.002±0.017
		C	-0.651±0.028	(0.013±0.028)
		D	-0.016±0.026	(-0.024±0.029)
	1.37	A	-0.205±0.022	-0.025±0.020
		B	-0.360±0.024	0.194±0.022
		C	-0.128±0.021	(-0.032±0.023)
		D	-0.073±0.023	(-0.038±0.022)
1588	0.47	A	[0.32 ±0.08]	[(0.07 ±0.09)]
		B	[(-0.19 ±0.08)]	[(-0.06 ±0.08)]
		C	(0.05 ±0.09)	(-0.05 ±0.08)
		D	0.47 ±0.08	(0.01 ±0.08)
	0.95	A	-0.05 ±0.05	-0.05 ±0.05
		B	-0.65 ±0.07	-0.06 ±0.06
		C	-0.63 ±0.07	(0.08 ±0.07)
		D	0.05 ±0.06	(-0.02 ±0.06)
	1.37	A	-0.350±0.040	-0.035±0.039
		B	-0.396±0.044	0.196±0.043
		C	-0.028±0.050	(0.036±0.050)
		D	-0.257±0.046	(-0.043±0.044)

theoretical predictions for both resonances, shown in Figs. 57 and 58, again indicate that the only possible overlap of all five bands occurs at the same large secondary admixture ratio. The poorer statistics obtained at the 1588-keV resonance are evident both in the larger error bars of Fig. 55 and in the wider allowed bands of Fig. 58.

The spin and parity assignments for the intermediate states, as determined from the predicted correlation functions at each of the resonances, are summarized in Table 6 along with the quadrupole-to-dipole amplitude ratios, as determined for the primary and secondary transitions. The error estimates for the latter are based upon the width of the allowed bands at the point of overlap and some consideration of the quality of the overlap. That is, in instances where the overlap was poor, an increase was made in the assigned

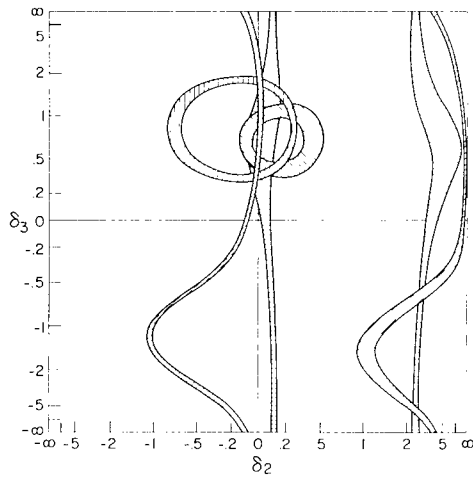


Fig. 56 - Contour plot for the 5/2 assignment to the 0.95-MeV state as observed at the 1599-keV resonance. See Fig. 50 for details of the representation.

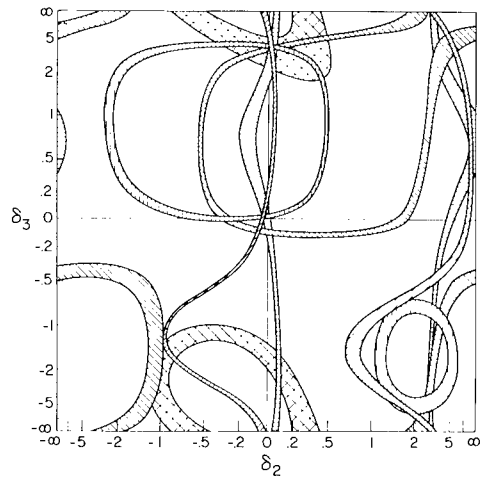


Fig. 57 - Contour plot for the 5/2 assignment to the 1.37-MeV state as observed at the 1599-keV resonance. See Figs. 50 and 51 for details of the representation.

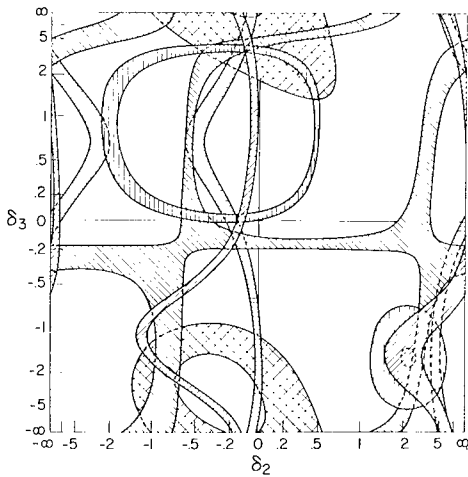


Fig. 58 - Contour plot for the 5/2 assignment to the 1.37-MeV state as observed at the 1599-keV resonance. See Figs. 50 and 51 for details of the representation.

errors. The weaker transitions in particular provide a problem in this regard. In those cases, a region of possible allowed values is indicated rather than a specific value with associated error.

Inferences for the probable parity may be based upon the observation of significant quadrupole admixtures as described in Sec. 1.4. Accordingly, probable negative parity has been proposed for each of the intermediate states for which spin has been assigned in this report (except the 1/2-unit spin states) on the basis of the observation of significant quadrupole admixtures in the secondary transitions as indicated in Table 6. As the secondary quadrupole admixture for the 1/2-unit spin states is indeterminate in the correlation measurements, negative parity cannot be assigned to them on this basis. The assignment of negative parity to the three capturing states is perhaps on less certain grounds, as the quadrupole admixtures for the primary transition are not so

Table 6
Summary of the Assignments From the Present Experiment for the Spin and Parity, J^π , of the Intermediate State and the Quadrupole Admixture Amplitude Ratios, δ_2 and δ_3 , for the Primary and Secondary Members, Respectively, of the Two-Part Cascade From the Capturing State Through the Intermediate State to the Ground State.

The values listed are identified as to the intermediate state and the resonance for which the triple correlation was observed. The spin assignments are all made on the basis of $3/2$ for the spin of both the capturing level (resonance) and for the ground state of ^{61}Cu (see Ref. 4). The three resonances are additionally assigned probable negative parity. Where assignments for the secondary admixture ratio were made at more than one resonance the last value listed in a weighted mean of the other values. The phase convention for δ is that of Devons and Goldfarb (2).

State (MeV)	Resonance (keV)	J^π	δ_2	δ_3
0.47	1588	$(1/2^-)^*$	-0.60 ± 0.07 or < -16 or > 26	
	1599	$(1/2^-)$	0.15 ± 0.02 or 1.25 ± 0.05	
	1620	$(1/2^-)$	-0.35 ± 0.02 or -5.8 ± 0.8	
0.95	1588	$5/2^-$	0.13 ± 0.06	$0.34^{+0.17}$ -0.12
	1599	$5/2^-$	0.01 ± 0.03	0.39 ± 0.05
	1620	$5/2^-$	0.03 ± 0.04	0.32 ± 0.04 0.35 ± 0.03
1.37	1588	$5/2^-$	-0.12 ± 0.06	$3.9^{+1.2}$ -0.8
	1599	$5/2^-$	0.04 ± 0.03	$3.63^{+0.39}$ -0.33
	1620	$5/2^-$	0.12 ± 0.02	$3.92^{+0.55}$ -0.43 $3.78^{+0.15}$ -0.13
1.63	1620	$(3/2^-)^\dagger$	-0.03 to 0.16^\ddagger	-0.29 to -1.68^\ddagger
		or $(5/2^-)$	0.56 to 1.05^\ddagger	-0.61 to -3.01^\ddagger
1.89	1620	$3/2^-$	-0.12 to -0.26^\ddagger	-0.08 to -0.42^\ddagger or -1.19 to -2.48^\ddagger
2.07	1620	$(1/2^-)^*$	0.05 ± 0.03	
			or 1.54 ± 0.09	

*Degeneracies associated with the $1/2$ assignment prevent a unique spin assignment, introduce an ambiguity in δ_2 , and make δ_3 completely indeterminant.

†The 1.63-MeV state was so weakly excited that it was impossible to distinguish on the basis of the correlations alone between a $3/2^-$ and a $5/2^-$ assignment.

‡The 1.63-MeV and 1.89-MeV states were so weakly excited that the δ values are better represented as a probable range of values rather than a value with associated error.

§Degeneracies associated with the $3/2$ assignment introduce an ambiguity in δ_3 ; however for the 1.63-MeV state the two regions are sufficiently indistinct that they are represented by a single range.

large* as those observed for the secondary transitions. However, penetrability arguments (see Ref. 1) favor the $3/2^-$ assignment of p-wave capture to the $3/2^+$ of d-wave capture. It is then possible on the basis of the observation of significant admixtures for the primary transitions to the $1/2$ -unit spin states to predict probable negative parity for them.

6.3 Discussion

In the present experiment the reaction $^{60}\text{Ni}(p,\gamma\gamma)^{61}\text{Cu}$ has been studied to obtain information on the low-lying excited states of one of the odd-A isotopes of copper. Because these isotopes contain a single proton outside a closed shell, they have attracted considerable attention with regard to the application of the core-excitation model. Although speculations on this model have been concerned with the location and spin of the levels and the application of the "center-of-gravity rule" of Lawson and Uretsky (15), additionally the arguments have been based upon the relationship of the transition probabilities between the presumed members of the expected quartet and the core level. These relationships, discussed by Cumming et al. (16), more recently summarized by Gove (17) and further treated by Vervier (18) and by Harvey (19), are based on absolute lifetime measurements with ^{63}Cu and ^{65}Cu , permitted by the stable nature of these nuclides. In this respect, of course, the present experiment does not contribute, as no information on the absolute lifetimes of the low-lying states can be determined by presently available techniques. The present measurements, however, do yield information on relative lifetimes through the measurement of the quadrupole admixture ratio, in addition to the predictions for the energy, spin, and parity.

Previous information on the low-lying states of ^{61}Cu is contained primarily in the article by Butler and Gossett (1). Subsequently, in an investigation of the decay of ^{61}Zn , Cumming (20) has observed gamma rays which he has fit into the level scheme reported in Ref. 1. On the basis of the intensities of the β^+ transitions inferred from these measurements, some limitations may be imposed on the possible spin values of the levels concerned, although no correlation measurements were made to predict definite values. Very recently Blair (21) has performed an experiment on the $^{60}\text{Ni}(^3\text{He},d)^{61}\text{Cu}$ reaction. He observes deuteron groups corresponding to the excitation of most of the states observed in the present experiment and makes ℓ -value assignments for the proton stripping on the basis of the forward-angle deuteron distributions.

The conclusions of the present report with regard to the positions of levels and their spin and probable parity assignments are summarized in the level diagram of Fig. 59, along with the results of Blair (21) and Cumming (20). There would appear to be agreement for the assignments to the first two excited states at 0.47 and 0.95 MeV. These spin assignments are also in agreement with assignments to presumably equivalent states in ^{63}Cu and ^{65}Cu , which have received considerable experimental attention. The quadrupole admixture for the 0.95-MeV state observed in the present experiment is in generally the same range of values as those observed for these states in ^{63}Cu (0.961 MeV) and ^{65}Cu (1.115 MeV), although there are some disagreements between different experiments for the same values as shown in Table 7. This discrepancy is particularly apparent for the recent resonance fluorescence result (22) compared to those from Coulomb excitation (23,24).

On the other hand, the situation with regard to the third excited state is less clear. In ^{63}Cu and ^{65}Cu the third excited states are reported (23,24) to be $7/2^-$, this assignment

*This effect is to be expected because large admixtures are generally associated with collective motions of the nucleus, which occur primarily for the relatively purer low-lying states. The capturing levels, on the other hand, occur at such high excitations that these states are probably highly mixed and would not be expected to contain sufficient relation to the lower states to provide large admixtures.

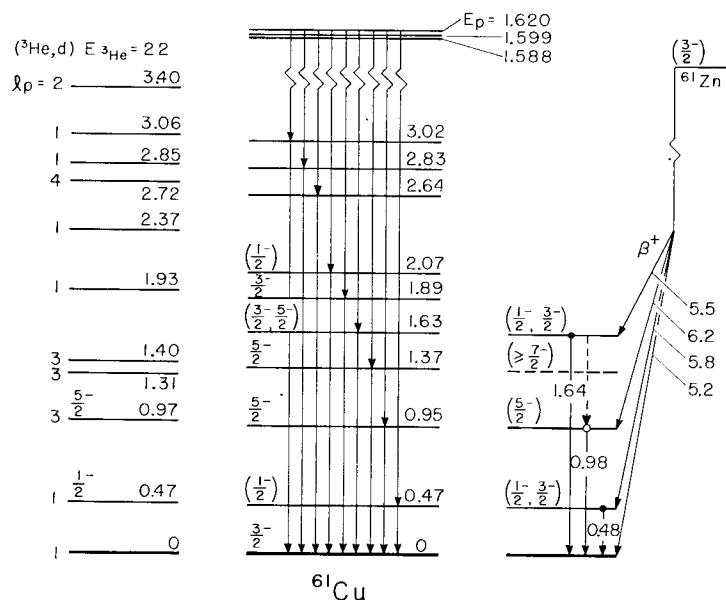


Fig. 59 - A level diagram for the nuclide ^{61}Cu showing the results of the present experiment in the center. Here only two-part cascades are shown, as the experimental arrangement preferentially selects these. Possible limitations on the spins of some of these states as inferred from the results of Cumming (20) in the decay of ^{61}Zn are shown on the right with the $\log ft$ values indicated for the β^+ transitions. Recent results by Blair (21) for the $(^3\text{He}, d)$ reaction are shown on the left with the ℓ -values determined from the proton stripping. His spin assignments for the first two excited states are based upon sum-rule considerations. The assignments for the excitation energies of the low-lying excited states are well within experimental errors for all experiments and the agreement for the spin assignments is good. The implications of the doublet at about 1.40 MeV reported by Blair are discussed in the text.

being in agreement with the expectations of the core-excitation model. Indeed, this is one of the levels for which absolute lifetime measurements have been made relating to the arguments for this model. Because Cumming observed no evidence of β^+ transitions to the level reported by Butler and Gossett (1) at 1.38 MeV in ^{61}Cu , it has been widely assumed (see Ref. 25) that this level has a spin of $7/2^-$. The assignment of $5/2^-$ of the present report is of course in disagreement with this conclusion. That the theoretical predictions for a $7/2^-$ assignment to the 1.37-MeV state do not agree with the experimental observations may readily be seen by a comparison of these predictions listed in Table 8 with the experimentally observed quantities listed in Tables 4 and 5. Blair's recent experiment offers an interesting possibility: he observes two $\ell = 3$ states at 1.31 and 1.40 MeV. As the $\ell = 3$ stripping leads to states of either $5/2^-$ or $7/2^-$, Blair's result is clearly not inconsistent with the $5/2^-$ assignment of the present report. Indeed, one is tempted to suggest that one member of Blair's doublet is the $5/2^-$ state, and that the other member is the missing $7/2^-$ state expected by analogy with ^{63}Cu and ^{65}Cu and required by the core-excitation model. It is not clear to which member of Blair's doublet the 1.37-MeV state of the present report corresponds, although the 1.40-MeV state may be

Table 7
Comparison of the Quadrupole-to-Dipole Amplitude Ratios, $\delta = (E2/M1)^{1/2}$, observed for the $5/2^-$ Second Excited States of Some of the Odd-A Isotopes of Cu

^{61}Cu	^{63}Cu	^{65}Cu
$+0.35 \pm 0.03^*$	$-0.41^{+0.07 \dagger}$ -0.11	$-0.22 \pm 0.06 \ddagger$
	$-0.27 \pm 0.08 \ddagger$	$-0.30 \pm 0.13 \ddagger$
	$\pm 0.40 \S$	$-0.52^{+0.07 \P}$ -0.05

*Present result. The difference of the sign of this result from the other measurements is due merely to different conventions: Devons and Goldfarb for the present results and Biedenharn and Rose for the others.

\dagger See Ref. 23.

\ddagger See Ref. 24.

\S See Ref. 16.

\P See Ref. 22.

Table 8
Predicted Correlation Functions for a $7/2^-$ Assignment to the 1.37-MeV State for Comparison With Those Actually Observed, as Listed in Tables 4 and 5.

These predictions contain the effects of finite solid angle of the detectors. Because M3 transitions are not expected to compete in reaction induced transitions, the predictions for the $3/2^-(E2)7/2^-(E2)3/2^-$ cascade are not a function of multipole admixtures.

Geometry	A_2	A_4
A	-0.166	0.068
B	-0.009	0.145
C	0.410	0
D	0.206	0

slightly favored. However, as the $7/2^-$ state is not observed in the $(p,\gamma\gamma)$ reaction, definite evidence for such an assignment is lacking.

The nonobservation of transitions involving a $7/2^-$ intermediate state, which would require a pure E2 transition from a $3/2^-$ capturing level, is perhaps not surprising in the present experiment. Although the transition de-exciting the intermediate state (secondary transition) may show an enhancement of the E2 transition probability if the state is analogous to those $7/2^-$ states observed in ^{63}Cu and ^{65}Cu , there is no reason to expect such an enhancement for the E2 transition from the capturing level to the $7/2^-$ state (primary transition). However, the strengths of the branching of transitions from the capturing level through various intermediate states, and the resultant observation in the present experiment, depend in part upon the transition probabilities of these primary transitions. Thus, the situation of the present experiment is not all comparable to that of the Coulomb excitation experiments in which the E2 transition probability between the $7/2^-$ state and the ground state is controlling.

Although no measurements had been made to determine the spin of the fourth excited state of ^{63}Cu (1.412 MeV), a value of $3/2^-$ had been assumed (15,17) for this state on the basis of the "center of gravity" rule. However, a recently published experiment by Blair (26) indicates $\ell = 3$ stripping for this state in disagreement with this assumption. Blair suggests that his observations favor the unified-model calculations of Bouten and Van Leuven (27) which predict $5/2^-$ for this state and allow the greater single particle strengths which Blair states his stripping measurements indicate. If the fourth excited state of ^{63}Cu is $5/2^-$, the situation in that nuclide is perhaps similar (but it is possible that the positions of the levels may be inverted) to the possibly existing in ^{61}Cu , as suggested above. (The small shifts in level positions, which would be required to invert the positions of the levels from the positions observed in ^{63}Cu , are not inconsistent with changes which may occur with the different neutron populations of these isotopes.)

Blair's observation of a doublet in ^{61}Cu , however, may raise the question of whether the presence of an undetected doublet could not so distort the results of the present experiment as to lead to an erroneous $5/2^-$ assignment with the unusually high secondary quadrupole admixture observed. That this is not the case is indicated by three arguments:

First, the full width at half maximum is 89 ± 6 keV for the peak at 1.37 MeV in the 1620-keV spectra, and this value is in good agreement with that observed for neighboring peaks. Further, as may be seen from the various spectra, the high-energy side of the Gaussian distribution for the 1.37-MeV peak is quite clear of evidence for an unresolved weaker transition; although the low-energy side of this peak is not so clear due to the presence of distortions (see Sec. 5.2). While it is difficult to make a quantitative estimate of the amount that could be present in the 1.37-MeV peak of a transition at either a 90-keV-higher or -lower energy, it seems unlikely that an amount sufficient to significantly distort the observed correlation could be present and remain undetected. Second, the transitions associated with the 1.37-MeV state are among the strongest at each resonance, and they produce excellent statistics. Thus the evidence for the $5/2^-$ assignment to this state probably represents better agreement of the predictions and experiment than that obtained for any of the other states of this report. It therefore seems unlikely that a contribution from the other unrelated member of a doublet could accidentally produce such an excellent agreement with the predictions at any one resonance, let alone three different resonances. This is particularly evident since the branching ratios for transitions to different states generally vary from resonance to resonance, and it would be highly unlikely that precisely the proper contribution be maintained at three different resonances. Third, the observation of a large A_4 term in only the B geometry is not what would be expected from the addition of unrelated angular correlations in an arbitrary manner. Thus, a distortion due to the effect of an undetected doublet would very likely also strongly affect the A_4 coefficients for the C and D geometries, whereas the predictions require that these coefficients vanish in any pure case. However, the values observed for these geometries do not appear to deviate significantly more from zero by the quoted errors than those observed for other states, and these values certainly are not comparable to that observed in the B geometry.

With regard to the remaining states at higher excitation energies: Blair does not report the observation of deuteron groups populating a state corresponding to that found at 1.63 MeV in the present report and in Ref. 1, and supported by the observations of Cumming. Of the two spin possibilities allowed by the present experiment for this state, the $3/2^-$ assignment may be preferred on the basis of Cumming's reported spin limitations. The state found by Blair at 1.93 MeV is in reasonable agreement with that assigned at 1.89 MeV in the present report, and the assignment of $\ell = 1$ is in agreement with the $3/2^-$ assignment of this report. Blair also does not report a state corresponding to the $1/2^-$ state at 2.07 MeV from the present experiment. The $\ell = 1$ state reported by Blair for a state at 2.37 MeV does not correspond to a state observed to be populated in the $(p, \gamma\gamma)$ reaction unless possibly it be that state at near this energy observed only at the 1588-keV resonance. Above this energy the agreement of states is problematical, due to the increased density of states and the difficulties of the sum-coincidence method in this region (see Sec. 6.1). It is in particular unlikely that the $\ell = 4$ state reported by Blair at 2.72 MeV corresponds to a state that is observed near this energy in the present experiment, as it is not expected that a $7/2^+$ or $9/2^+$ level would be populated by a double cascade in the $(p, \gamma\gamma)$ reaction.

Thus, the agreement of the present experiment with other experimental evidence appears to be quite good, although the agreement with theory, or at least with some of the existing versions of the core-excitation model (18,19), would appear less satisfactory. The assignments to the first two excited states in the present experiment are of course consistent with that model; and the absence of the observation of a $7/2^-$ state may not be serious, in that the possibility that the unobserved member of the doublet reported by Blair could be such a state; however, these versions of the core-excitation model, at least as applied to the neighboring Cu isotopes, apparently do not explain the unusual character of the state which is here reported at 1.37 MeV for ^{61}Cu . Thus, if the state in ^{61}Cu at 0.95 MeV is the $5/2^-$ member of the core excitation quartet, as is to be expected if the apparently equivalent states in ^{63}Cu and ^{65}Cu are the $5/2^-$ members essential to the reduced (E2) transition probability arguments now being used to support the model

(17-19), then the 1.37-MeV state cannot be the $5/2^-$ member of this quartet. If, as is generally assumed, the enhancement of the E2 transition probability, reflected in the unusually high quadrupole admixture, is indeed an index of collective effects, why then does a model which purports to represent the effects of collective motions in these nuclides not explain the existence of a level which apparently has stronger collective features than those states presumably explained by the model?

ACKNOWLEDGMENTS

The authors are pleased to acknowledge the assistance of Dr. P.A. Treado of Georgetown University and of this Laboratory for his participation in some of the data accumulation and analysis and in helpful discussions of the interpretation of the results. The authors wish to gratefully acknowledge the assistance of many members of the staff of this Laboratory including: Mr. Jack Brotzman, for design of the sum-coincidence and gain-stabilizer circuits used in this experiment, and Messrs. Paul Shifflett, John Robinson, and Richard Prom for advice and assistance in other phases of the electronic instrumentation; Messrs. Claude Martin, Walter Aleksiewicz, and Bernard Taubersmith, for assistance in the design of some of the physical apparatus, and Mr. Joe Schumacher and other members of ESD for fabrication of the apparatus; Dr. Charlotte Davisson, for providing the computer programming for the Monte Carlo calculations to generate the finite-geometry-correction coefficients; Miss Doris Ellis, of the Research Computation Center, ODR, for programming the predictions of the correlation functions, and various members of the RCC for advice on programming other aspects of the data analysis; Mr. Carl Starling, and in earlier phases of the work, Mr. Frank Marchetti, for general assistance with construction and maintenance of the instrumentation; Messrs. Larry Robinson, Niel Reid, and Arnold Eskin, summer students, for participation in various phases of the operation; Mrs. Edwina Cecchini and others of the division secretarial staff for assistance with the manuscript; and especially Dr. L. A. Beach, for his interest in and support of the work throughout. The authors also wish to express their appreciation to Dr. A.G. Blair, of the Los Alamos Scientific Laboratory, for communicating his results prior to publication.

REFERENCES

1. Butler, J.W., and Gossett, C.R., Phys. Rev. 108:1473 (1957)
2. Devons, S., and Goldfarb, L.J.B., in "Handbuch der Physik," Vol. 42, p. 362, Ed. by S. Flügge, Berlin:Springer-Verlag 1957
3. Ferguson, A.J., and Rutledge, A.R., "Coefficients for Triple Angular Correlation Analysis in Nuclear Bombardment Experiments," Atomic Energy of Canada, Ltd., CRP-615, AECL-420, 1957, revised and reprinted 1962
4. Nierenberg, W.A., Shugart, H.A., and Silsbee, H.B., Bull. Am. Phys. Soc. 2:200 (1957); Reynolds, J.B., Christensen, R.L., Hamilton, D.R., Hooke, W.M., and Stroke, H.H., Phys. Rev. 109:465 (1958)
5. Hoogenboom, A.M., Nucl. Instr. Methods 3:57 (1958)
6. Draper, J.E., and Fleischer, A.A., Nucl. Instr. Methods 9:67 (1960)
7. Butler, J.W., Nucl. Instr. Methods 8:211 (1960)
8. Reich, C.W., Merrill, J.A., and Klema, E.D., Nucl. Instr. Methods 23:36 (1963)
9. Grodstein, G.W., "X-Ray Attenuation Coefficients From 10 kev to 100 Mev," National Bureau of Standards Circular 583, 1957
10. Rose, M.E., Phys. Rev. 91:610 (1953)
11. Gossett, C.R., and Davisson, C.M., Bull. Am. Phys. Soc. 7:9 (1962); Gossett, C.R., and Davisson, C.M., NRL Quar. on Nuc. Sci. and Tech., Oct. 1, 1961, p. 38. Values for 3 in. diam \times 3 in. and 5 in. diam \times 6 in. NaI crystals are available from the authors.
12. Falvey, J.P., "A NAREC Program for Least Square Error Fitting," NRL Report 5788, June 15, 1962
13. Gossett, C.R., August, L.S., and Treado, P.A., Bull. Am. Phys. Soc. 9:472 (1964)
14. Harris, G.I., and Seagondollar, L.W., Phys. Rev. 131:787 (1963); Van Rinsvelt, H., and Smith, P.B., Physica 30:59 (1964)
15. Lawson, R.D., and Uretsky, J.L., Phys. Rev. 108:1300 (1957)
16. Cumming, J.B., Schwarzschild, A., Sunyar, A.W., and Porile, N.T., Phys. Rev. 120:2128 (1960); Cumming, J.B., and Porile, N.T., Phys. Rev. 122:1267 (1961)
17. Gove, H.E., Phys. Letters 4:249 (1963)
18. Vervier, J., Nuovo Cimento 28:1412 (1963)
19. Harvey, M., Nucl. Phys. 48:578 (1963)
20. Cumming, J.B., Phys. Rev. 114:1600 (1959)
21. Blair, A.G., private communication
22. Beard, G.B., Phys. Rev. 135:B577 (1964)
23. Robinson, R.L., McGowan, F.K., and Stelson, P.H., Phys. Rev. 134:B567 (1964)
24. Elbek, B., Gove, H.E., and Herskind, B., to be published in Mat. Fys. Medd. Dan. Vid. Selsk.

25. "Nuclear Data Sheets," compiled by K. Way et al., Printing and Publishing Office, National Academy of Sciences-National Research Council, Washington, D.C., 1960, NRC 60-5-40,41
26. Blair, A.G., Phys. Letters 9:37 (1964)
27. Bouten, M., and Van Leuven, P., Nucl. Phys. 32:499 (1962)

DOCUMENT CONTROL DATA - R&D

(Security classification of title, body of abstract and indexing annotation must be entered when the overall report is classified)

1. ORIGINATING ACTIVITY (Corporate author)		2a. REPORT SECURITY CLASSIFICATION	
U.S. Naval Research Laboratory Washington, D.C. 20390		UNCLASSIFIED	
		2b. GROUP	
3. REPORT TITLE DETERMINATION OF THE SPIN AND PARITY OF NUCLEAR EXCITED STATES BY THE EXPERIMENTAL MEASUREMENT OF TRIPLE CORRELATIONS IN (p, $\gamma\gamma$) REACTIONS			
4. DESCRIPTIVE NOTES (Type of report and inclusive dates) A final report on one phase of the problem.			
5. AUTHOR(S) (Last name, first name, initial) Gossett, C.R. August, L.S.			
6. REPORT DATE February 12, 1965	7a. TOTAL NO. OF PAGES 94	7b. NO. OF REFS 27	
8a. CONTRACT OR GRANT NO. NRL Problem H01-10	9a. ORIGINATOR'S REPORT NUMBER(S) NRL Report 6186		
b. PROJECT NO. RR 002-06-41-5006	9b. OTHER REPORT NO(S) (Any other numbers that may be assigned this report)		
c.			
d.			
10. AVAILABILITY/LIMITATION NOTICES Unlimited availability. Copies available from Clearinghouse for Federal Scientific and Technical Information (CFSTI) Sills Building, 5285 Port Royal Road, Springfield, Virginia 22151.			
11. SUPPLEMENTARY NOTES		12. SPONSORING MILITARY ACTIVITY Dept. of the Navy (Office of Naval Research)	
13. ABSTRACT The measurement of triple correlations in (p, $\gamma\gamma$) reactions to determine spin and parity of nuclear excited states has not been widely used in the past despite the capability of such measurements to produce generally unambiguous assignments. This lack of usage has arisen primarily because of the low efficiency, the complexity, and the difficulty of such measurements when performed by standard techniques. This report describes an experimental arrangement which allows the measurement of triple correlations with an exceptionally high efficiency and multiplicity (the capability of measuring many different correlations simultaneously). This improvement has been obtained primarily from the successful application of a three-crystal double sum-coincidence spectrometer. An explanation of the method and detailed descriptions of the physical apparatus, electronic circuitry, experimental procedures, and data analysis are given, including explanations of a number of deviations from normal in both the design and procedures. As an illustration of the effectiveness and limitations of the experimental arrangement, the results of an extensive triple correlation experiment on the $^{60}\text{Ni}(p, \gamma\gamma)^{61}\text{Cu}$ reaction are presented with the conclusions regarding the spin and probable parity of six of the lowest-lying energy levels and a discussion of the applicability of certain nuclear models to this nucleus.			

14. KEY WORDS	LINK A		LINK B		LINK C	
	ROLE	WT	ROLE	WT	ROLE	WT
Nuclear spectroscopy Nuclear excited states Nuclear spins Parity Triple correlations Sum-coincidence Double sum-coincidence (p, γ) reactions ⁶⁰ Ni(p, γ) ⁶¹ Cu reaction Experimental arrangement Electronic circuitry Data analysis Predicted correlations						

INSTRUCTIONS

1. **ORIGINATING ACTIVITY:** Enter the name and address of the contractor, subcontractor, grantee, Department of Defense activity or other organization (*corporate author*) issuing the report.

2a. **REPORT SECURITY CLASSIFICATION:** Enter the overall security classification of the report. Indicate whether "Restricted Data" is included. Marking is to be in accordance with appropriate security regulations.

2b. **GROUP:** Automatic downgrading is specified in DoD Directive 5200.10 and Armed Forces Industrial Manual. Enter the group number. Also, when applicable, show that optional markings have been used for Group 3 and Group 4 as authorized.

3. **REPORT TITLE:** Enter the complete report title in all capital letters. Titles in all cases should be unclassified. If a meaningful title cannot be selected without classification, show title classification in all capitals in parenthesis immediately following the title.

4. **DESCRIPTIVE NOTES:** If appropriate, enter the type of report, e.g., interim, progress, summary, annual, or final. Give the inclusive dates when a specific reporting period is covered.

5. **AUTHOR(S):** Enter the name(s) of author(s) as shown on or in the report. Enter last name, first name, middle initial. If military, show rank and branch of service. The name of the principal author is an absolute minimum requirement.

6. **REPORT DATE:** Enter the date of the report as day, month, year; or month, year. If more than one date appears on the report, use date of publication.

7a. **TOTAL NUMBER OF PAGES:** The total page count should follow normal pagination procedures, i.e., enter the number of pages containing information.

7b. **NUMBER OF REFERENCES:** Enter the total number of references cited in the report.

8a. **CONTRACT OR GRANT NUMBER:** If appropriate, enter the applicable number of the contract or grant under which the report was written.

8b, 8c, & 8d. **PROJECT NUMBER:** Enter the appropriate military department identification, such as project number, subproject number, system numbers, task number, etc.

9a. **ORIGINATOR'S REPORT NUMBER(S):** Enter the official report number by which the document will be identified and controlled by the originating activity. This number must be unique to this report.

9b. **OTHER REPORT NUMBER(S):** If the report has been assigned any other report numbers (*either by the originator or by the sponsor*), also enter this number(s).

10. **AVAILABILITY/LIMITATION NOTICES:** Enter any limitations on further dissemination of the report, other than those

imposed by security classification, using standard statements such as:

- (1) "Qualified requesters may obtain copies of this report from DDC."
- (2) "Foreign announcement and dissemination of this report by DDC is not authorized."
- (3) "U. S. Government agencies may obtain copies of this report directly from DDC. Other qualified DDC users shall request through _____."
- (4) "U. S. military agencies may obtain copies of this report directly from DDC. Other qualified users shall request through _____."
- (5) "All distribution of this report is controlled. Qualified DDC users shall request through _____."

If the report has been furnished to the Office of Technical Services, Department of Commerce, for sale to the public, indicate this fact and enter the price, if known.

11. **SUPPLEMENTARY NOTES:** Use for additional explanatory notes.

12. **SPONSORING MILITARY ACTIVITY:** Enter the name of the departmental project office or laboratory sponsoring (*paying for*) the research and development. Include address.

13. **ABSTRACT:** Enter an abstract giving a brief and factual summary of the document indicative of the report, even though it may also appear elsewhere in the body of the technical report. If additional space is required, a continuation sheet shall be attached.

It is highly desirable that the abstract of classified reports be unclassified. Each paragraph of the abstract shall end with an indication of the military security classification of the information in the paragraph, represented as (TS), (S), (C), or (U).

There is no limitation on the length of the abstract. However, the suggested length is from 150 to 225 words.

14. **KEY WORDS:** Key words are technically meaningful terms or short phrases that characterize a report and may be used as index entries for cataloging the report. Key words must be selected so that no security classification is required. Identifiers, such as equipment model designation, trade name, military project code name, geographic location, may be used as key words but will be followed by an indication of technical context. The assignment of links, roles, and weights is optional.